HIGH ENERGY SCATTERING.

by

Raymond William Moore.

Thesis presented for the Doctor of
Philosophy of the University of London
and
Diploma of the Membership of Imperial College.

Physics Department,
Imperial College
LONDON S.W.7.

October 1970.

Contents.

Page.

PREFACE.

The work presented in this thesis was carried out between October 1968 and September 1970 under the supervision of Professor P.T. Matthews to whom the author is grateful for guidance. Except where stated, the work is original and has not been presented for a degree of this or any other university.

The author wishes to thank S.A. Adjei, P.A. Collins, B.J. Hartley and K.J.M. Moriarty with whom he has collaborated on a series of absorptive Regge, absorptive Veneziano and multiparticle Veneziano models in an attempt to explain a wide range of experimental data, for permission to include the work in the thesis. He also thanks members of the Theoretical Physics Department for valuable discussions. Finally, the author acknowledges the financial support of the Science Research Council.

ABSTRACT.

This thesis consists of six chapters and deals with the application of cuts as generated by the absorption model to both Regge models, in chapters 1 to 4, and to Veneziano models in chapter 5 and 6.

Chapter 1 consists of a discussion of the fixed pole peripheral model together with the motivation for the introduction of both a Regge form for the pole graph and an absorption model for the cuts. In chapter 2, we start constructing our model with the development of a form for the Regge term which has couplings to inter-relate all two body processes. The required two-body kinematics are given. This is followed in chapter 3 by a brief discussion of cut models leading into the parameterization used for the cuts. Finally, chapter 4 deals with the application of our model to $0^{-}\frac{1}{2}^{+}$ hypercharge exchange processes and the relation to other similar models.

In an attempt to form a Veneziano model out of our previous Regge absorption model, a general review of the subject is given in Chapter 5, with particular reference to $\bar{K}N$ and KN charge-exchange reactions. In chapter 6, we give an 'improved' U(6,6) Regge formalism which is then converted into a dual model. The physical properties required are discussed, followed by the application to $\bar{K}N$ and KN charge-exchange reactions.

A review of the computer program is given in the appendix.

CHAPTER I. REGGE POLES AND CUTS.

In the original form of the peripheral model for two-body meson-baryon scattering at high energies, it is believed that the differential cross-sections at small momentum transfers are dominated by the exchange of 'low mass' fixed pole meson particles in the t-channel[1].

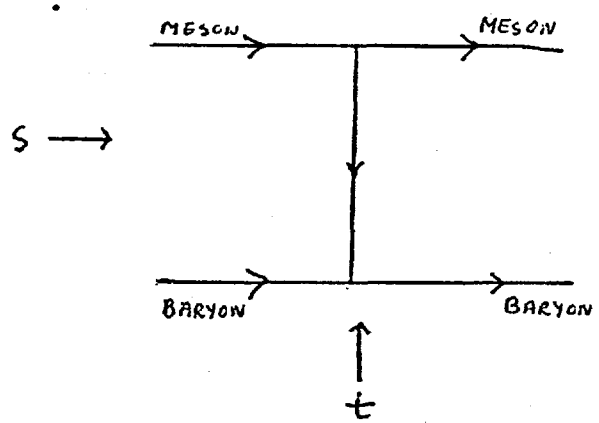

These lowest mass particles are expected to dominate as they lie nearest the physical scattering region in the t-plane i.e. negative t-region, and lead to an amplitude $T \sim \frac{s^J}{t-M_J^2}$ where J defines the spin of the particle exchanged in the process[2]. However, as the quantum numbers of the external particles may allow more than one 'low mass' exchange, symmetry schemes, e.g. U(6,6) are essential to give the ratio of the contributions from the various Feynman graphs[3].

For fixed pole exchange, we have $\left.\frac{d\sigma}{dt}\right|_{t=0} \sim s^{2J-2}$, so pseudoscalar exchange gives, e.g. in $pn \to np$, $\left.\frac{d\sigma}{dt}\right|_{t=0} \sim s^{-2}$, which is the correct s-dependence of the experimental data of the forward peak, although the forward peaking is not obtained as conservation of angular momentum makes the pseudoscalar contribution vanish at t=0. However, for the exchange of mesons of $J>0$, the energy dependence in the forward direction is incorrect. For example, in πN charge-exchange scattering, $\left.\frac{d\sigma}{dt}\right|_{t=0}(\text{experiment}) \sim s^{-1}$, but as we have ρ exchange (J=1), $\left.\frac{d\sigma}{dt}\right|_{t=0}(\text{theory}) \sim s^{0}$. The correction of this s-dependence problem

is suggested by Chew-Frautschi plots of J against t, $t \geqslant 0$[4], for particles of the same parity, strangeness and isospin. These come out to be approximately linear for all plots, so if $\alpha(t)$ defines the equation of the linear plot, $\alpha(t) = \alpha_0 + \alpha' t$ with $\alpha(M_J^2) = J$, where J is the spin of a particle of mass M_J. The exchanged poles may therefore be thought of as 'moving', with a generalized spin $\alpha(t)$, and the amplitude in the negative t region is generalized to $T \sim (1 \pm e^{-i\pi\alpha(t)}) \frac{s^{\alpha(t)}}{\sin \pi\alpha(t)}$. Hence, the 'moving' or Regge pole model gives $\left.\frac{d\sigma}{dt}\right|_{t=0}(\text{theory}) \sim s^{2\alpha(t)-2}$. Thus, by choosing $\alpha_0 \approx 0$ for pseudoscalar exchange, $\left.\frac{d\sigma}{dt}\right|_{t=0} \sim s^{-2}$ still and $\alpha_0 \approx \frac{1}{2}$ for vector exchange, $\left.\frac{d\sigma}{dt}\right|_{t=0} \sim s^{-1}$, so solving the s-dependence problem.

In the Regge pole model, the necessity for placing the coupling constants of the Reggeons, or exchanged Regge poles, within a symmetry scheme exists as in the fixed pole model.

Up to now, we have not discussed the t-dependence of the differential cross-sections predicted by pole models. This is poor with, in general, not enough damping at increasing $|t|$. However, this can be overcome in the Regge pole model by the use of the t-dependent spin together with a residue function which is taken to be a function of t. However, similarly to the fixed pole model, no forward peaking is obtained for pseudoscalar exchange. Hence, there are good reasons why cuts, as generated by the absorption model, should be used to correct the momentum transfer dependence rather than a t-dependent residue. These are:

(1) That for elastic scattering at increasing energies, more and more inelastic channels become accessible as required by unitarity. Thus,

as far as the elastic channel is concerned, absorption (or loss) of a particle occurs. This will tend to occur more at low partial waves, or small impact parameters where the force is stronger, and leave the high energy scattering dominated by high partial waves, as indicated by the impact parameter representation[5].

A similar idea exists for inelastic scattering with particles being absorbed out of a channel containing the incident particles into another one.

(2) That in some reactions where only one known pole can be exchanged (e.g. the ρ pole in πN charge-exchange scattering) or where a pair of exchange degenerate poles are exchanged (e.g. the ρ and A_2 poles in $\bar{K}N$ charge-exchange scattering or the $K^*(890)$ and $K_N(1420)$ poles in $\pi^+ p \to K^+ \Sigma^+$), a non-zero polarization exists[6,7,8,9]. As polarization is proportional to $Im(\phi_1 \phi_2^*)$ where ϕ_1 and ϕ_2 are the two independent $0^-\frac{1}{2}^+$ s-channel helicity amplitudes defined by $\phi_1 = \langle \frac{1}{2}0 | \phi | \frac{1}{2}0 \rangle$, $\phi_2 = \langle \frac{1}{2}0 | \phi | -\frac{1}{2}0 \rangle$, a single-pole or a pair of exchange-degenerate poles exchanged predicts zero polarization for all scattering angles.

However, in πN charge-exchange scattering where polarization data exists, it turns out to be small and positive at small $|t|$. Previous explanations of this have used an unsubstantiated pole, the ρ', but recent experimental tests searching for this pole have shown that if it exists, it has a very small coupling constant[10].

(3) That for pion exchange reactions where a pion peak of width $\sim m_\pi^2$ and slope $\sim e^{50t}$ occurs, the conservation of angular momentum leads to an evasive pole i.e. goes to zero in the forward direction, t=0. A proposed solution to this problem, not involving cuts, was conspiracies.

To see how these worked, consider, for example, pn charge-exchange scattering[11]. Here, quantum numbers allow the pion to contribute to the s-channel helicity amplitudes,

$$\phi_2 = \langle \tfrac{1}{2}\tfrac{1}{2} | \phi | -\tfrac{1}{2} -\tfrac{1}{2} \rangle \quad , \quad \phi_4 = \langle \tfrac{1}{2} -\tfrac{1}{2} | \phi | -\tfrac{1}{2}\tfrac{1}{2} \rangle$$

with the pion contribution such that $\phi_2^{\pi} = \phi_4^{\pi}$. As ϕ_4 is a helicity flip amplitude, the conservation of angular momentum implies $\phi_4(t=0) = 0$. Hence, $\phi_2^{\pi}(t=0) = \phi_4^{\pi}(t=0) = 0$.

Defining the pion conspirator, π^c, as the parity doublet of the pion, positive parity gives $\phi_2^{\pi^c} = -\phi_4^{\pi^c}$. Hence $\phi_2 = \phi_2^{\pi} + \phi_2^{\pi^c} + \dots$ and $\phi_4 = \phi_4^{\pi} + \phi_4^{\pi^c} + \dots = \phi_2^{\pi} - \phi_2^{\pi^c} + \dots$. Hence, by putting $\phi_2^{\pi} = \phi_2^{\pi^c}$, $\phi_4 = 0$ to agree with angular momentum conservation, but the part of ϕ_2 associated with the pion does not vanish and so the forward peak is obtained.

The undesirable effects of conspiracies are, firstly, that no known meson exists of the required mass and parity. Secondly, Le Bellac[12] showed that while experimentally, the reactions $\pi N \to \rho \Delta$, $K N \to K^* \Delta$ and $\pi N \to f^0 \Delta$ exhibit peaks, conspiracies predict dips in the forward direction.

The absorption model solves the peaking problem in the following manner. As before, the rotation functions ensure the flip amplitudes such as ϕ_4 in pn charge-exchange scattering remain equal to zero in the forward direction. However, as ϕ_2 , in this reaction, is non-flip, the rotation function does not put this amplitude equal to zero. Now,

$$\phi_2^{\pi} \sim \frac{t}{t - m_\pi^2} \quad \text{for } t \text{ small}$$
$$= 1 + \frac{m_\pi^2}{t - m_\pi^2}$$

The first term is the high energy limit of the s-wave term $P_0(\cos\theta)$ and so violates unitarity at high energies. Absorption has the effect such that ϕ_2^{π} (absorbed) $\sim \frac{m_\pi^2}{t-m_\pi^2}$ i.e. takes out the s-wave term, so allowing a forward peak.

(4) That the behaviour of total cross sections at energies which have now become available through the advent of the Serpukov accelerator which can give results up to 70 GeV/c for negative pion and kaon beams. Barger and Phillips have shown that for $\pi^- p$ and $K^- p$ elastic scattering[13], the Regge pole graph does not explain the flattening of the total cross sections at high energy and so to explain the data, cuts are introduced.

(5) That cross-over effects, which might be due to zeros in pole residues e.g. the ω in $K^{\pm} p$ elastic scattering and NN and $N\bar{N}$ elastic scattering, do not appear to be consistent with factorization of the residues of the poles[14]. Returning to the example of the vanishing of the ω in NN and $N\bar{N}$ elastic scattering to explain the 'crossover' effect, factorization gives $\beta_\omega = [\beta_{\omega NN}]^2$ up to a sign. However, in a reaction such as $\pi N \to \rho^0 N$ which has a contribution from ω exchange, factorization gives $\beta_\omega = \beta_{\pi\rho\omega}\,\beta_{\omega NN}$ which makes the ω exchange amplitude of $\pi N \to \rho^0 N$ vanish at the cross-over point of NN and $N\bar{N}$ elastic scattering. No such dip exists in the experimental data.

The remedy is to use the destructive interference between the absorption cut and, say, the ω to generate the required zero at the cross-over point.

(6) That in Regge amplitudes, which use the nonsense choosing ghost-killing mechanism as predicted by the Veneziano model, zeros occur which are not present in the data. However, dips which do not go to zero exist at these points[15]. Hence, cuts are required to fill in these nonsense dips.

(7) That elastic $p\,\bar{p}$ scattering has an expanding rather than a shrinking diffractive peak. Cuts are required to explain this[16].

(8) That, besides the problem of the forward peak, $pn \to np$ and $p\bar{p} \to n\bar{n}$ are difficult to reconcile in just pole models.[16]

Hence, we have a motivation for using a Reggeized absorption model with couplings related by a higher symmetry scheme in an attempt to explain the features of forward scattering data.

CHAPTER 2. THE REGGE FORMALISM

2.1 Introduction.

As discussed in chapter 1, a Regge form is necessary for the pole graph in order to get the correct s-dependence of two-body meson-baryon cross-sections. It was also indicated that the couplings ought to be incorporated within a symmetry scheme, so that the amplitudes for various exchanges in a given process are inter-related as are the various processes. The fact that the known baryon and meson particle spectrum is given correctly by the lower SU(6) multiplets was used as a motivation by Watson et al[3] who used a fixed pole model with couplings inter-related by the relativistic generalization of U(6), U(6,6). This has the advantage over SU(3) that processes involving different baryon and meson vertices simultaneously can be inter-related although it is of course more badly broken. However, in this model only mesons lying in $(6,\bar{6},0)$ [notation is such that $(6,\bar{6})$ describes the U(6) ⊗ U(6) (the rest symmetry of U(6,6)) multiplet containing the SU(3) meson 0^- octet and 1^- nonet, and the '0' is the Casimir of O(3) describing the lowest angular momentum excitation] could be exchanged. In order to incorporate such reactions as $\pi^- p \to \eta n$ where there is only 2^+ exchange, within this model, it is necessary to include higher multiplets of U(6,6) or U(6) ⊗ U(6) ⊗ O(3).

The SU(3) 2^+ nonet containing such particles as the A_2 and the $K_N(1420)$ lie in the U(6,6) 4212 multiplet or the $(6,\bar{6};1)$ U(6) ⊗ U(6) ⊗ O(3) multiplet. Hence, there are two methods of incorporating higher spin exchanges into the model. These are either

using higher U(6,6) multiplets or higher $U(6) \otimes U(6) \otimes O(3)$ multiplets i.e. $(6,\bar{6},N)$, N = 0,1,2.. The latter method of using O(3) excitations is preferable as here, only J^P is altered and hypercharge and isospin is left unaltered so avoiding exotic mesons. This latter approach was used successfully by Shafi[17] in explaining $2^+, 1^+$ and 0^+ decay rates and by Delbourgo et al.[18] in a Regge pole model.

Taking these arguments into account leads us to use a Reggeized U(6) ⊗ U(6) ⊗ O(3) model to construct the pole graph s-channel helicity amplitudes, which provide the most convenient form for introducing absorptive cuts.

2.2. U(6) ⊗ U(6) ⊗ O(3) Fields[18,19]

The basic representation of U(6,6) is the 'quark' representation of dimensionality 12. However, this corresponds to no known physical particles. Thus we have to construct higher irreducible representations of U(6,6) in order to include physical particle fields.

The lowest meson fields are constructed out of the product of quark and anti-quark:

$$\underline{12} \otimes \underline{\bar{12}} = \underline{1} \oplus \underline{143} \qquad (2.1)$$

where the $\underline{143}$ is the traceless meson field which reduces to $(6,\bar{6})$ under the rest group U(6) ⊗ U(6) decomposition.

Similarly, the lowest baryon fields are given by the product of three quarks:

$$\underline{12} \otimes \underline{12} \otimes \underline{12} = \underline{220} \oplus \underline{364} \oplus \underline{572} \oplus \underline{572} \qquad (2.2)$$

where the fully symmetric field 364 reduces to (56,1) under the U(6) ⊗ U(6) decomposition.

The SU(3) composition of these fields can be seen under SU(3) ⊗ $\mathcal{U}_4 u(2,2)$ decomposition

$$\underline{143} = (8,15) \oplus (1,15) \oplus (8,1) \tag{2.3}$$

$$\underline{364} = (10,20) \oplus (8,20) \oplus (1,4) \tag{2.4}$$

(2.3) shows that the 143 contains the SU(3) 0^- octet and 1^- nonet, while (2.4) shows that the 364 contains the $\frac{1}{2}^+$ octet and $\frac{3}{2}^+$ decuplet.

As SU(3) can relate mesons among themselves and also baryons among themselves for a given $(J)^P$, a sensible decomposition is U(6,6) ⊃ U(2,2) ⊗ SU(3). Under this decomposition, the 144 generators of U(6,6) are:

$$(\gamma_R T^i)^B_A \qquad \text{where } A,B = 1 \ldots 12, \tag{2.5}$$

$\gamma_R = 1, \gamma_\mu, i\gamma_\mu\gamma_5, \gamma_5, \frac{1}{2}\sigma_{\mu\nu}$, $R = 1 \ldots 16$ are the sixteen Dirac matrices forming the generators of U(2,2), and $T^i = \frac{1}{2}\lambda^i$, where the λ^i are the nine Gell'Mann matrices forming the generators of SU(3).

The traceless 143 meson field is constructed as follows :

$$\Phi^B_A(P) = (\gamma_R T^i)^B_A \, \phi^i_R(P) \tag{2.6}$$

where the $\phi^i_R(P)$ are the free particle meson fields of momentum P and mass μ. The U(6,6) fields satisfy the Bargmann-Wigner equations :

$$(P-\mu)^A_C \, \Phi^B_A(P) = \Phi^B_A(P) \, (P+\mu)^C_B = 0 \; ; \tag{2.7}$$

$$P^A_c = P_\alpha \delta^a_c .$$

and taking the fields 'on-shell' gives

$$p^2 \bar{\Phi}_A^B(p) = \mu^2 \bar{\Phi}_A^B(p) \tag{2.8}$$

(2.7) and (2.8) give:

$$\phi^i(p) = 0$$

$$i p_\mu \phi^i_{\mu 5}(p) = \mu \phi^i_5(p), \qquad i\mu \phi^i_{\mu 5}(p) = p_\mu \phi^i_5(p)$$

$$i p_\mu \phi^i_{\mu\nu}(p) = \mu \phi^i_\nu(p), \qquad i\mu \phi^i_{\mu\nu}(p) = p_\mu \phi^i_\nu(p) - p_\nu \phi^i_\mu(p) \tag{2.9}$$

Using (2.9) and the equation of continuity for a vector field

$$p_\mu \phi^i_\mu(p) = 0 \tag{2.10}$$

gives

$$\bar{\Phi}_A^B(p) = \frac{1}{2\mu}\left[(\not{p} + \mu)(\gamma_\mu \phi_\mu(p) - \gamma_5 \phi_5(p))\right]_A^B \tag{2.11}$$

where $\not{p} = p_\mu \gamma_\mu$ and $\phi_\mu(p)$, $\phi_5(p)$ are the free particle fields corresponding to the SU(3) 1^- nonet and 0^- nonet respectively.

Similarly, the symmetric (56,1) decomposition is

$$\begin{aligned} u_{(ABC)}(p) = \varepsilon_{abc}\Big[& C_{\alpha\beta} V'_\gamma + (\gamma_5 C)_{\alpha\beta} V_\gamma + (i\gamma_\mu \gamma_5 C)_{\alpha\beta} \\ & V_{\mu\gamma} \Big] + (\gamma_\mu C)_{\alpha\beta} D_{\mu\gamma(abc)} + \tfrac{1}{2}(\sigma_{\mu\nu} C)_{\alpha\beta} D_{\mu\nu\gamma(abc)} \\ & + \Big[\varepsilon_{abd}\Big\{ C_{\alpha\beta} N'^d_{\gamma c} + (\gamma_5 C)_{\alpha\beta} N^d_{\gamma c} + (i\gamma_\mu \gamma_5 C)_{\alpha\beta} \\ & N^d_{\mu\gamma c}\Big\} + \text{cyclic permutations}\Big] \end{aligned} \tag{2.12}$$

where $\alpha, \beta, \gamma = 1, \ldots 4$ are the U(2,2) labels, a,b,c,d = 1,2,3 are the

SU(3) labels, and $C_{\alpha\beta}$ is the charge conjugation matrix. Also
$V=\gamma_5 V'$, $V_\mu = -i\gamma_\mu^{\alpha\beta}\gamma_5 V$, $N' = \gamma_5 N + i\gamma_5\gamma_\mu N_\mu$, $\gamma_\mu D_\mu = 0$

Applying the Bargmann-Wigner equation to (2.12)

$$(P-m)_D^A \, U_{(ABC)}(P) = 0 \tag{2.13}$$

gives

$$V = 0$$

$$imN_\mu(P) = P_\mu N(P), \quad imD_{\mu\nu}(P) = P_\mu D_\nu(P) - P_\nu D_\mu(P) \tag{2.14}$$

leading to

$$U_{(ABC)}(P) = \frac{1}{2\sqrt{6}m}\Big[\{(\not{P}+m)\gamma_5 C\}_{\alpha\beta}\varepsilon_{abd}N_c^d{}_\gamma + \text{cyclic permutations} + 3\{(\not{P}+m)\gamma_\mu C\}_{\alpha\beta} D_{\mu\gamma(abc)}\Big] \tag{2.15}$$

where $N_{c\gamma}^{d} = N_\gamma^i (T^i)_c^d$

with N_μ^i and $D_{\mu\gamma}$ are the free particle fields corresponding to the SU(3) $\frac{1}{2}^+$ octet and $\frac{3}{2}^+$ decuplet respectively.

(2.11) and (2.15) correspond respectively to $(6,\bar{6};0)$ and $(56,1;0)$ multiplets respectively in $U(6) \otimes U(6) \otimes O(3)$. To construct higher O(3) multiplets we take note of the fact that experimentally $(6,\bar{6};N)$, N = 0,1, occur and $(56,1;N)$, N = 0,2... occur in nature. Also, the knowledge that the 2^+ fields etc. which lie in $(6,\bar{6};1)$ are of the form $\phi^i_{(\mu\nu)}(P)$ suggests that the fields for $O_N(3)$, N = 0,1,2.... are of the form $\phi^i_{(\mu_1\cdots\mu_N)}(P)$. These are symmetric, but not traceless in their indices

and satisfy conditions

$$p_{\mu_i}\,\phi^{(p)}_{(\mu_1\cdots\mu_i\cdots\mu_N)} = 0$$
$$p^2\,\phi^{(p)}_{(\mu_1\cdots\mu_N)} = \mu^2\,\phi^{(p)}_{(\mu_1\cdots\mu_N)} \qquad (2.16)$$

Hence, the field for $(6,\bar{6};N)$ is

$$\Phi^{B\,(p)}_{A(\mu_1\cdots\mu_N)} = \frac{1}{2\mu}\left[(\not{p}+\mu)(\gamma_\mu\,\phi^{(p)}_{\mu(\mu_1\cdots\mu_N)} - \gamma_5\,\phi^{(p)}_{(\mu_1\cdots\mu_N)})\right]^B_A \qquad (2.17)$$

and for $(56,1;2N)$,

$$u^{(p)}_{(ABC)(\mu_1\cdots\mu_{2N})} = \frac{1}{2\sqrt{6}\,m}\Big[\{(\not{p}+m)\gamma_5 C\}_{\alpha\beta}\,\varepsilon_{abd}\,N^{d}_{c\gamma(\mu_1\cdots\mu_{2N})} \qquad (2.18)$$
$$+ \text{cyclic permutations} + 3\{(\not{p}+m)\gamma_\mu C\}_{\alpha\beta}$$
$$D_{\mu\gamma(abc)(\mu_1\cdots\mu_{2N})}\Big]$$

2.3. Three-point Functions.

The present state of experiments enable us to carry out essentially two types of two-body scattering. These are $0^-\tfrac{1}{2}^+ \to \ldots$ and $\tfrac{1}{2}^+\tfrac{1}{2}^+ \to \ldots$ using J^P notation, with the 0^- lying in $(6,\bar{6};0)$ and the $\tfrac{1}{2}^+$ in the $(56,1;0)$. As we are interested in $0^-\tfrac{1}{2}^+ \to 0^-\tfrac{1}{2}^+$, we need to compute two three-point functions for forward scattering invariant under the subgroup $U(6) \otimes O(2)$

(a) $(6,\bar{6};0)_{p_2} - (\bar{6},6;0)_{p_4} - (6,\bar{6};N)_{p_4-p_2}$

(b) $(56,1;0)_{p_1} - (\bar{56},1;0)_{p_3} - (6,\bar{6};N)_{p_3-p_1}$

where the subscripts specify the field momenta.

The Lagrangians are computed by carrying out the SU(6) decomposition of the $U(6) \otimes U(6) \otimes O(3)$ multiplets giving

$$(6,\bar{6};0) = \underline{1} \oplus \underline{35} \tag{2.19a}$$

$$(56,1;0) = \underline{56} \tag{2.19b}$$

The decomposition for $(6,\bar{6};N)$ is the same as (2.19a) but with the appropriate excitation labels on the fields. The construction of the Lagrangians is carried out explicitly as follows :

(a) The two external multiplets give

$$(\underline{1} \oplus \underline{35}) \otimes (\underline{1} \oplus \underline{35}) \tag{2.20}$$

of which we want the $\underline{35}$ or $\underline{1}$ multiplets as these lie in $(6,\bar{6};N)$

$$\underline{1} \otimes \underline{1} = \underline{1} \tag{2.21}$$

$$\underline{35} \otimes \underline{1} = \underline{35} \tag{2.22}$$

$$\underline{1} \otimes \underline{35} = \underline{35} \tag{2.23}$$

$$\underline{35} \otimes \underline{35} = \cdots \oplus 2 \times \underline{35} \oplus \underline{1} \tag{2.24}$$

The fields for the singlet are given by contracting the momentum tensor $\frac{1}{2}(P_2+P_4)_A^B = \frac{1}{2}(P_2+P_4)_\alpha^\beta \delta_a^b$ on the U(6,6) fields, i.e. taking the trace of the SU(3) labels. Thus the couplings for (2.21) and the singlet of (2.24) are given by

$$h_0^{(-)} \frac{\mu^{-(2+N)}}{2^{N+3}} P_A^{'B} \bar{\Phi}_B^A(P_2) P_C^{'D} \bar{\Phi}_D^C(-P_4) P'_{\mu_1} \cdots P'_{\mu_N} P_E^{'F} \bar{\Phi}_{F(\mu_1\cdots\mu_N)}^E(P_4-P_2) \tag{2.25}$$

and

$$h_0^{(-)} \frac{\mu^{-N}}{2^{N+1}} \bar{\Phi}_A^B(P_2) \bar{\Phi}_B^A(-P_4) P'_{\mu_1} \cdots P'_{\mu_N} P_{\bar{E}}^{'F} \bar{\Phi}_{F(\mu_1\cdots\mu_N)}^{\bar{E}}(P_4-P_2) \tag{2.26}$$

respectively where μ is a mass associated with the vertex and $P' = (P_2+P_4)$ and we have saturated the O(3) labels by momentum tensors to give the correct s-dependence in the T-matrix. The superscript (-) on the coupling constants satisfies the Bose requirement that the term is only non-zero for N odd and vice versa for (+).

From the four 35's constructed in (2.22) to (2.24) we want an even and odd signature Regge pole eventually. Such a requirement is met by the two couplings

$$h_1^{(+)} \frac{\mu^{1-N}}{2^N}\left[\bar{\Phi}_A^B(p_2)\,\bar{\Phi}_B^C(-p_4) + \bar{\Phi}_A^B(-p_4)\,\bar{\Phi}_B^C(p_2)\right] p'_{r_1}\cdots p'_{r_N} \bar{\Phi}_{C(r_1\cdots r_N)}^{A}(p_4-p_2) \tag{2.27}$$

and

$$h_1^{(-)} \frac{\mu^{1-N}}{2^N}\left[\bar{\Phi}_A^B(p_2)\,\bar{\Phi}_B^C(-p_4) - \bar{\Phi}_A^B(-p_4)\,\bar{\Phi}_B^C(p_2)\right] p'_{r_1}\cdots p'_{r_N} \bar{\Phi}_{C(r_1\cdots r_N)}^{A}(p_4-p_2) \tag{2.28}$$

where h_1's couple to both $\underline{1}$ and $\underline{35}$.

Hence the effective Lagrangian is

$$\begin{aligned}\mathcal{L}_{(a)} = \frac{\mu^{-N}}{2^{N+1}}\bar{\Phi}_A^B(p_2)\bar{\Phi}_C^D(-p_4)\Big[& h_0^{(-)}\delta_B^C\delta_D^A + h_0'^{(-)}\frac{\mu^{-2}}{4}p'^A_B\,p'^C_D \\ & + 2\mu\, h_1^{(+)}\left(\delta_B^C\frac{\partial}{\partial p'^D_A} + \delta_D^A\frac{\partial}{\partial p'^B_C}\right) \\ & + 2\mu\, h_1^{(-)}\left(\delta_B^C\frac{\partial}{\partial p'^D_A} - \delta_D^A\frac{\partial}{\partial p'^B_C}\right)\Big]\bar{\Phi}_{(N)}(p_2,p_4)\end{aligned} \tag{2.29}$$

where $\bar{\Phi}_{(N)}(p_2;\,p_4)$ is the fully contracted $(6,\bar{6};N)$ field and is given by

$$\Phi_{(N)}(P_2,P_4) = P'_{\mu_1} \cdots P'_{\mu_N} P'^{B}_{A} \bar{\Phi}^{A}_{B(\mu_1 \cdots \mu_N)}(P_4 - P_2) \qquad (2.30)$$

(b) Here, the two external multiplets give:

$$\underline{56} \otimes \underline{56} \qquad (2.31)$$

from which we want $\underline{35}$ or $\underline{1}$. We get

$$\underline{56} \otimes \underline{56} = \cdots \oplus \underline{35} \oplus \underline{1} \qquad (2.32)$$

Carrying out the arguments as in (a), we get the effective Lagrangian to be:

$$\mathcal{L}_{(b)} = \frac{m^{-(N+1)}}{2^{N+1}} \bar{u}^{(ACD)}(P_3) U_{(BCD)}(P_1) \left[g_0 \delta^{B}_{A} + 2m g_1 \frac{\partial}{\partial P^{A}_{B}} \right] \Phi_{(N)}(P_1,P_3) \qquad (2.33)$$

where m is a mass associated with vertex b and $P = (P_1+P_3)$.

From now on, as we are only interested in $O^{-\frac{1}{2}+}$ hypercharge and charge-exchange scattering, we will neglect $h_0^{(-)}$, $h_0'^{(-)}$ and g_0.

2.4 Supermultiplet Propagators

To construct propagators corresponding to the exchange of a $(6,\bar{6};N)$ supermultiplet, the following heuristic argument is used.

The propagator for two fields with one orbital label each is the vacuum expectation value :

$$\langle \phi^{i}_{\mu}(P)\, \phi^{j}_{\nu}(-P) \rangle = \frac{\delta_{ij}}{P^2 - M^2} \left(-g_{\mu\nu} + \frac{P_\mu P_\nu}{M^2} \right) \qquad (2.34)$$

where M is a mass associated with the fields.

Generalizing to the $[N]$ representation of O(3) gives:

$$\langle \phi^{i}_{(\mu_1\cdots\mu_N)}(p)\,\phi^{j}_{(\mu_1'\cdots\mu_N')}(-p)\rangle = \frac{\delta^{ij}}{p^2-M^2}\sum_{\mu_1\mu_1'}\left(-g_{\mu_1\mu_1'}+\frac{p_{\mu_1}p_{\mu_1'}}{M^2}\right)\cdots\cdots\left(-g_{\mu_N\mu_N'}+\frac{p_{\mu_N}p_{\mu_N'}}{M^2}\right) \tag{2.35}$$

The propagator for $(6,\bar{6};0)$ is constructed using the Bargmann-Wigner Equations for the fields:

$$(p-M)^{A}_{D}\,\bar{\Phi}_{A}^{B}(p) = \bar{\Phi}_{A}^{B}(p)\,(p+M)_{B}^{D} = 0 \tag{2.36}$$

and the 'on-shell'condition:

$$p^2\,\bar{\Phi}_{A}^{B}(p) = M^2\,\bar{\Phi}_{A}^{B}(p) \tag{2.37}$$

A propagator satisfying these conditions is

$$\langle \bar{\Phi}_{A}^{B}(p)\,\bar{\Phi}_{B'}^{A'}(-p)\rangle = \frac{(M+p)_{A}^{A'}(M-p)_{B'}^{B}}{4M^2(p^2-M^2)} \tag{2.38}$$

Combining (2.35) and (2.38) heuristically, we have for $(6,\bar{6};N)$ exchange

$$\langle \bar{\Phi}^{B}_{A\,(\mu_1\cdots\mu_N)}(p)\,\bar{\Phi}^{A'}_{B'\,(\mu_1'\cdots\mu_N')}(-p)\rangle = \sum_{\mu_1\mu_1'}\left(-g_{\mu_1\mu_1'}+\frac{p_{\mu_1}p_{\mu_1'}}{M^2}\right)\cdots\cdots \left(-g_{\mu_N\mu_N'}+\frac{p_{\mu_N}p_{\mu_N'}}{M^2}\right)\frac{(M+p)_{A}^{A'}(M-p)_{B'}^{B}}{4M^2(p^2-M^2)} \tag{2.39}$$

In the case which we wish to consider (2.30) and (2.33) imply that we need to know the fully contracted supermultiplet propagator

$$\Delta_{(N)} = \frac{1}{2^{2(N+1)}}\langle \bar{\Phi}_{(N)}(-q')\,\bar{\Phi}_{(N)}(-q)\rangle, \tag{2.40}$$

$$q = p_1-p_3,\quad q' = p_2-p_4$$

This is

$$\Delta_{(N)} = \left(-\frac{p.p'}{4}\right)^{N+1} \frac{1}{t-M^2} \tag{2.41}$$

$$= \left(\frac{p.p'}{4}\right)^{N+1} \frac{(\cos\theta)^{N+1}}{t-M^2} \tag{2.42}$$

for pair-wise equal mass kinematics where θ is the angle between $(\underline{P}')$ and $(\underline{P})$.

In (2.42), $(\cos\theta)^N$ is the rotation function $d^N_{[1][1]}(\theta)$ for the U(3) representation of the supersinglet exchange, and $\cos\theta$ is a spin factor coming from the U(6,6) rotation function $d^{(6,\bar{6})}_{[1][1]}(\theta)$. The generalized rotation function $d^N_{[w][w']}(\theta)\; d^{(6,\bar{6})}_{[w][w']}(\theta)$ is obtained by differentiation. Specifically, we are interested in

$$4\frac{\partial^2}{\partial p^{\beta}_{A}\,\partial p'^{A'}_{B'}}\Delta_{(N)} = \left(\frac{p.p'}{4}\right)^{N} \frac{(M-q)^{B'}_{\beta}(M+q)^{A}_{A'}}{4M^2(t-M^2)} \tag{2.43}$$

2.5. The Reggeized Invariant Amplitudes for $0^{\frac{-1}{2}+}$ Hypercharge and Charge-Exchange Scattering

The covariant T-matrix is constructed according to the usual rules such that :

$$T = \langle p_3 p_4 | T\,(\mathcal{L}_{(a)}\,\mathcal{L}_{(b)}) | p_1 p_2 \rangle \quad \text{up to a } \delta\text{-function} \tag{2.44}$$

$$= D_p\, D_{p'}\, \Delta_{(N)} \tag{2.45}$$

where the D's are differential operators depending on the external quantum numbers at the respected vertices. Using (2.31) and (2.35) gives for $0^{-}\tfrac{1}{2}^{+}$ charge-exchange scattering:

$$T = \frac{m\mu^2}{(m+\mu)^{N+1}}\,\bar{u}^{(ACD)}_{(P_3)}\,u^{(P_1)}_{(BCD)}\,g_1\Big\{h_1^{(+)}\Big\{\bar{\Phi}(P_2),\bar{\Phi}(-P_4)\Big\}^{A'}_{B'} + h_1^{(-)}\big[\bar{\Phi}(P_2),\bar{\Phi}(-P_4)\big]^{A'}_{B'}\Big\}\,4\frac{\partial^2}{\partial P_B^A\,\partial P'^{A'}_{B'}}\,\Delta_{(N)}$$

$$= \frac{g_1\mu}{t-M^2}\left(\frac{P\cdot P'}{4mP}\right)^N \bar{u}\,\Gamma_-\Big\{h_1^{(+)}\Big\{\bar{\Phi},\bar{\Phi}\Big\} + h_1^{(-)}\big[\bar{\Phi},\bar{\Phi}\big]\Big\}\,\Gamma_+\,u \tag{2.46}$$

using (2.43) and where

$$\left(\Gamma_\pm\right)^B_A = \frac{(M\pm q\!\!\!/)^B_A}{2M} \tag{2.47}$$

where $q = P_1 - P_3$. Carrying out the decomposition of the U(6,6) meson tensors with respect to U(2,2) ⊗ SU(3) as shown in (2.11), extracting the pseudoscalar part., and noting that :

$$2\{\,,\}_{u(6,6)} = \{\,,\}_{u(2,2)}(,)_D + [\,,]_{u(2,2)}(,)_F \tag{2.48}$$

and

$$2[\,,]_{u(6,6)} = [\,,]_{u(2,2)}(,)_D + \{\,,\}_{u(2,2)}(,)_F \tag{2.49}$$

where $(\,,\,)_D$ and $(\,,\,)_F$ are the SU(3) anticommutators and commutators respectively

and are given by

$$(\phi_5, \phi_5)_F = [\phi_5, \phi_5]_a^b \tag{2.50}$$

$$(\phi_5, \phi_5)_D = \{\phi_5, \phi_5\}_a^b \tag{2.51}$$

with the extra tensor being implied by (2.38), we obtain

$$T = -g_1 \frac{M}{t-M^2} \left(\frac{p\cdot p'}{4mp}\right)^N \bar{u} \left(\frac{\not{p} - \not{p}' \not{p}}{2p}\right) u$$
$$\left[h_1^{(+)}(\phi_5, \phi_5)_F + h_1^{(-)}(\phi_5, \phi_5)_D\right]\left(1 + \frac{M}{2p}\right) \tag{2.52}$$

Similarly, carrying out the U(2,2) ⊗ SU(3) decomposition of the (56,1;0) fields as in (2.15) and extracting the $\frac{1}{2}^+$ octet part, gives

$$T = \frac{g_1}{t-M^2} \frac{1}{2}\sqrt{\frac{3}{2}}\, p \left(\frac{p\cdot p'}{4mp}\right)^N \left(1 + \frac{2m}{M}\right)\left(1 + \frac{M}{2p}\right)$$
$$\left\{\left(\frac{p\cdot p'}{4mp}\right)\left[(\bar{N}, N)_D + \left(\frac{2}{3} - \frac{M}{2m}\right)(\bar{N} N)_F\right] + \frac{1}{2p}\right.$$
$$\left.\left(1 - \frac{M^2}{4m^2}\right)(\bar{N} \not{p}' N)_{D+\frac{2}{3}F}\right\}\left\{h_1^{(+)}(\phi_5, \phi_5)_F\right. \tag{2.53}$$
$$\left. + h_1^{(-)}(\phi_5, \phi_5)_D\right\}$$

To Reggeize (2.53), we use a first-order Taylor expansion about the pole, $t = M^2$, and obtain

$$\frac{1}{t-M^2} = \pm \left.\frac{d\alpha}{dt}\right|_{t=M^2} \Gamma(\alpha)\Gamma(1-\alpha) \tag{2.54}$$

where the + or − depends on the spin of the exchange. We also let

$$N \longrightarrow \alpha - 1 \tag{2.55}$$

and extract out of $h^{(\pm)}$ the signature factors $\frac{1}{2}\left(1 \mp e^{-i\pi\alpha}\right)$ whose

presence is required to remove wrong signature poles as demanded by the presence of exchange forces.

To remove the nonsense poles at $\alpha = -1, -3, \ldots$ for $h^{(+)}$ and $\alpha = 0, -2, \ldots$ for $h^{(-)}$ we need a 'ghost-killing' mechanism or else we have the violation of the conservation of angular momentum at these points. To show how this is done in $0^{-}\tfrac{1}{2}^{+}$ scattering[11], consider, for example, the pole at $\alpha = 0$ in $h^{(-)}$. (We shall carry out the same mathematical operation on $h^{(+)}$ so that a nonsense dip is created in this contribution). The non-flip amplitude is a sense-sense one (no net helicity flip at both t-channel vertices) while the flip amplitude is sense-nonsense (helicity flip at the baryon vertex). Every nonsense vertex introduces a $\sqrt{\alpha}$, so to overcome branch points and to conserve angular momentum, a factor of α is introduced in the sense-sense amplitude and a factor of $\sqrt{\alpha}$ in the sense nonsense amplitude. This is repeated at poles $\alpha = -j$ by replacing α in the above argument by $(\alpha + j)$.

Thus to remove all 'ghosts' and to create nonsense zeros at the alternate integers in α, we use the 'Gell-Mann ghost killing mechanism' and divide the T-matrix by $\Gamma(\alpha)$.

Hence, the Reggeized T-matrix is

$$
\begin{aligned}
T = \left(1+\frac{M}{2\mu}\right)\left(1+\frac{2m}{M}\right)\Bigg\{ & -\left(\frac{s+\frac{t}{2}-m^2-\mu^2}{2m\mu}\right)\Big[(\bar{N},N)_D \\
& +\left(\frac{2}{3}-\frac{M}{2m}\right)(\bar{N},N)_F\Big] + \frac{1}{2\mu}\left(1-\frac{M^2}{4m^2}\right)(\bar{N}\not{q}\,'N)_{D+\frac{2}{3}F}\Bigg\} \\
& \Bigg\{ \beta_- \Gamma(1-\alpha_-)\left(1-e^{-i\pi\alpha_-}\right) h_F \left(\frac{s+\frac{t}{2}-m^2-\mu^2}{2m\mu}\right)^{\alpha_- -1} \\
& + \beta_+ \Gamma(1-\alpha_+)\left(1+e^{-i\pi\alpha_+}\right) h_D \left(\frac{s+\frac{t}{2}-m^2-\mu^2}{2m\mu}\right)^{\alpha_+ -1}\Bigg\}
\end{aligned}
$$

(2.56)

where the exchange degeneracy of $\alpha_\pm$ has been broken and the meson tensors dropped as they are just equal to unity and

$$\beta_\pm = \frac{g_1 L_1^{(F)} \sqrt{6}}{8} \mu (-1)^N \left. \frac{d\alpha}{dt} \right|_{t=M^2} \qquad (2.57)$$

As (2.56) was evaluated at $t = M^2$, M must be replaced by $\sqrt{t}$ in here; so leading to a branch point at $t = 0$ on the edge of the physical region.

A solution to this problem was suggested by Gribov[20], where for $t \leq 0$, a conjugate conspiring trajectory is introduced. Thus, using the natural doubling afforded by quarks and pseudoquarks within a multispinor framework, we consider for mesons two trajectories corresponding to $(6,\bar{6})$ and $(\bar{6},6)'$ where the prime indicates a pseudoquark composite. By analogy with Macdowell symmetry for fermions, the $(\bar{6},6)'$ has terms with $\sqrt{t} \to -\sqrt{t}$.

Taking the total T-matrix as

$$T = \frac{1}{2}\left(T(6,\bar{6}) + T(\bar{6},6)' \right) \qquad (2.58)$$

to remove the singularity, we need $\alpha_\pm(0) = \alpha_\pm'(0)$ and $\beta_\pm(0) = \beta_\pm'(0)$ By analogy with fermions, it is speculated that for small t,

$$\alpha_\pm(t) = \alpha_\pm'(t) \quad , \quad \beta_\pm(t) = \beta_\pm'(t) = \text{constant} \qquad (2.59)$$

In (2.56), the 'N' spinors have both U(2,2) and SU(3) labels. However, the brackets around them imply SU(3) traces, so the SU(3) labels are completely saturated leaving the 'N' spinors to be treated as Dirac spinors.

Defining the covariant M-function, M by

$$T = \bar{N} M N \tag{2.60}$$

and writing

$$M = A 1 + \tfrac{1}{2} \not{p}' B \tag{2.61}$$

where 1 is the unit matrix, enables us to write (2.57) subject to (2.58) and (2.59), as

$$A = \left[\left(1 + \frac{t}{4m_p}\right) g_F - \left(1 + \frac{m}{\mu}\right) g_{D+\frac{2}{3}F} \right] \left[\beta_- \Gamma(1-\alpha_-)\left(1 - e^{-i\pi\alpha_-}\right) h_F \left(\frac{s + \frac{t}{2} - m^2 - \mu^2}{2m_p}\right)^{\alpha_-} + \beta_+ \Gamma(1-\alpha_+)\left(1 + e^{-i\pi\alpha_+}\right) h_D \left(\frac{s + \frac{t}{2} - m^2 - \mu^2}{2m_p}\right)^{\alpha_+} \right]$$

$$B = \frac{1}{\mu}\left(1 + \frac{m}{\mu}\right)\left(1 - \frac{t}{4m^2}\right) g_{D+\frac{2}{3}F} \left[\beta_- \Gamma(1-\alpha_-)\left(1 - e^{-i\pi\alpha_-}\right) h_F \left(\frac{s + \frac{t}{2} - m^2 - \mu^2}{2m_p}\right)^{\alpha_- - 1} + \beta_+ \Gamma(1-\alpha_+)\left(1 + e^{-i\pi\alpha_+}\right) h_D \left(\frac{s + \frac{t}{2} - m^2 - \mu^2}{2m_p}\right)^{\alpha_+ - 1} \right] \tag{2.62}$$

where g and h are the SU(3) couplings at the baryon and meson vertices respectively.

As explained in the discussion on 'ghost-killing' , (2.62) contains nonsense dips for $\alpha_- = 0, -2 \ldots$ and $\alpha_+ = -1, -3 \ldots$. These are borne out experimentally, e.g. in π N charge-exchange scattering at $\alpha_- = 0$.

2.6 S-channel Helicity Amplitudes and Experimental Quantities[21]

For the two-body process $a + b \to c + d$, the differential cross section is defined in terms of the s-channel helicity amplitudes by :

$$\frac{d\sigma}{dt} = \frac{\pi}{QK} \frac{1}{(2s_1+1)(2s_2+1)} \frac{K}{Q} \sum_{\substack{\text{helicity} \\ \text{amplitudes}}} |\phi_i|^2 \qquad (2.63)$$

where s_j is the spin of particle j; Q (K) is the initial (final) centre-of-mass three-momenta and ϕ_i is a helicity amplitude. For $0^-\tfrac{1}{2}^+ \to 0^-\tfrac{1}{2}^+$, i goes from 1 to 4, and the individual amplitudes are defined by

$$\phi_1 = \langle \tfrac{1}{2}0 | \phi | \tfrac{1}{2}0 \rangle \quad , \quad \phi_2 = \langle \tfrac{1}{2}0 | \phi | -\tfrac{1}{2}0 \rangle$$
$$\phi_3 = \langle -\tfrac{1}{2}0 | \phi | \tfrac{1}{2}0 \rangle \quad , \quad \phi_4 = \langle -\tfrac{1}{2}0 | \phi | -\tfrac{1}{2}0 \rangle \qquad (2.64)$$

where

$$\langle \tfrac{1}{2}0 | \phi | \tfrac{1}{2}0 \rangle = \frac{\langle \tfrac{1}{2}0 | T | \tfrac{1}{2}0 \rangle}{8\pi W} \quad \text{etc.} \qquad (2.65)$$

where $W = \sqrt{s}$ and $\langle \tfrac{1}{2}0 | T | \tfrac{1}{2}0 \rangle$ is that spin component of the T-matrix.

Conservation of parity gives

$$\langle -\lambda_3 -\lambda_4 | \phi | -\lambda_1 -\lambda_2 \rangle = \frac{\eta_3\eta_4}{\eta_1\eta_2} (-1)^{\lambda-\mu} (-1)^{s_3+s_4-s_1-s_2} \langle \lambda_3 \lambda_4 | \phi | \lambda_1 \lambda_2 \rangle \qquad (2.66)$$

where η_i is the intrinsic parity of particle i, $\lambda = \lambda_3 - \lambda_4$ and $\mu = \lambda_1 - \lambda_2$

For $0^-\tfrac{1}{2}^+$ scattering,

$$\frac{\eta_3\eta_4}{\eta_1\eta_2} = 1 \qquad (2.67)$$

and (2.66) gives

$$\phi_4 = \phi_1 \,, \qquad \phi_2 = -\phi_3 \tag{2.68}$$

Thus,

$$\frac{d\sigma}{dt} = \frac{\pi}{Q^2}\left[\,|\phi_1|^2 + |\phi_2|^2\,\right] \tag{2.69}$$

Similarly, the polarization of the outgoing nucleon is:

$$P(t) = 2\,\mathrm{Im}\,(\phi_1\phi_2^*)\Big/\left[|\phi_1|^2+|\phi_2|^2\right] \tag{2.70}$$

However, in order to use (2.69) and (2.70), we must write the pole term helicity amplitudes in terms of the invariant amplitudes A and B. Treating the N spinors as Dirac ones (in (2.56) $N \equiv N_\alpha^i (\tau^i)_a^b$ so the N_α^i is the Dirac spinor part), the relativistic boost condition is :

$$N^{(\lambda_1)}(p_1) = \frac{\not{p}_1 + m_1}{\sqrt{E_1+m_1}}\;\psi^{(\lambda_1)}(\theta,\phi) \tag{2.71}$$

where ψ is the Pauli rest spinor and θ , ϕ specifies the particle direction with respect to the positive z-direction. Similarly,

$$\bar{N}^{(\lambda_3)}(p_3) = \psi^{+(\lambda_3)}(\theta,\phi)\;\frac{(\not{p}_3+m_3)}{\sqrt{E_3+m_3}} \tag{2.72}$$

where for positive intrinsic parity

$$\gamma_0\,\psi = \psi \tag{2.73}$$

Using $\underline{\gamma} = \gamma_0 \underline{\sigma}\,\gamma_5$ where $\underline{\sigma} = \begin{pmatrix}\sigma & 0\\ 0 & \sigma\end{pmatrix}$, σ = Pauli spin matrices, (2.71) and (2.72) become

$$N^{(\lambda_1)}(p_1) = \sqrt{E_1+m_1}\left[1 + \frac{i\underline{\sigma}.\underline{p}_1\gamma_5}{E_1+m_1}\right]\chi^{(\lambda_1)}(\theta,\phi) \tag{2.74}$$

$$\bar{N}^{(\lambda_3)}(p_3) = \sqrt{E_3+m_3}\;\chi^{\dagger(\lambda_3)}(\theta,\phi)\left[1 - \frac{i\underline{\sigma}.\underline{p}_3\gamma_5}{E_3+m_3}\right] \tag{2.75}$$

respectively.

In the centre-of-mass-frame, the following conventions which preserve parity and forbid particle-antiparticle mixing are used

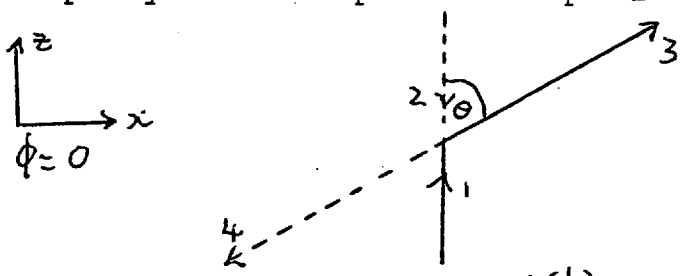

$$\chi^{(\frac{1}{2})}(\theta=0) = \begin{pmatrix}1\\0\\0\\0\end{pmatrix}, \qquad \chi^{\dagger(\frac{1}{2})}(\theta) = \left(\cos\tfrac{\theta}{2}, \sin\tfrac{\theta}{2}, 0, 0\right)$$

$$\chi^{(-\frac{1}{2})}(\theta=0) = \begin{pmatrix}0\\1\\0\\0\end{pmatrix}, \qquad \chi^{\dagger(-\frac{1}{2})}(\theta) = \left(-\sin\tfrac{\theta}{2}, \cos\tfrac{\theta}{2}, 0, 0\right) \tag{2.76}$$

Using (2.60), (2.61) and pair-wise equal mass kinematics gives

$$\phi_1 = \frac{1}{4\pi W}\cos\tfrac{\theta}{2}\left[m_1 A + (E_1 W - m_1^2)\,B\right] \tag{2.77}$$

$$\phi_2 = \frac{1}{4\pi W}\sin\tfrac{\theta}{2}\left[E_1 A + m_1(W - E_1)\,B\right] \tag{2.78}$$

where m_1, E_1 are the mass and c.m. energy respectively of the target nucleon.

2.7 t-Channel Trajectories

As Chew-Frautschi plots of the meson trajectories in the resonance region show them to be approximately straight lines, it has long been traditional to regard Regge traejctories in the scattering region as linear extensions of the plots. However, except for certain specialized models such as the Veneziano model, this is not necessary if potential scattering and perturbation theory are to be believed.

Generally, in potential scattering, the trajectories are dependent of the form of the potential employed in the scattering model and in most cases are certainly non-linear[22]. However, what is most important is that a definite asymptotic behaviour is predicted.

Taking the example of a potential formed by the superposition of Yukawa potentials of the form

$$V(\underline{r}) = \int_{\mu_0}^{\infty} d\mu\, \rho(\mu)\, \frac{e^{-\mu \underline{r}}}{\underline{r}} \quad , \mu_0 > 0 \tag{2.79}$$

the trajectories $\alpha(t)$ are non-linear with an asymptotic behaviour

$$\alpha(t) \rightarrow -\tfrac{1}{2}(N+1), \; t \rightarrow -\infty \tag{2.80}$$

where N is a positive integer defining satellite trajectories. The leading trajectory (N=1) thus has the asymptotic limit [23]

$$\alpha(t) \rightarrow -1 \quad , \quad t \rightarrow -\infty \tag{2.81}$$

Other evidence for the existence of non-linear trajectories is the scattering region comes from perturbation theory in the relativistic domain[24]. If one evaluates a generalized Feynman ladder graph, which is well known to the equivalent to a Regge pole, we obtain :

$$\alpha(t) = -N + \sum_{n=1}^{\infty} g^{2n} K_n(t) \qquad (2.82)$$

where the $K_n(t)$ are integrals associated with the self-energy loops contained in the ladder and the g's are 'end contributions'. N is an integer depending on the 'order' of the trajectory. The asymptotic behaviour of (2.82) is such that

$$K_n(t) \to 0, \quad t \to -\infty \qquad (2.83)$$

Again the leading trajectory has the asymptotic limit

$$\alpha(t) \to -1 \ , \ t \to -\infty \qquad (2.84)$$

Experimental confirmation of the conclusions (2.81) and (2.82) has been carried out by Owen et al[25], who fitted the parametric form $\frac{d\sigma}{dt} \sim s^{2(\alpha(t)-1)}$ to the $\pi^- p$ elastic scattering data from the foward to the backward region. They found (2.81) and (2.84) to be approximately true.

Taking into account these facts, we parameterized our trajectories as

$$\alpha(t) = \alpha_0 + \alpha_1 e^{\alpha_2 t} \qquad (2.85)$$

which gives

$$\alpha(t) \to \alpha_0, \quad t \to -\infty \qquad (2.86)$$

The α_0 were found to be compatible with -1 to within experimental error (see chapter 4).

To show that our trajectory is not too remote from the general idea of linear trajectories, we see that in the peripheral region

$$\alpha(t) \simeq (\alpha_0+\alpha_1) + (\alpha_1\alpha_2)t \qquad (2.87)$$

i.e. linear. Continuing the trajectories into the resonance region using this limit, we see that the meson poles are acceptably close to the trajectory (Fig. 2).

We further notice that $|\alpha(t)|<1$ is the scattering region considered in Chapter 4 so only one nonsense point occurs at $\alpha=0$. As we use the Gell'Mann 'ghost-killing' mechanism, we have a zero in the pole graph of the odd-signature trajectory as this is a wrong-signature point. However, as $\alpha=0$ is a right signature point for the even-signature trajectory, there is no dip in its pole graph at this point.

CHAPTER 3. ABSORPTIVE CORRECTIONS.

3.1 Absorptive Cut Models.

Later in this chapter, in fact in section 3.4, the equivalence of cuts in the J-plane and absorptive corrections to the pole graph are discussed, so we shall assume this equivalence in the preceeding sections.

Chapter 1 provided us with the motivation for introducing absorptive corrections to the pole graph. We are now faced with the problem of how to do this. Basically, there are two points of view which may be adopted for the introduction of the Pomeron-Reggeon type of absorptive cuts. These are:

a) The weak cut model as used by us[26,27,28]. Here, the pole contribution is larger than the cut and dips in differential cross-sections are obtained by using a 'nonsense choosing' mechanism as indicated by the Veneziano model.

b) The strong cut model as used by the Michigan group[29]. Here the Regge residues are featureless and do not have a nonsense choosing mechanism in them. Dips, and like features, are obtained by pole-cut interference, undoubtedly facilitated by the wealth of parameters present in this model. Phillips[30] has stated that by suitable choice of parameters, dips can be obtained practically anywhere.

In this version of the absorptive cut model, the cuts are multiplied by a factor λ, where

$$\lambda = \left|\text{inelastic cut} + \text{elastic cut}\right| \Big/ \left|\text{elastic cut}\right| \qquad (3.1)$$

as a method of introducing particles other than Pomerons into the cut. λ is typically taken to be of the order of 1.5, as inelastic cut $\sim \frac{1}{2}$ elastic cut and thus gives cuts stronger by about 50% than the weak cut model which has $\lambda = 1$.

Up to the present, only Pomeron-Reggeon type cuts have been considered. No models for Reggeon-Reggeon type cuts have been constructed as judging from the ratio of $\left[\text{elastic } \frac{d\sigma}{dt} \Big/ \text{inelastic } \frac{d\sigma}{dt}\right]$ which is just $\left[\text{Pomeron}^2/\text{Reggeon}^2\right]$ in the forward direction, Reggeon-Reggeon cuts are expected by an order of magnitude lower than Pomeron-Reggeon cuts and so are only expected to be important at very wide angles or very low energies where the Pomeron contribution is expected to have vanished.

3.2 Absorptive Corrections to the Pole Graph.

To introduce these, the pole s-channel helicity amplitudes are first expanded in a partial-wave series[21].

$$\langle \lambda_3 \lambda_4 | \phi(s,\theta) | \lambda_1 \lambda_2 \rangle = \sum_J (2J+1) \langle \lambda_3 \lambda_4 | T^J(s) | \lambda_1 \lambda_2 \rangle d^J_{\mu\lambda}(\theta) \qquad (3.2)$$

where θ is the c.m. s-channel scattering angle, $\mu = \lambda_1 - \lambda_2$, $\lambda = \lambda_3 - \lambda_4$ where 1,2,3,4 describe the incoming baryon and meson, and the outgoing baryon and meson respectively. λ_i is the helicity

of particle i and $\langle \lambda_3 \lambda_4 | T^J(s) | \lambda_1 \lambda_2 \rangle$ is the partial-wave amplitude.

In particular, for $0^- \tfrac{1}{2}^+ \to 0^- \tfrac{1}{2}^+$ scattering, the two independent helicity amplitudes defined by equations (2.64) and (2.68) have the partial wave expansions

$$\phi_1(s,t) = \sum_J (2J+1) \langle \tfrac{1}{2} 0 | T^J(s) | \tfrac{1}{2} 0 \rangle \; d^J_{\frac{1}{2}\frac{1}{2}}(\theta) \qquad (3.3)$$

$$\phi_2(s,t) = \sum_J (2J+1) \langle \tfrac{1}{2} 0 | T^J(s) | -\tfrac{1}{2} 0 \rangle \; d^J_{-\frac{1}{2}\frac{1}{2}}(\theta) \qquad (3.4)$$

where the rotation functions $d^J_{\mu\lambda}(\theta)$ are given in terms of Legendre polynomials by

$$d^J_{\frac{1}{2}\frac{1}{2}}(\theta) = \left[P_{\ell+1}(\cos\theta) + P_\ell(\cos\theta) \right] \Big/ \left[2(1+\cos\theta) \right]^{\frac{1}{2}} \qquad (3.5)$$

$$d^J_{-\frac{1}{2}\frac{1}{2}}(\theta) = -\left[P_{\ell+1}(\cos\theta) - P_\ell(\cos\theta) \right] \Big/ \left[2(1-\cos\theta) \right]^{\frac{1}{2}} \qquad (3.6)$$

with $J = \ell + \tfrac{1}{2}$.

To write the partial-wave amplitudes in terms of the helicity amplitudes, we make use of the orthonormality relation :

$$\int_{-1}^{+1} d^J_{\mu\lambda}(\theta) \, d^{J'}_{\mu\lambda}(\theta) \, d(\cos\theta) = \frac{2\,\delta_{JJ'}}{(2J+1)} \qquad (3.7)$$

Thus, we have for the partial-wave amplitudes:

$$\langle \lambda_3\lambda_4 | T^J(s) | \lambda_1\lambda_2 \rangle = \tfrac{1}{2} \int_{-1}^{+1} \langle \lambda_3\lambda_4 | \phi(s,t) | \lambda_1\lambda_2 \rangle d^J_{\mu\lambda}(\Theta) d(\cos\theta) \quad (3.8)$$

These are determined in practice by numerical integration as explained in the appendix.

To introduce the absorptive corrections, we approximate the modified production amplitude by the Watson formula to first order[5,31].

$$\langle \lambda_3\lambda_4 | T'^J(s) | \lambda_1\lambda_2 \rangle = \tfrac{1}{2} \sum_{\alpha,\beta} \Big[\langle \lambda_3\lambda_4 | S^{el\,J} | \alpha\beta \rangle$$

$$\langle \alpha\beta | T^J(s) | \lambda_1\lambda_2 \rangle + \langle \lambda_3\lambda_4 | T^J(s) | \alpha\beta \rangle \langle \alpha\beta | S^{el\,J} | \lambda_1\lambda_2 \rangle \Big] \quad (3.9)$$

where $\langle \lambda_3\lambda_4 | T'^J(s) | \lambda_1\lambda_2 \rangle$ is the production amplitude modified by absorptive corrections, and $\langle \lambda_3\lambda_4 | S^{el\,J} | \alpha\beta \rangle$ and $\langle \alpha\beta | S^{el\,J} | \lambda_1\lambda_2 \rangle$ are the S-matrix elements for single elastic scattering in the final and initial states respectively. To get nearer a true modification to the production amplitude, we really need to introduce all orders of elastic scattering in both the final and initial states.

In (3.9), we can write

$$\langle \lambda_3\lambda_4 | S^{el\,J} | \alpha\beta \rangle = \langle \lambda_3\lambda_4 | \alpha\beta \rangle + 2i\rho \langle \lambda_3\lambda_4 | T^{el\,J} | \alpha\beta \rangle \quad (3.10)$$

and similarly for $\langle \alpha\beta | S^{el\,J} | \lambda_1 \lambda_2 \rangle$, where ρ is a phase-space factor. Hence, using (3.10) in (3.9) we obtain

$$\langle \lambda_3 \lambda_4 | T^{J}_{(s)} | \lambda_1 \lambda_2 \rangle = \langle \lambda_3 \lambda_4 | T^{J}_{(s)} | \lambda_1 \lambda_2 \rangle + i\rho \sum_{\alpha,\beta}$$

$$\left[\langle \lambda_3 \lambda_4 | T^{J}_{(s)} | \alpha\beta \rangle \langle \alpha\beta | T^{el\,J} | \lambda_1 \lambda_2 \rangle + \langle \lambda_3 \lambda_4 | T^{el\,J} | \alpha\beta \rangle \langle \alpha\beta | T^{J}_{(s)} | \lambda_1 \lambda_2 \rangle \right] \quad (3.11)$$

The components of the right-hand side of (3.11) correspond to diagrams (a), (b) and (c) respectively of Fig.1. The elastic scattering elements in (3.11) are just equivalent to a fixed pole Pomeron, so it is apparent immediately how Pomeron-Reggeon cuts arise.

In the actual computation of the absorptive corrections, we make the following assumptions above the elastic scattering elements.

1). That the elastic scattering in the final state is the same as the elastic scattering in the initial state purely for the technical reason that no-one has yet done, for example, $K^+\Sigma^+$ elastic scattering experimentally, and our elastic scattering parameters are determined by the experimental data (see section 3.3).

2). That the elastic scattering is purely non-flip. This assumption is based on the fact that for high-energy meson-baryon elastic scattering in the near forward direction, the non-flip amplitude is dominant.

Under 1) and 2), (3.11) becomes:

$$\langle \lambda_3\lambda_4 | T'^{J}(s) | \lambda_1\lambda_2 \rangle = \langle \lambda_3\lambda_4 | T^{J}(s) | \lambda_1\lambda_2 \rangle + 2i\rho \langle \lambda_3\lambda_4 | T^{J}(s) | \lambda_1\lambda_2 \rangle \quad (3.12)$$
$$\langle \lambda_1\lambda_2 | T^{\dagger J} | \lambda_1\lambda_2 \rangle$$

$$= \langle \lambda_3\lambda_4 | T^{J}(s) | \lambda_1\lambda_2 \rangle \langle \lambda_1\lambda_2 | S^{\dagger J} | \lambda_1\lambda_2 \rangle \quad (3.13)$$

Having calculated the modified partial-waves in (3.13), these are then resummed to give the modified helicity amplitudes:

$$\langle \lambda_3\lambda_4 | \phi'(s,\theta) | \lambda_1\lambda_2 \rangle = \sum_J (2J+1) \langle \lambda_3\lambda_4 | T'^{J}(s) | \lambda_1\lambda_2 \rangle \, d^{J}_{\mu\lambda}(\theta) \quad (3.14)$$

The modified helicity amplitudes, ϕ_i', calculated as in (3.14) then replace the pole term helicity amplitudes, ϕ_i, in (2.69) and (2.70) for the purposes of comparing $\frac{d\sigma}{dt}$ and P(t) with experiment.

A calculational point worth noting is that in the partial-wave summations (3.2), (3.3), (3.4) and (3.14), the sum $\sum_J$ is approximated by $\sum_J^N$, where N is the smallest number such that the contributions to the (N+1)th partial wave from the helicity amplitudes are zero and:

a) $$\langle \lambda_1\lambda_2 | S^{\dagger N} | \lambda_1\lambda_2 \rangle = 1.0 \quad (3.15)$$

b) after using (3.8) to find the partial-waves, the application of (3.2), using N as the upper limit of the sum, to these partial-waves yields the original pole helicity amplitudes.

Both a) and b), of course, are taken to be true to an appropriate number of decimal places.

3.3 Parameterization of the Elastic Scattering Elements.

A parameterization for the elastic scattering elements S^{el} (matrix labels are dropped for the spinless case) is obtained by a non-relativistic method for spinless particles[2,3]. A generalization to include spin is then made afterwards.

The differential cross section for elastic scattering with equal mass spinless particles is

$$\left(\frac{d\sigma}{d\Omega}\right)_{el} = |f(\theta)|^2 \tag{3.16}$$

where θ is the C.M. scattering angle. Here, we use a partial-wave expansion for $f(\theta)$ in terms of the orbital angular momentum, ℓ,

$$f(\theta) = \sum_{\ell=0}^{\infty} (2\ell+1)\left(\frac{S_\ell^{el} - 1}{2iQ}\right) P_\ell(\cos\theta) \tag{3.17}$$

where Q is the centre of mass 3-momentum and S_ℓ^{el} is the elastic scattering S-matrix for partial wave ℓ, $0 \le |S_\ell^{el}| \le 1$.

In the peripheral region, θ is small, so for $s \to \infty$,

$$P_\ell(\cos\theta) \longrightarrow J_0(b\sqrt{|t|}) \tag{3.18}$$

where J_0 is the Bessel function of the first kind of order zero, b is a continuous parameter called the 'impact parameter' and $\sqrt{|t|} \approx Q\theta$. b is defined by the equation,

$$Qb = \ell + \tfrac{1}{2} \tag{3.19}$$

implying that b gives a measure of the 'distance' of interaction.

At high energies, we expect many partial-waves to contribute so we make the approximate replacement:

$$\sum_{\ell=0}^{\infty} \cdots \longrightarrow \int_0^{\infty} d\ell \cdots \longrightarrow \int_0^{\infty} Q\, db \cdots \tag{3.20}$$

Hence,

$$f(\theta) = iQ \int_0^{\infty} b\, db \left[1 - S^{el}(b)\right] J_0(b\sqrt{|t|}) \tag{3.21}$$

For S_ℓ^{el}, a complex Gaussian model is assumed,

$$S_\ell^{el} = 1 - \left[C_1 e^{-\ell(\ell+1)/\nu_1^2 Q^2} + iC_2 e^{-\ell(\ell+1)/\nu_2^2 Q^2} \right] \tag{3.22}$$

implying that

$$S^{el}(b) = 1 - \left[C_1 e^{-b^2/\nu_1^2}\, e^{1/4\nu_1^2 Q^2}_{\ell} + iC_2 e^{-b^2/\nu_2^2}\, e^{1/4\nu_2^2 Q^2}_{\ell} \right] \tag{3.23}$$

where c_1 and c_2 are related to the opacity of the target i.e. strength of interaction, as shown below, and where ν_1, ν_2 can be thought of as radii of interactions typically associated with a Gaussian model. This occurs as

$$\left[1 - S^{el}(b)\right] = C_1 e^{-b^2/\nu_1^2}\, e^{1/4\nu_1^2 Q^2}_{\ell} + iC_2 e^{-b^2/\nu_2^2}\, e^{1/4\nu_2^2 Q^2}_{\ell} \tag{3.24}$$

where e^{-b^2/r_1^2} has the form for a given r_1

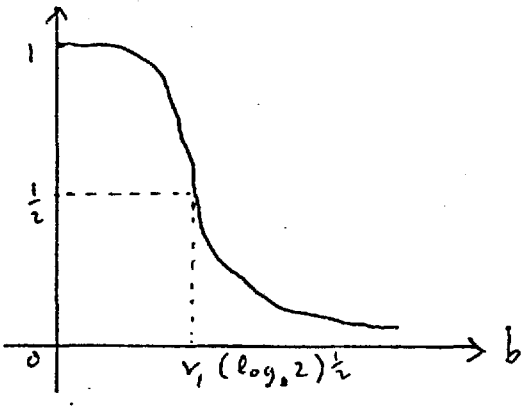

To show how c_1 and c_2 are related to the mean opacity, we determine σ_{el} and σ_{tot}.

Now

$$\sigma_{el} = \frac{\pi}{Q^2} \sum_{\ell=0}^{\infty} (2\ell+1) \left| S_\ell^{el} - 1 \right|^2 \tag{3.25}$$

$$\longrightarrow 2\pi \int_0^\infty b\,db \left[c_1^2 e^{-2b^2/r_1^2} e^{1/2r_1^2Q^2} + c_2^2 e^{-2b^2/r_2^2} e^{1/2r_2^2Q^2} \right]$$

$$= \frac{\pi}{2} \left[r_1^2 c_1^2 e^{1/2r_1^2Q^2} + 2r_2^2 c_2^2 e^{1/2r_2^2Q^2} \right] \tag{3.26}$$

Similarly

$$\sigma_{tot} = \frac{2\pi}{Q^2} \sum_{\ell=0}^{\infty} (2\ell+1) \left[1 - R_e\left(S_\ell^{el}\right) \right] \tag{3.27}$$

$$\longrightarrow 4\pi \int_0^\infty b\,db\, c_1 e^{-b^2/r_1^2} e^{1/4r_1^2Q^2}$$

$$= 2\pi c_1 r_1^2 e^{1/4 r_1^2 Q^2} \tag{3.28}$$

Hence,

$$\text{Mean Opacity} = \frac{2\sigma_{el}}{\sigma_{tot}} \tag{3.29}$$

$$= \frac{r_1^2 c_1^2 e^{1/2r_1^2Q^2} + r_2^2 c_2^2 e^{1/2r_2^2Q^2}}{2c_1 r_1^2 e^{1/4 r_1^2 Q^2}} \tag{3.30}$$

As in practice, we put $\nu_2 = \nu_1$,

$$\text{Mean Opacity} = \frac{c_1^2 + c_2^2}{2c_1} \, e^{-1/4\nu_1^2 Q^2} \tag{3.31}$$

and as typically, $\nu_1 \sim 4$, $Q \sim 2$, $e^{-1/4\nu_1^2 Q^2} \sim 1$ (3.32)

$$\text{Mean Opacity} = \frac{c_1^2 + c_2^2}{2c_1} \tag{3.33}$$

The physical interpretation of mean opacity is that it represents the 'strength of the interaction' in the sense that it describes how much of the total scattering is elastic and so due to the short range forces in the completely black disc, radius ν_1 , area of the target. These particles are then lost to (or absorbed from) the given inelastic channel which we are considering in the peripheral region, which occurs within a radius μ . The situation is easily visualized for $\mu > \nu_1$

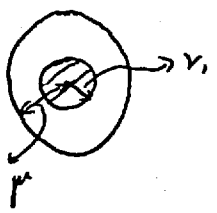

but equally true for $\nu_1 > \mu$.

Neglecting $e^{-1/4\nu_1^2 Q^2}$ again, (3.28) gives the expression for the determination of c_1 from a given set of data. This is

$$c_1 = \frac{\sigma_{Tot}}{2\pi\nu_1^2} \tag{3.34}$$

To determine ν_1 , we take (3.21), which gives

$$f(\theta) = \frac{iQ}{2}\left[C_1 \nu_1^2 \, e^{1/4\nu_1^2Q^2} \, e^{\frac{-\nu_1^2|t|}{4}} + iC_2\nu_2^2 \, e^{1/4\nu_2^2Q^2} \, e^{-\frac{\nu_2^2|t|}{4}} \right]$$

$$\xrightarrow[\nu_1=\nu_2]{\text{for}} \frac{iQ}{2}\left[C_1 + iC_2\right]\nu_1^2 \, e^{1/4\nu_1^2Q^2} \, e^{-\nu_1^2|t|/4} \qquad (3.35)$$

Hence, $\left(\frac{d\sigma}{d\Omega}\right)_{el} = |f(\theta)|^2$

$$= \frac{Q^2}{4}\left[C_1^2 + C_2^2\right]\nu_1^4 \, e^{1/2\nu_1^2Q^2} \, e^{-\nu_1^2|t|/2} \qquad (3.36)$$

In general, $C_2 << C_1$, so (3.36) reduces to

$$\left(\frac{d\sigma}{d\Omega}\right)_{el} = \frac{C_1^2Q^2\nu_1^4}{4} \, e^{1/2\nu_1^2Q^2} \, e^{-\nu_1^2|t|/2} \qquad (3.37)$$

Hence, at a given centre-of-mass momentum Q,

$$\left[\frac{d\sigma}{dt} \Big/ \frac{d\sigma}{dt}\Big|_{t=0}\right]_{el} = e^{-\nu_1^2|t|/2}$$

$$\therefore \log_e\left[\frac{d\sigma}{dt} \Big/ \frac{d\sigma}{dt}\Big|_{t=0}\right]_{el} = -\frac{\nu_1^2|t|}{2} \qquad (3.38)$$

Hence, the slope of a log - linear plot of the elastic scattering differential cross-section, after normalization, gives $\frac{\nu_1^2}{2}$.

Practically, we always take $\nu_1 = \nu_2$, giving

$$S_\ell^{el} = 1 - (C_1 + iC_2) \, e^{-\ell(\ell+1)/\nu_1^2Q^2} \qquad (3.39)$$

To include spin, we have an obvious generalization of (3.39). Taking, as stated in section 3.2, the matrix element $S^{el\,J}_{flip} = 0$, the non-flip element is obtained by replacing ℓ by J in (3.39) giving,

$$\langle \lambda_1\lambda_2 | S^{el\,J} | \lambda_1\lambda_2 \rangle = 1 - (c_1 + ic_2)\, e^{-J(J+1)/\gamma_1^2 Q^2} \tag{3.40}$$

We can think of this as being a weighted mean as

$$\ell = J+\tfrac{1}{2}, J-\tfrac{1}{2} \tag{3.41}$$

Judging purely on physical reasons, we see that (3.40) is just what we require for the absorption model, as neglecting c_2 , we get

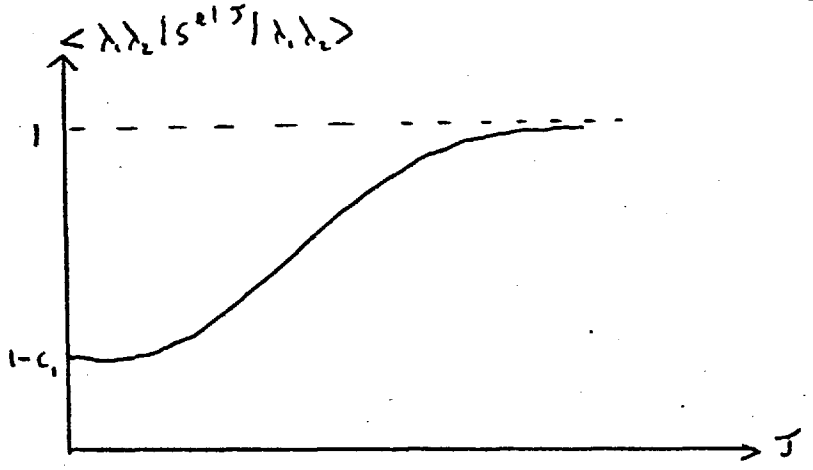

i.e. attenuation of the low partial waves.

It now just remains to determine c_2. As we have assumed that the $0^- \tfrac{1}{2}^+$ elastic scattering is pure non-flip, at t=0,

$$\left(\frac{d\sigma}{d\Omega}\right)^{el}_{t=0} = |f(\theta=0)|^2 = |\phi_i^{el}(\theta=0)|^2 \tag{3.43}$$

Implying

$$\phi_1^{el}(t=0) = f(t=0) \tag{3.44}$$

Hence,

$$\frac{c_2}{c_1} = -\frac{Re\,\phi_1^{el}(t=0)}{Im\,\phi_1^{el}(t=0)} \tag{3.45}$$

The ratio $Re\,\phi_1^{el}(t=0)/Im\,\phi_1^{el}(t=0)$ has been measured experimentally for $\pi^{\pm}p$ elastic scattering, but not for $K^{\pm}p$ elastic scattering. Thus c_2 can be determined for $\pi^{\pm}p$ processes, but for processes where this data is missing, c_2 is put equal to zero, making the elastic scattering purely imaginary. (c_2=0 always in chapter 4).

For small momentum transfers, we can also determine ϕ_1^{el} as here it is fair to assume the complete dominance of the non-flip amplitude. Extending (3.44) to small $t \neq 0$,

$$\phi_1^{el}(t) = f(t) \quad , t \text{ small} \tag{3.44a}$$

Hence, from (3.35),

$$\langle \tfrac{1}{2}0 | \phi^{el}(s,t) | \tfrac{1}{2}0 \rangle = \frac{\sqrt{s}}{4} \nu_1^2 \left[ic_1 - c_2\right] e^{1/\nu_1^2 s} \; e^{-\nu_1^2 |t|/4} \tag{3.35a}$$

where $q^2 \simeq \frac{s}{4}$

As $c_2 << c_1$ and $e^{1/\nu_1^2 s} \simeq 1$,

$$\langle \tfrac{1}{2}0 | \phi^{el}(s,t) | \tfrac{1}{2}0 \rangle = \frac{\sqrt{s}}{4} \nu_1^2 \, ic_1 \, e^{-\nu_1^2 |t|/4} \tag{3.35b}$$

On comparison of (3.35b) with (2.77), we see that for small θ, the s-dependence implies that our elastic scattering Gaussian is equivalent to a fixed pole of spin J=1.

3.4 Regge Cuts and Absorptive Corrections.

Here, we aim to discuss both Regge Cuts as discussed by Amati, Fubini and Stangellini (AFS) [32] and Mandelstam [33] and Absorptive corrections as applied to Regge Poles and show that they have sufficient features in common for us to believe that Absorptive Corrections generate cuts in the complex J plane.

The introduction of cuts as opposed to absorptive corrections follows from the work carried out by AFS, who considered an amplitude with a 'crossed Regge Pole' behaviour

$$T(s,t) = \frac{\beta(t)}{\sin \pi\alpha(t)} \left(\frac{s}{s_0}\right)^{\alpha(t)} \qquad (3.46)$$

and found that when this was inserted into the right-hand side of the elastic unitarity equation:

$$\mathrm{Im}\, T(s,t) = \int_{\substack{\text{phase}\\ \text{space}}} \rho \, d\Omega \; T(s,t') \, T(s,t'') \qquad (3.47)$$

and a dispersion integral taken over $\mathrm{Im}\, T(s,t)$, a behaviour more complicated than (3.46) was obtained which AFS put down to diagrams of the form:

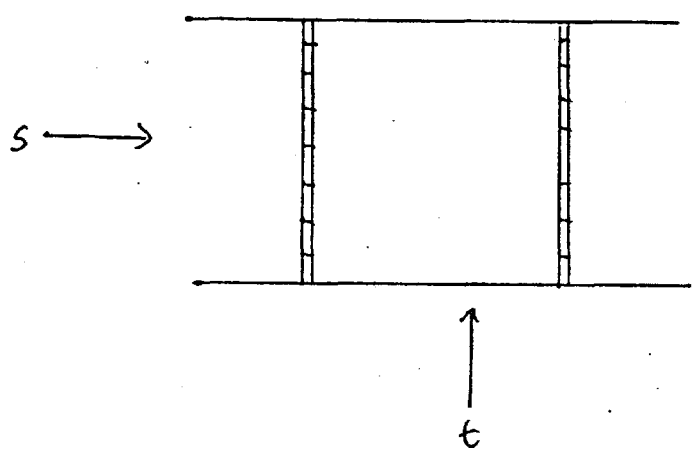

Although Mandelstam showed that when all dispersion graphs were added to form the Feynman graph, no cut resulted in the J-plane, the idea was enough to generate modified graphs, which do give cuts.

Mandelstam showed that the simplest graph which gives cuts is :

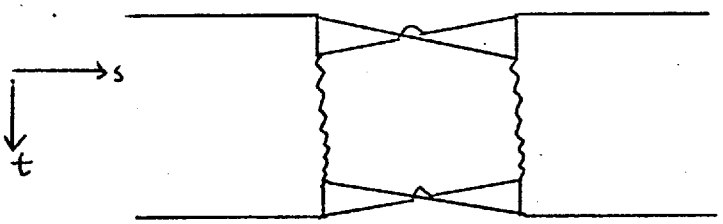

where ~~~ is an effective trajectory ≡ ⊏⊏⊏⊏ .
As this graph has a third double spectral function ρ_{tu}, a cut results in the J-plane.

The absorptive corrections give diagrams similar to that obtained by AFS as shown by Figs 1(b) and 1(c), but as shown by equations (3.8) and (3.12), the equation evaluated is of the form:

$$T(s,t) = \int_{\substack{\text{phase}\\ \text{space}}} d\Omega\, \rho\, T_1(s,t')\, T_2(s,t'') \qquad (3.48)$$

AFS and Mandelstam diagrams give a similar energy behaviour as does the absorption model[34,35,36], but the latter two have the opposite sign so the pole term and cut term have desctuctive interference which seems to be experimentally verified.

Symbolically, we can write (3.12) in the following form

$$T_{ab} \simeq R + 2i\, P \otimes R \qquad (3.49)$$

where R defines the pole term, P, the Pomeron (or elastic scattering)

term, and a and b, two-particle states. In this notation Caneschi[37] showed that there may not be a 'phase contradiction' after all. From (3.47), extracting the elastic intermediate state, we write

$$I_m T_{ab} = R_e\left(T^*_{ab} \otimes T_{aa} + T^*_{bb} \otimes T_{ab}\right) + \sum_{n \neq a,b} \int d\Omega_n \rho_n T^*_{bn} T_{an} \qquad (3.50)$$

Putting $T_{aa} = T_{bb} = P$, $T_{ab} = R$, and as $s \to \infty$

$$\sum_{n \neq a,b} \int d\Omega_n \rho_n T^*_{bn} T_{an} = I_m R \quad + \text{low-lying cut},$$

we have, with P pure imaginary,

$$I_m T_{ab} \simeq I_m R + 2 R_e (P^* \otimes R) \qquad (3.51)$$

which has the sign disagreement with (3.49). If however, for $n \neq a,b$ we apply absorptive corrections to the inelastic intermediate amplitudes according to the Watson formula, (3.9) (neglecting absorption in intermediate states).

$$T'_{an} \simeq T_{an} \otimes (1 + iP) + T_{bn} \otimes iR \qquad (3.52)$$

we obtain (3.49).

As far as the energy behaviour is concerned, we first show an expression for a leading Regge cut derived for a spinless case. A Somerfeld-Watson transform is first taken for the t-channel partial wave decomposition of the amplitude:

$$T(s,t) = \sum_{J=0}^{\infty} (2J+1)\, T^J(t)\, P_J(\cos\theta) \qquad (3.53)$$

$$= \frac{i}{2} \oint_C (2J+1) \frac{T(J,t)\, P_J(-\cos\theta)}{\sin \pi J}\, dJ \qquad (3.54)$$

where the contour c encloses integers along the real axis of the J-plane.

Assuming cuts and poles only exist in the right-half of the J-plane, the contour can be deformed as follows from c to include c'.

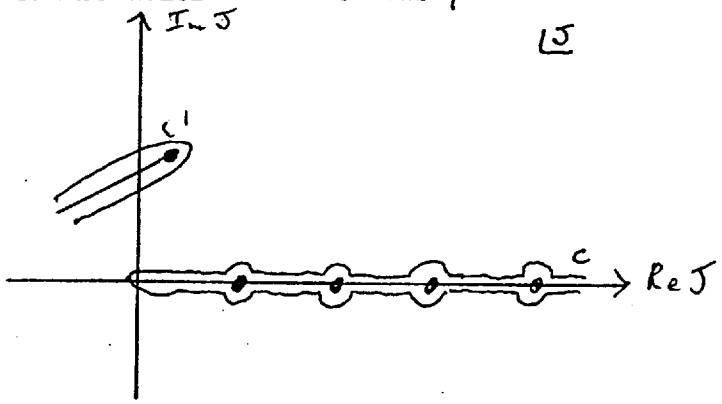

to obtain

$$T(s,t) = \sum_{\alpha} \frac{\beta(\alpha,t)\, P_\alpha(-\cos\theta)}{\sin \pi\alpha} + \sum_{cuts} \oint_{cuts} \frac{P_\alpha(-\cos\theta)}{\sin\pi\alpha} T(\alpha,t)\, d\alpha$$

+ left-hand contour integral (3.55)

$$\xrightarrow[\text{limit}]{\text{high-energy}} \sum_{\alpha} \frac{\beta(\alpha,t)\left(\frac{s}{s_0} e^{-i\pi}\right)^\alpha}{\sin\pi\alpha} + \sum_{cuts} \int \frac{\left(\frac{s}{s_0} e^{-i\pi}\right)^\alpha}{\sin\pi\alpha} \text{Disc}_\alpha\, T(\alpha,t)\, d\alpha \qquad (3.56)$$

For a leading order Mandelstam cut near $\alpha^c = j$

$$\text{Disc}_j\, T(j,t) \sim \Gamma(t) \qquad (3.57)$$

giving an asymptotic cut contribution :

$$T^c(s,t) \sim \frac{\Gamma'(t)\left(\frac{s}{s_0}\right)^{\alpha(t)}}{\left(\log_e\left(\frac{s}{s_0} + \frac{i\pi}{2}\right)\right)} \qquad (3.58)$$

An expression similar to (3.58) is shown in Moriarty's[38] thesis for the absorption model, using spinless particles in the impact parameter representation.

Thus the evidence seems to indicate that the absorption model does indeed lead to a cut in the J-plane.

CHAPTER 4. APPLICATION OF THE REGGEIZED ABSORPTION MODEL TO $0^-\frac{1}{2}^+$ HYPERCHARGE-EXCHANGE REACTIONS.

4.1 Discussion of Results.

In this section, we apply the Reggeized U(6) ⊗ U(6) ⊗ O(3) absorption model to the $0^-\frac{1}{2}^+$ hypercharge-exchange reactions[28]

(i) $\pi^- p \to K^0 \Lambda (\Sigma^0)$

(ii) $\pi^- p \to K^0 \Lambda$

(iii) $K^- n \to \pi^- \Lambda$

(iv) $K^- n \to \pi^- \Sigma^0$

(v) $\pi^+ p \to K^+ \Sigma^+$

(vi) $K^- p \to \pi^- \Sigma^+$

The model, as applied to these reactions, consisted of the Reggeized U(6) ⊗ U(6) ⊗ O(3) pole term as developed in Chapter 2, to which was added the absorptive corrections as shown in chapter 3. In the above reactions, we have both $K^*(890)\left[J^P = 1^-\right.$,odd-signature$\left.\right]$ and $K_N(1420)\left[J^P = 2^+\right.$,even-signature$\left.\right]$ exchanges, neither of which can be isolated in a single reaction due to the absence of G-parity. Hence, we cannot determine the parameters for a given trajectory separately from the other. Thus we chose the reaction with the best statistics in the differential cross-section data over a wide range of energy and carried out a χ^2 minimization using MINUITS (CERN Program

Library No: D506) to fit the theoretical pole + cut differential cross-section to the experimental data and so determine the parameters. The reaction chosen was $\pi^- p \to K^0 Y^0 \left[\pi^- p \to K^0 \Lambda(\Sigma^0)\right]$ where the Y^0 includes both Λ's and Σ^0's as the resolution of the experiment was not sufficient to differentiate these. The parameters determined in this way were β_-, β_+, α_1^-, α_2^-, α_1^+ and α_2^+. α_0^- and α_0^+ were fixed by the knowledge of the values of α_1^-, α_2^-, α_1^+ and α_2^+ respectively and the constraint that the $K^*(890)$ and $K_N(1420)$ trajectories must pass through their respective poles. This latter condition was imposed using equation (2.87). Pair-wise equal mass kinematics were used in the calculation with $m = 1.15\ GeV/c^2$, the average mass of the $\frac{1}{2}^+$ octet, and $\mu = 0.42\ GeV/c^2$, the average mass of the 0^- nonet.

The SU(3) D- and F-type couplings used in this analysis are shown in Table 1, and the elastic scattering absorption coefficients as determined by equations (3.34) and (3.38) are shown in Table 2 (Since no differential cross-section data exists for K^-n elastic scattering (required to determine γ_1), K^-p elastic scattering coefficients are used). In Table 3, the results of the minimization for the parameters of the trajectories are given.

As stated before, Fig.1 displays diagramatically the scattering amplitude in its components specified by equation (3.11). Fig.2 shows the Chew-Frautschi plot for the $K^*(890)$ and $K_N(1420)$ trajectories. The trajectories turn out to be almost degenerate although this was not imposed as a condition. This agrees with the absorption models discussed later, although they use the strong form of exchange degeneracy which was found not to be valid in our case (Table 3 shows $|\beta_{K^*}| > |\beta_{K_N}|$).

We will now discuss the results of each reaction separately and after in Section 4.2, compare our model with others applied to $0^-\frac{1}{2}^+$ hypercharge-exchange.

(i) $\pi^- p \to K^o \Lambda(\Sigma^o)$

As stated earlier in this section, the mass resolution of the recoil hyperon in this experiment was such that the Λ and Σ^o could not be distinguished. Since, in principle, these are distinguishable reactions:

$$\frac{d\sigma}{dt}(\pi^- p \to K^o \Lambda(\Sigma^o)) = \frac{d\sigma}{dt}(\pi^- p \to K^o \Lambda) + \frac{d\sigma}{dt}(\pi^- p \to K^o \Sigma^o) \tag{4.1}$$

Using this condition, we minimized on the data, to get the momentum transfer distributions shown in Fig.3. The s- and t-dependence are extremely well represented.

Having determined the Regge parameters, we calculated the following reactions and compared the predictions with experiment.

(ii) $\pi^- p \to K^o \Lambda.$

Differential cross-section data for this process exists at 7.91 GeV/c. Figures 4, 5 and 6 illustrate the momentum transfer distributions obtained with the various possible exchanges using the parameterization determined using (i). The ($K^*(890) + K_N(1420)$) 'pole + cut' distribution forms a good representation of the data. All three figures show the various pole, cut, and 'pole+cut' distributions, the last formed from the destructive interference of the first two.

In detail, we see that in Fig.4, the pole graph has a nonsence zero, caused by $\alpha_{K^*} = 0$, at around $t \simeq -0.35\ (GeV/c)^2$. The cut has a kinematic dip slightly further in at $t \simeq -0.3\ (GeV/c)^2$. Fig.5 displays the $K_N(1420)$ contribution . Here we have no nonsense zeros or dips as $\alpha_{K_N} = 0$ is a right-signature point. Fig. 6 shows the $K^*(890) + K_N(1420)$ contribution which is compared with experiment. The data exhibits a dominance of the non-flip amplitude in the forward direction, and this is correctly reproduced by our model.

Similarly figures 7,8, and 9 show the contributions to the Polarization for $\pi^- p \to K^0 \Lambda$ at 6 GeV/c. As expected, all pole contributions are zero, and for the $K^*(890)$ exchange, the cut graph has a dip in approximately the same place as the cut contribution to the differential cross-section. Hence, we get a corresponding dip in the 'pole+cut' graph.

Fig.9 shows the 'pole+cut' contribution for $\left(K^*(890) + K_N(1420)\right)$ exchanges compared with experiment. Agreement is obtained for $|t| < 0.3\ (GeV/c)^2$, but we fail to obtain the turnover required to get the negative polarization at $t \simeq -0.35\ (GeV/c)^2$. We notice that we have $K^*(890)$ dominance in the 'pole+cut' graph.

(iii) $\underline{K^- n \to \pi^- \Lambda.}$

The theoretical prediction for the differential cross section for this reaction is plotted against the experimental data at 4.25 GeV/c[45] in Fig.10 . The normalization in the forward direction is reproduced, but the theory predicts too much scattering for large t.

In Fig.11 the theoretical and experimental polarizations[45] compared. The theory does not represent the data.

(iv) $\underline{K^- n \to \pi^- \Sigma^o}$.

Fig. 12 shows a comparison of the recent data[45] on the differential cross section for this reaction at 4.25 GeV/c with the prediction of this model. The agreement is most encouraging. Both the forward normalization and the t-dependence are well reproduced.

The polarization distribution for which no data exists at present is shown in Fig.13.

(v) $\underline{\pi^+ p \to K^+ \Sigma^+}$.

The high energy experimental data on $d\sigma/dt$ for this reaction has been measured by two experimental groups [8,9]. In Fig.14 the results of our calculations are compared with the data of Ref.8. Both the normalization and t-dependence of the model are consistent with the data. A plot of the momentum-transfer distributions and the corresponding experimental data of Ref.9 is shown in Fig.15. We observe that in this case we do not obtain the correct normalization. The right t-dependence is obtained out to about $t = -.4\,(GeV/c)^2$, but beyond this there appears to be some structure which is not reproduced by our model. Since much of this data is at low energy, and this structure is not present at the highest available energy, we do not take this disagreement in t-dependence too seriously.

In Fig. 16, 17, 18 the polarization predictions are compared with the available data[8, 9, 10]. Fig. 16 and 18 show that the

polarization is small and negative for $|t| < .3$. However, between $t = -.3$ and $t = -.5$ the data shows a dramatic change to a large positive value of about $.7$ at all energies, and this persists to larger values of t. Our model correctly reproduces the polarization for $|t| < .3$, which corresponds to the forward peak region in the differential cross-section but beyond this the model fails.

(vi) $\underline{K^- p \to \pi^- \Sigma^+}$.

Our prediction of the differential cross section for this reaction is compared with the available experimental data[46, 47] in Fig.19. As in the previous reaction, (v), we fail to obtain the correct normalization, although the t-dependence is reasonable. Since reactions (v) and (vi) are related by charge conjugation at the meson vertex, the $K^*(890)$ contribution simply changes sign from one reaction to the other. However, the $K^*(890)$ residue is approximately twice the $K_N(1420)$ residue and therefore this change in sign produces little difference in the forward normalizations of these two reactions, and in the forward direction $\frac{d\sigma}{dt}(K^- p \to \pi^- \Sigma^+) \approx 2 \frac{d\sigma}{dt}(\pi^+ p \to K^+ \Sigma^+)$ experimentally. Fig. 20 shows the prediction for the polarization of reaction (vi) at 8.0 GeV/c. The only data existing for this is at 3 GeV/c. This data has the opposite sign to our prediction.

As explained circa equation (3.15), in the numerical work involving the partial-wave expansion, a finite number of partial-waves was employed. 20 were used together with a 48-point Gaussian quadrature for the numerical integration. This was checked using 30-partial waves together with a 512-point Gaussian quadrature. The results did not alter significantly.

4.2 Other phenomenological models applied to $0^-\frac{1}{2}^+$ hypercharge-exchange reactions.

We feel that within the limitations and restrictions of our model, the agreement with experiment is satisfactory except for the polarizations of $\pi^- p \to K^0 \Lambda$, $K^- n \to \pi^- \Lambda$ and $\pi^+ p \to K^+ \Sigma^+$ for $|t| > 0.3\ (GeV/c)^2$. These crossover effects have been obtained in 3 other models, but in 2 this is a somewhat artificial effect. We shall now discuss these models in detail.

A previous model was that of Reeder and Sarma[39], who used a pure Regge pole model with SU(3) symmetry for the residues. As this symmetry is not large enough to relate the F/D ratios for $K^*(890)$ and $K_N(1420)$ exchanges, these were left free and not related by SU(6) as in our model. In fact, the SU(6) relations were not verified by Reeder and Sarma. The detailed breakdown of the model was as follows. They had 17 free parameters of which 8 were residue ones corresponding to vector and tensor exchanges in the non-flip and flip amplitudes of the Λ and Σ reactions; 4 were the 'so-called' scale parameters for vector and tensor exchanges and flip and non-flip amplitudes; 4 were the F/D ratio parameters for vector and tensor exchanges in the flip and non-flip amplitudes; and finally, a 'crossover' parameter in the form $\left(1 + \frac{t_0}{t}\right)$. Their trajectories were not varied, but obtained from those of the ρ and A_2 determined in $0^-\frac{1}{2}^+$ charge-exchange scattering by breaking SU(3) symmetry. They just displaced them to make them pass through the $K^*(890)$ and $K_N(1420)$ poles expectively. However, the $K^*(890)$ trajectory was linear while the $K_N(1420)$ one was quadratic. Of course, with this number of parameters they could not help, but be reasonably successful in explaining the data.

The other two models were both Reggeized absorption models and were published after our work. They were both constructed using non-flat Pomerons in the cut, and were specifically constructed to explain polarizations mentioned in the first paragraph.

The first model was that of Krzywicki and Tran Thanh Van[40], who used both strong exchange degeneracy for their trajectories and a non-flat Pomeron of slope 0.4 $(GeV/c)^{-2}$. Absorptive corrections were introduced using an impact parameter representation, but their model was rather limited in the sense that they just tried to predict one polarization given another. In fact, they considered just four reactions. They fitted the 3 GeV/c polarization data, including the cross-overs of $\pi^- p \to K^0 \Lambda$ and $\pi^+ p \to K^+ \Sigma^+$ and from this, they predicted the reactions which have the same SU(3) couplings, but the sign of the vector contribution reversed, $K^- n \to \pi^- \Lambda$ and $K^- p \to \pi^- \Sigma^+$ with considerable success.

A more complete analysis was carried out by Myers, Noirot, Rimpault and Salin[41], who again used strong exchange degeneracy for the $K^*(890)$ and $K_N(1420)$ trajectories, but this time the Pomeron had a shallower slop of 0.28 $(GeV/c)^{-2}$. They had essentially one free parameter, which was a SU(3) mixing one in the B invariant amplitude. However, an interesting feature of their model that they chose their B to be crossing symmetric as the antisymmetric solution gave too large a non-flip amplitude. Hence, an extra (s-u) factor was required external to the B.

Meyers et. al successfully fitted the differential cross-section data of the 6 reactions named in (4.1) and $K^- n \to \pi^0 \Sigma^-$ and $\pi^- p \to K^0 \Sigma^0$ and also successfully explained the experimental fact

$$\frac{d\sigma}{dt}(K^-p \to \pi^-\Sigma^+) \approx 2\frac{d\sigma}{dt}(\pi^+p \to K^+\Sigma^+) \qquad (4.2)$$

which is difficult to obtain for exchange-degenerate trajectories without cuts. From these differential cross-sections, they successfully predicted the polarizations for $\pi^-p \to K^0\Lambda$ at 3.1 GeV/c, and $\pi^+p \to K^+\Sigma^+$ between 3 and 7 GeV/c, but failed for $K^-n \to \pi^-\Lambda$ at 3.1 and 4.25 GeV/c, where a non-existent crossover is predicted.

4.3 Conclusion.

We feel that the great virtue of our model is that we have a large enough symmetry scheme to relate all non-exotic two-body meson baryon scattering processes and also that the integration involved in the absorptive corrections is carried out numerically. This latter point means that we can avoid approximating such functions as the Γ-function or trignometric functions, which are not expressible as polynomials or exponentials, in the Fourier-Bessel transform so as to do this integral analytically. The Γ-function and trignometric functions, as appearing in the Regge formalism, are an essential part of the physics.

However, largely from 'hindsight', we are able to make several suggestions for the improvement of this model. Firstly, the diagrams show that a considerable relative normalization problem may exist, in spite of the fact that normalization errors in the data, typically of the order of 20-30% (e.g. as shown in Figs. 14 and 15) are present. This normalization problem may be related to the fact that

considerable difficulties are known to exist in the determination of the Λ KN and Σ KN coupling constants and their agreement with SU(6) symmetry. However, SU(6) seemed to work well for $K^*(890)$ exchange in the U(6,6) absorptive peripheral model as applied to photoproduction reactions, but not in the Reader and Sarma's analysis of $0^-\frac{1}{2}^+$ hypercharge-exchange reactions. Also the $K_N(1420)$ remains largely an unknown quantity, so a considerable amount of work needs to be carried out in this field.

Secondly, we put the final state absorption parameters equal to the initial state ones as no elastic scattering data exists for $K^+\Sigma^+$ elastic scattering etc. Obviously, resolution of this questionable solution must await data.

Thirdly, the use of unequal mass kinematics may have been important. This was certainly the case in the Reggeized U(6) ⊗ U(6) ⊗ O(3) absorption model as applied, using the vector dominance model, to $\gamma p \to \pi^- \Delta^{++}$. In the differential cross-sections, the forward turnover was due completely to the unequal mass kinematics.

Finally, as discussed before, a Gaussian using a ~~travelling~~ moving pole could have been used.

Reaction	Baryon vertex		Meson vertex	
	$K^*(890)$ and $K_N(1420)$		$K_N(1420)$	$K^*(890)$
	$D + \frac{2}{3}F$	F	D-type	F-type
$\pi^- p \to K^o \Lambda$	$-\sqrt{3}$	$-\sqrt{3}$	$\sqrt{2}$	$-\sqrt{2}$
$\pi^- p \to K^o \Sigma^o$	$\frac{1}{3}$	-1	$\sqrt{2}$	$-\sqrt{2}$
$K^- n \to \pi^- \Lambda$	$-\sqrt{3}$	$-\sqrt{3}$	$\sqrt{2}$	$\sqrt{2}$
$K^- n \to \pi^- \Sigma^o$	$-\frac{1}{3}$	1	$\sqrt{2}$	$\sqrt{2}$
$\pi^+ p \to K^+ \Sigma^+$	$\frac{\sqrt{2}}{3}$	$-\sqrt{2}$	$\sqrt{2}$	$-\sqrt{2}$
$K^- p \to \pi^- \Sigma^+$	$\frac{\sqrt{2}}{3}$	$-\sqrt{2}$	$\sqrt{2}$	$\sqrt{2}$

TABLE 1.

D and F couplings.

Channel	p_{lab}	ν_i^{-1} (GeV)	c_i
$\pi^+ p$	3.00	.27	.89
	3.25	.27	.87
	4.00	.27	.84
	5.05	.27	.82
	5.40	.27	.81
	7.00	.27	.79
$\pi^- p$	6.00	.26	.79
	7.91	.26	.76
	8.00	.26	.76
	10.00	.26	.74
	11.20	.26	.73
$K^- p$	3.50	.26	.79
	4.07	.26	.78
	4.25	.26	.77
	5.47	.26	.73

TABLE 2.

Absorption coefficients.

Trajectory	$K^*(890)$	$K_N(1420)$
α_o	- 0.829	- 0.984
α_1	1.098	1.177
α_2 (GeV/c)$^{-2}$	0.840	0.761
β (GeV/c)$^{-1}$	- 7.162	4.712
No. of data points	76	
χ^2	65	

TABLE 3.

Regge parameters.

FIGURE CAPTIONS

Figure 1. The pole + cut diagram.

Figure 2. Plot of $\alpha(t)$ against t for the $K^*(890)$ trajectory (—) and the $K_N(1420)$ trajectory (------). Parameters from Table 3.

Figure 3. Differential cross section for $\pi^- p \to K^0 \Sigma^0$. Data from ref. 42.

Figure 4. Contributions from the pole (----), cut (—— - ——), and pole + cut (—) to the differential cross-section for $\pi^- p \to K^0 \Lambda$ using only the $K^*(890)$ exchange with parameters from Table 3.

Figure 5. Contributions from the pole (-----), cut (— - — -), and pole + cut (—) to the differential cross-section for $\pi^- p \to K^0 \Lambda$ using only the $K_N(1420)$ exchange with parameters from Table 3.

Figure 6. Contributions from the pole (----), cut (— - — -), and pole + cut (—) to the differential cross-section for $\pi^- p \to K^0 \Lambda$ using the $K^*(890)$ + $K_N(1420)$ exchanges with parameters from Table 3. Data from Ref.43.

Figure 7. Contributions from the pole (---), cut (— - —— -), and pole + cut (—) to the polarization for $\pi^- p \to K^0 \Lambda$ using only the $K^*(890)$ exchange with parameters from Table 3.

Figure 8. Contributions from the pole (---), cut (— - — - —) and pole + cut (—) to the polarization for $\pi^- p \to K^0 \Lambda$ using only the $K_N(1420)$ exchange with parameters from Table 3.

Figure 9. Contributions from the pole (----), cut (— - — - —), and pole + cut (—) to the polarization for $\pi^- p \to K^0 \Lambda$ using the $K^*(890)$ + $K_N(1420)$ exchanges with parameters from Table 3. Data from ref. 44.

Figure 10. Differential cross-section for $K^- n \to \pi^- \Lambda$. Data from Ref.45.

Figure 11. Polarization for $K^- n \to \pi^- \Lambda$. Data from ref.45.

Figure 12. Differential cross-section for $K^- n \to \pi^- \Sigma^0$. Data from ref.45.

Figure 13. Polarization for $K^- n \to \pi^- \Sigma^0$.

Figure 14. Differential cross-section for $\pi^+ p \to K^+ \Sigma^+$. Data from ref.8.

Figure 15. Differential cross-section for $\pi^+ p \to K^+ \Sigma^+$. Data from ref. 9.

Figure 16. Polarization for $\pi^+ p \to K^+ \Sigma^+$. Data from ref.10.

Figure 17. Polarization for $\pi^+ p \to K^+ \Sigma^+$. Data from ref.8.

Figure 18. Polarization for $\pi^+ p \to K^+ \Sigma^+$. Data from ref.9.

Figure 19. Differential cross-section for $K^- p \to \pi^- \Sigma^+$. Data from refs. 46 and 47.

Figure 20. Polarization for $K^- p \to \pi^- \Sigma^+$.

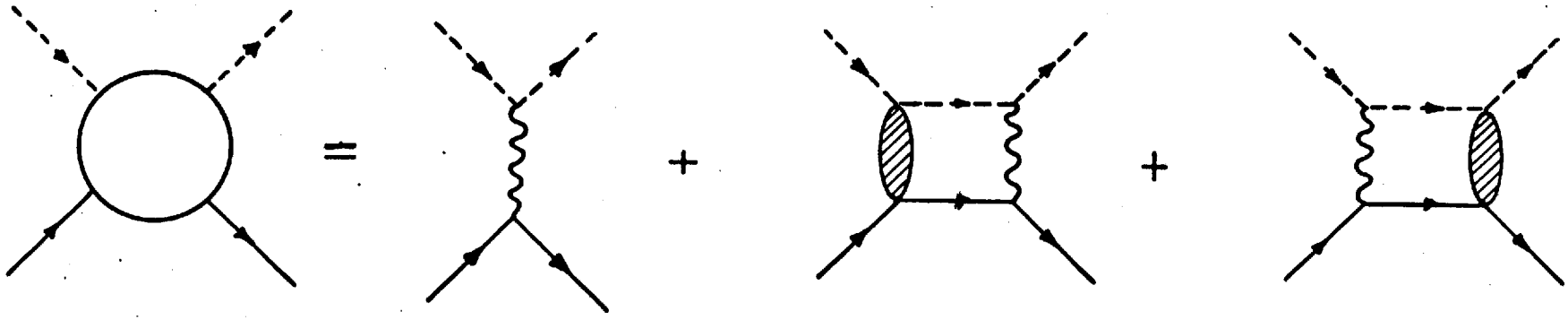

Fig. 1.

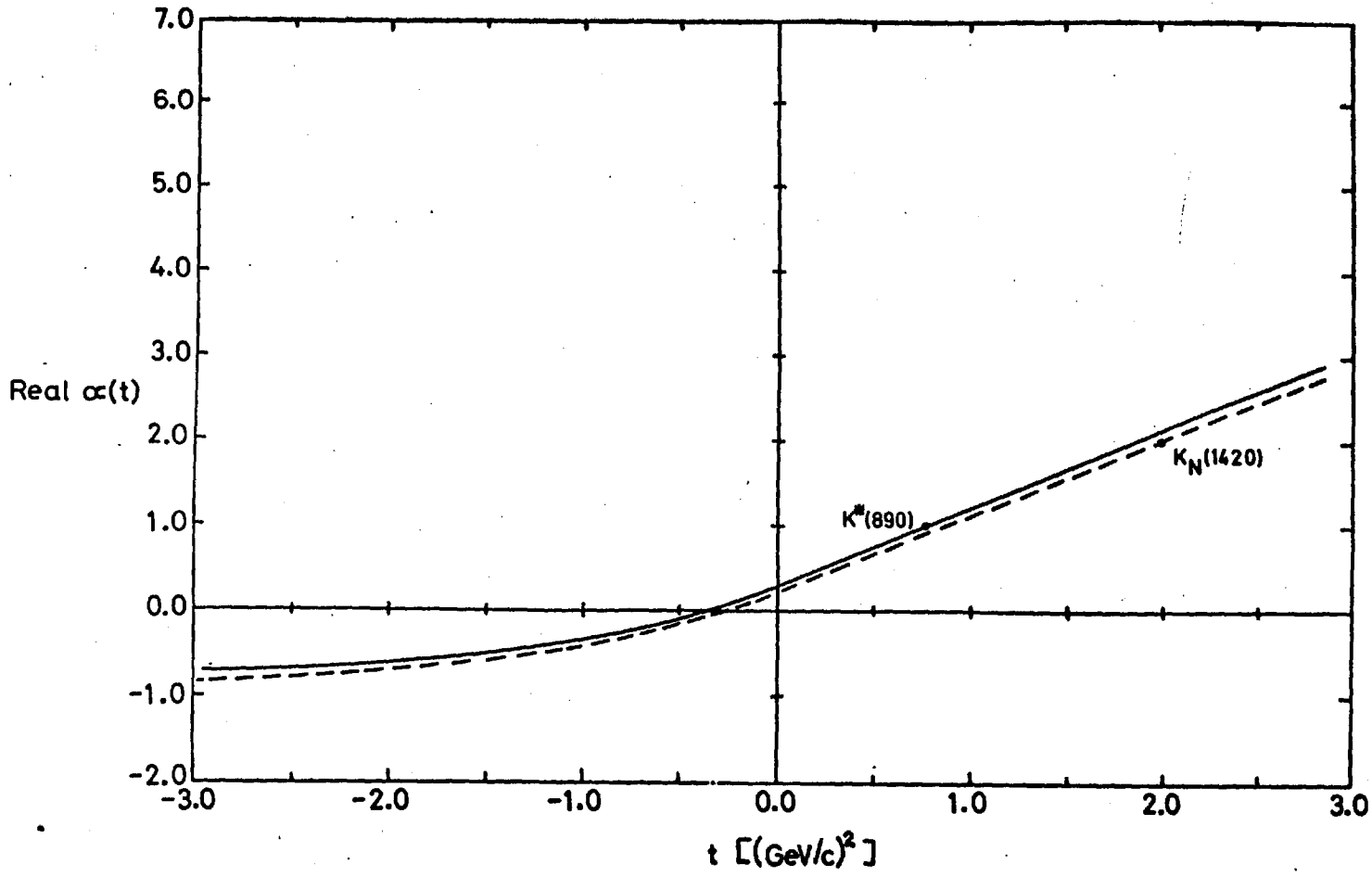
7.0
6.0
5.0
4.0
3.0
2.0
1.0
0.0
-1.0
-2.0
Real α(t)
-3.0
-2.0
-1.0
0.0
1.0
2.0
3.0
t [(GeV/c)²]
K*(890)
K_N(1420)

Fig. 2.

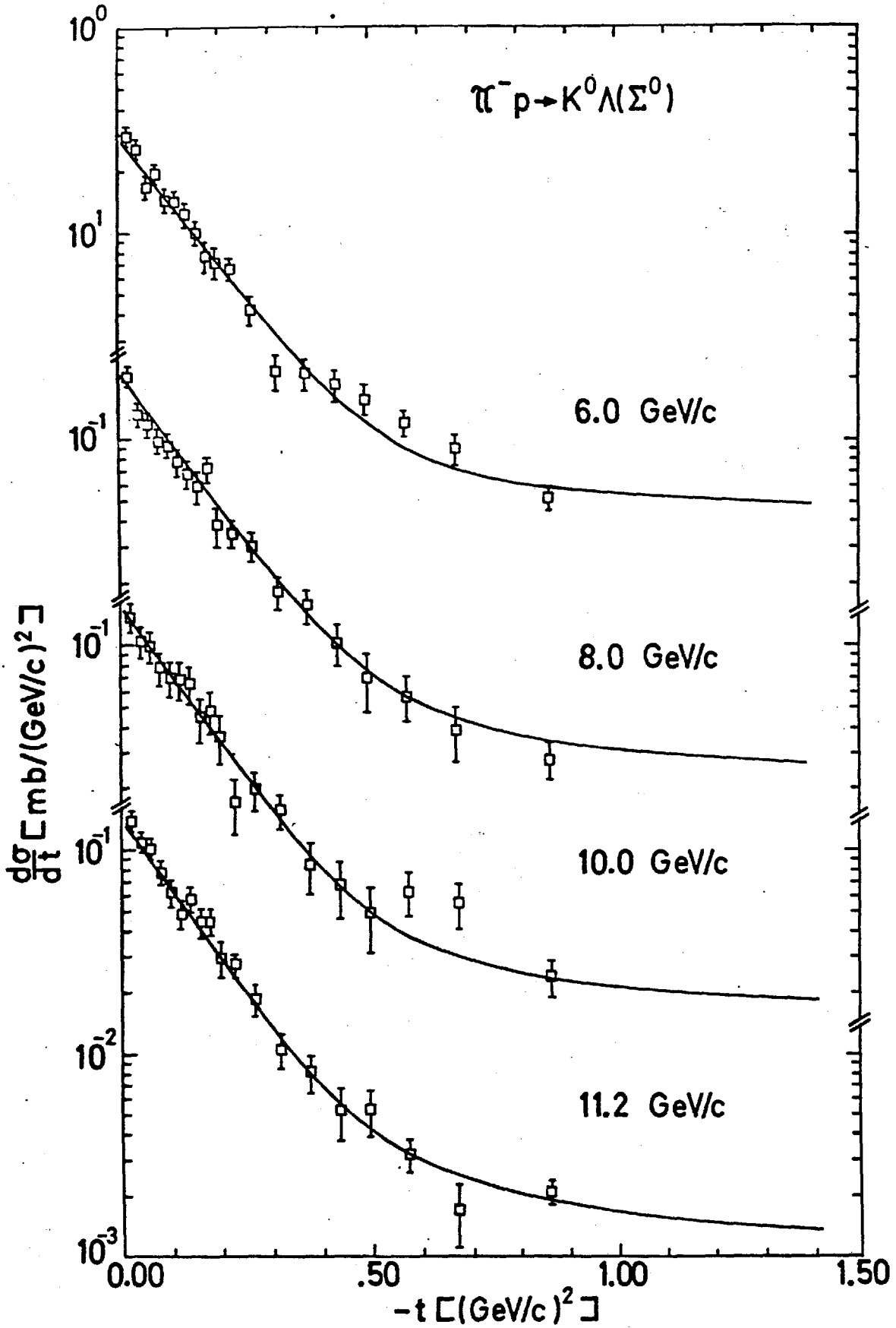
$\pi^- p \to K^0 \Lambda(\Sigma^0)$
6.0 GeV/c
8.0 GeV/c
10.0 GeV/c
11.2 GeV/c
$\frac{d\sigma}{dt}$ [mb/(GeV/c)^2]
$-t$ [(GeV/c)^2]
10^0
10^{-1}
10^{-1}
10^{-1}
10^{-2}
10^{-3}
0.00
.50
1.00
1.50

Fig. 3.

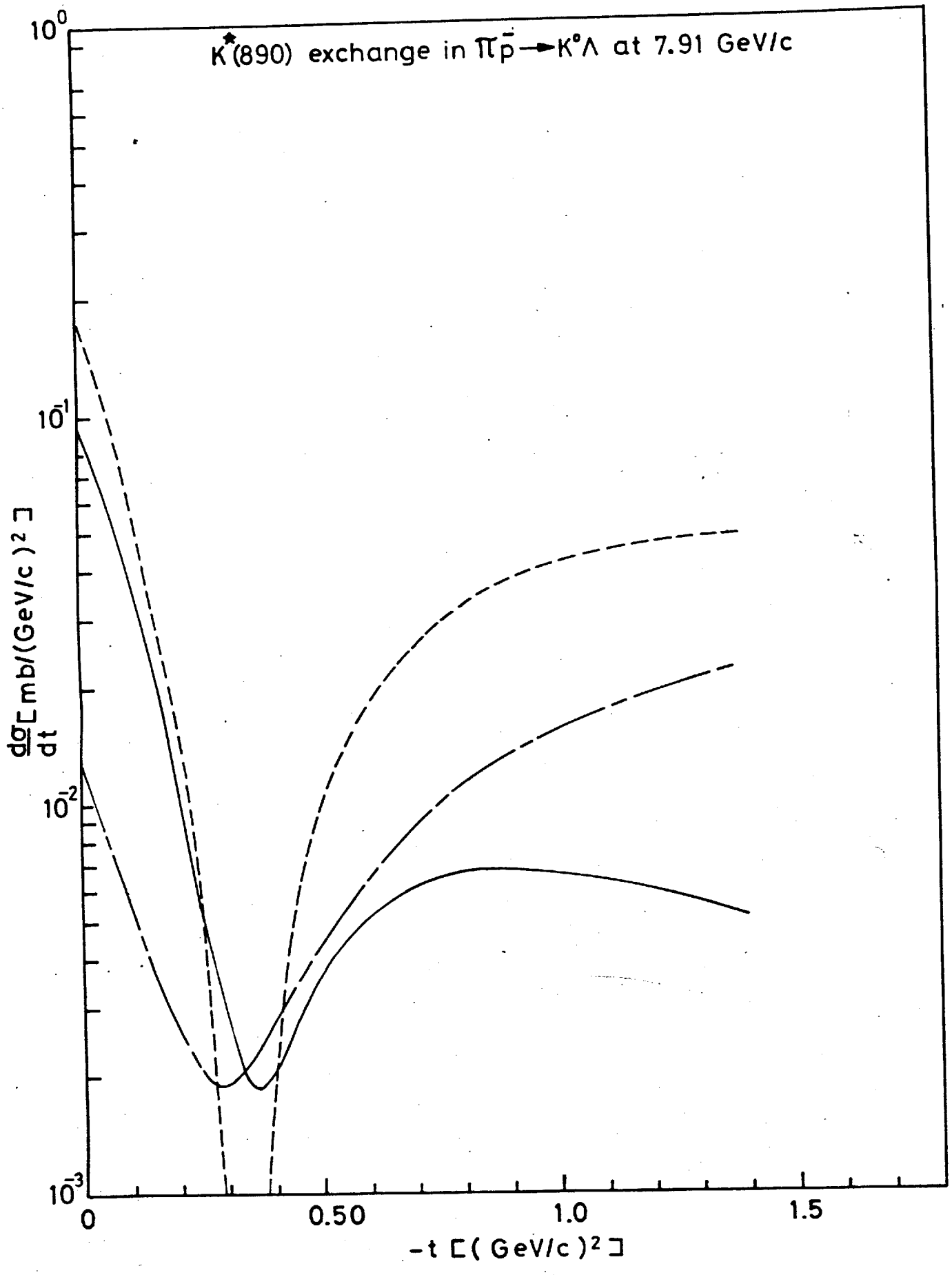
K*(890) exchange in π⁻p → K°Λ at 7.91 GeV/c
10⁰
10⁻¹
10⁻²
10⁻³
dσ/dt [mb/(GeV/c)²]
0
0.50
1.0
1.5
-t [(GeV/c)²]

Fig. 4.

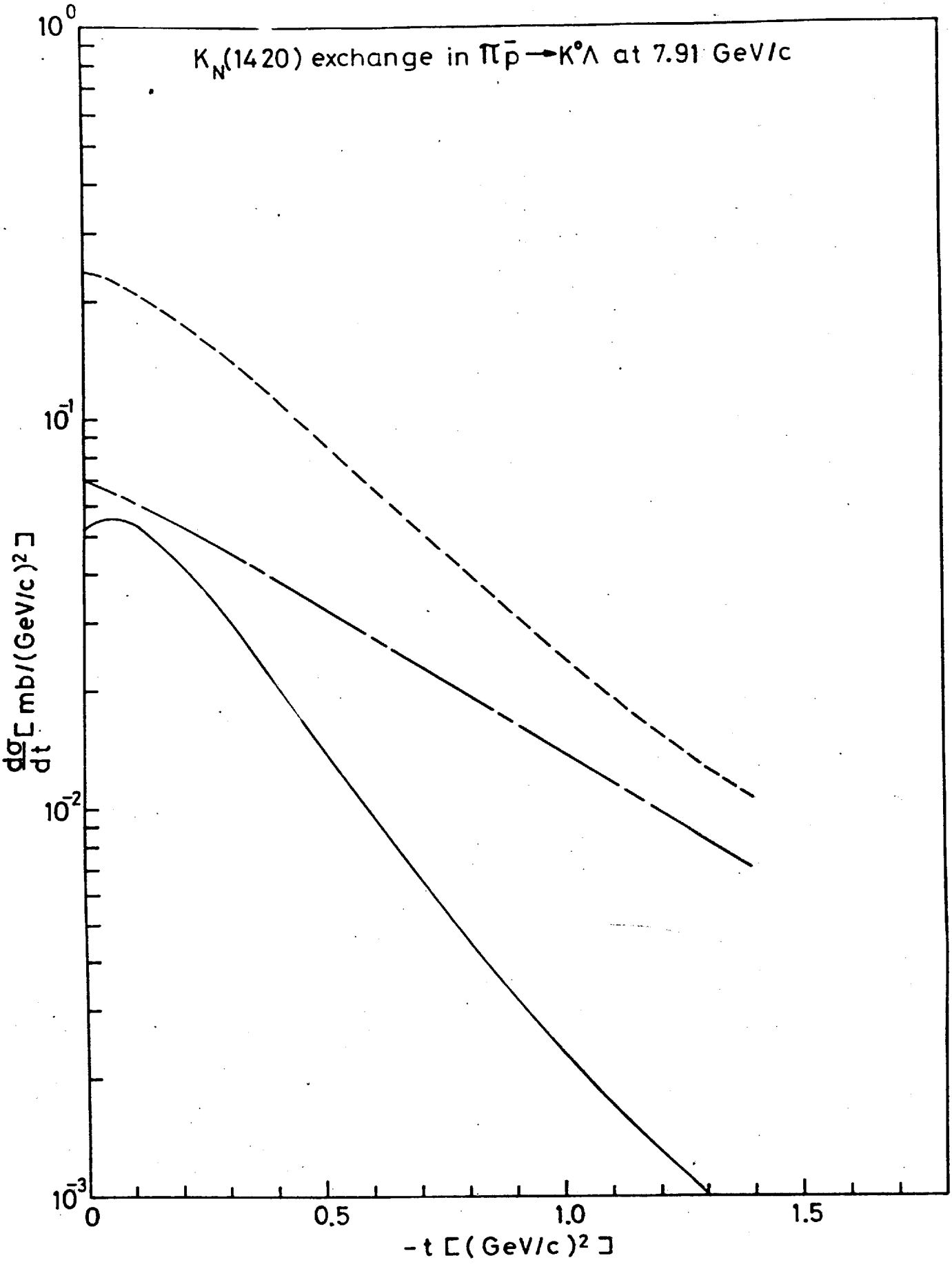
$K_N(1420)$ exchange in $\pi^- p \rightarrow K^0 \Lambda$ at 7.91 GeV/c
10^0
10^{-1}
10^{-2}
10^{-3}
$\frac{d\sigma}{dt}$ [mb/(GeV/c)^2]
0
0.5
1.0
1.5
$-t$ [(GeV/c)^2]

Fig. 5

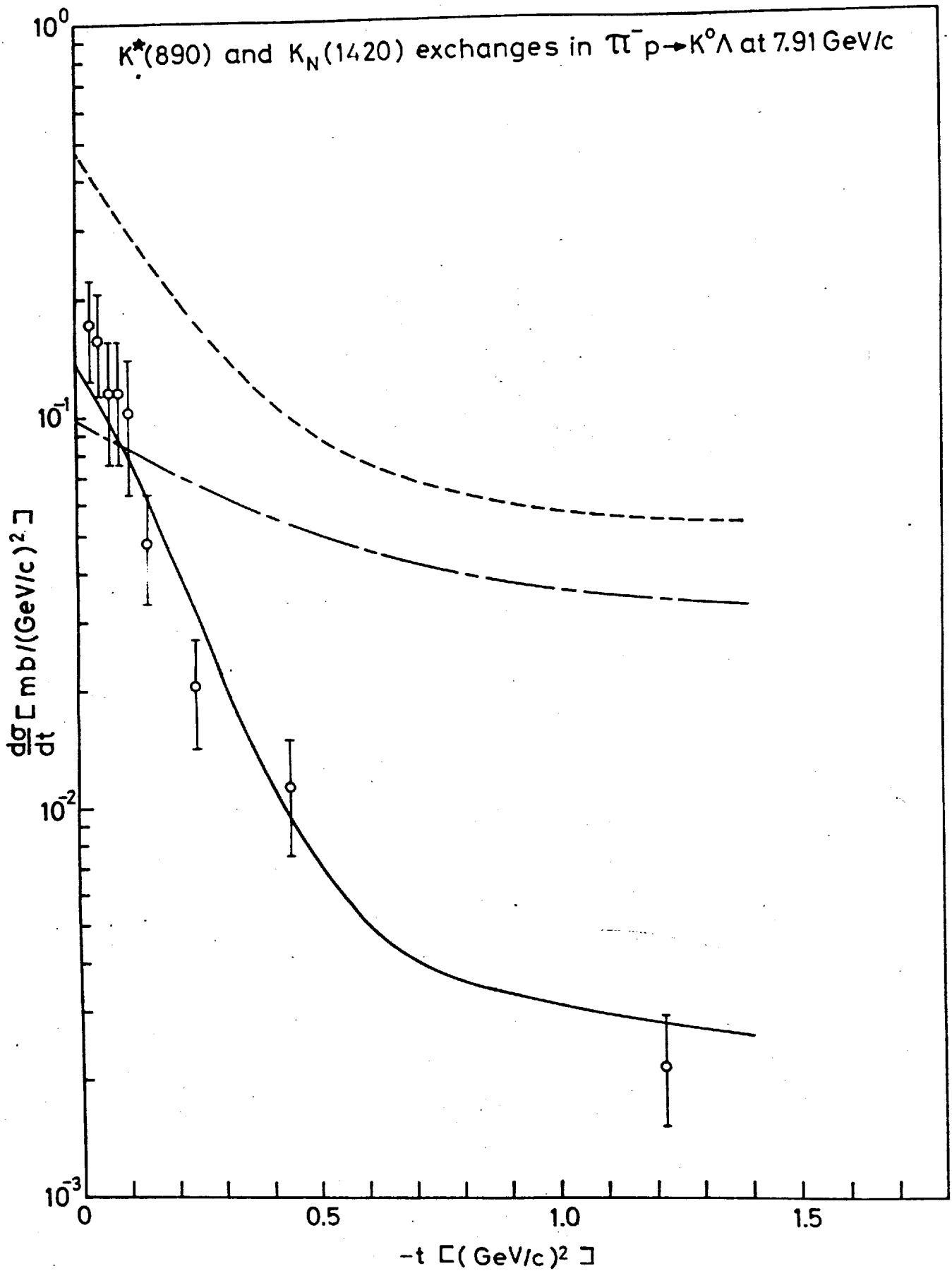
$K^*(890)$ and $K_N(1420)$ exchanges in $\pi^- p \to K^0 \Lambda$ at 7.91 GeV/c
10^0
10^{-1}
10^{-2}
10^{-3}
$\frac{d\sigma}{dt}$ [mb/(GeV/c)^2]
0
0.5
1.0
1.5
$-t$ [(GeV/c)^2]

Fig. 6.

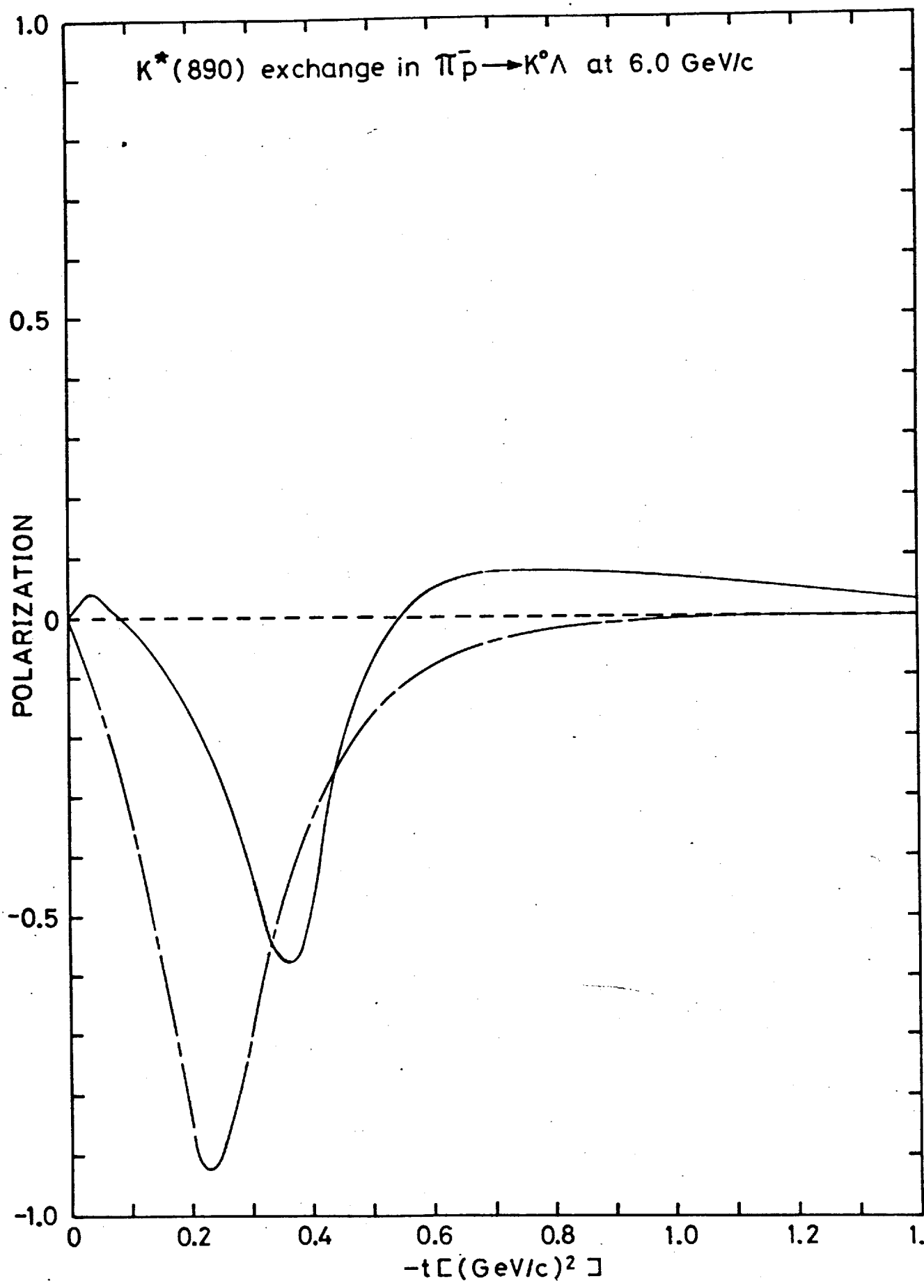
K*(890) exchange in π⁻p → K°Λ at 6.0 GeV/c
POLARIZATION
1.0
0.5
0
-0.5
-1.0
0
0.2
0.4
0.6
0.8
1.0
1.2
1.4
-t [(GeV/c)²]

Fig. 7.

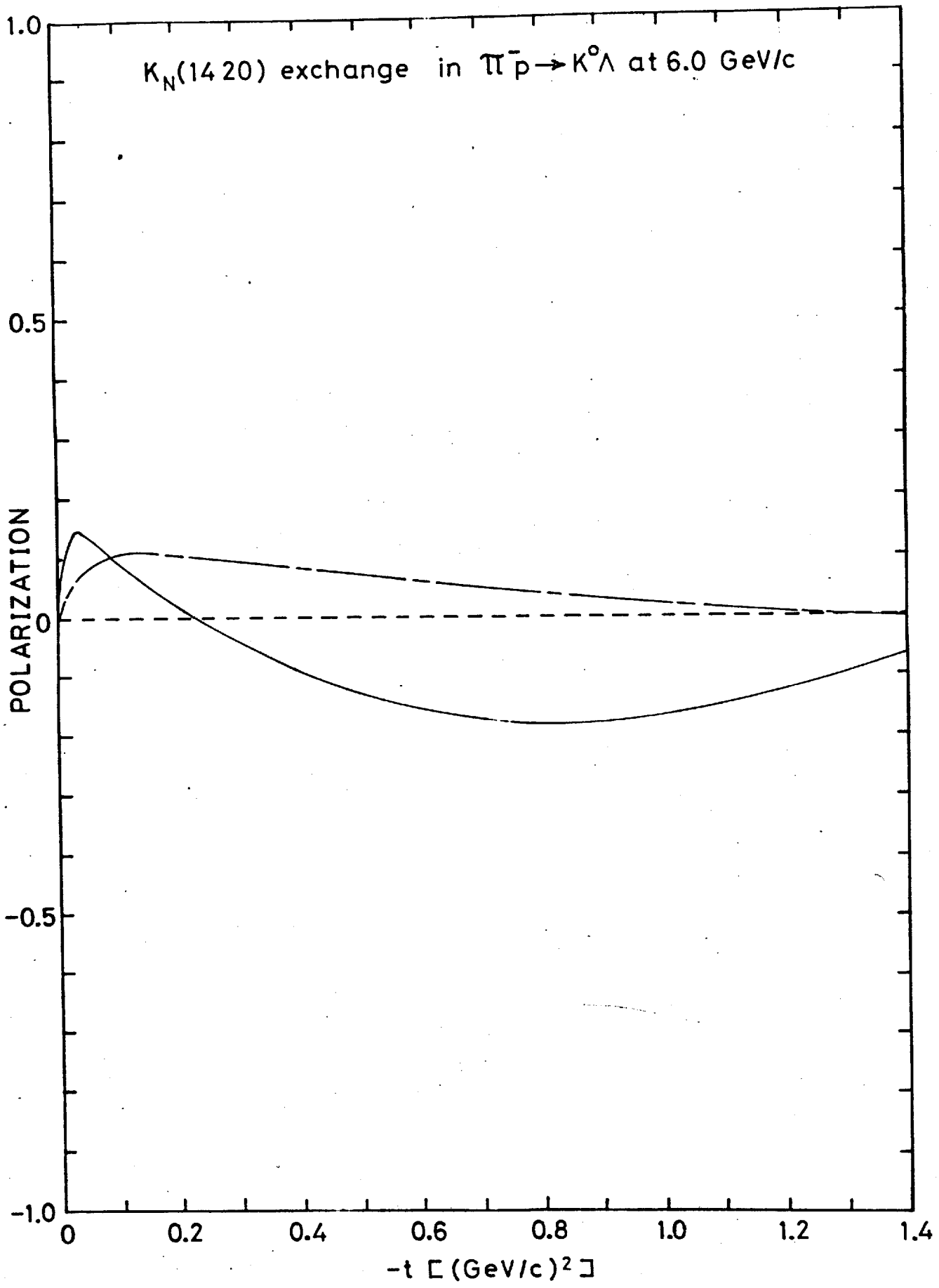
$K_N(1420)$ exchange in $\pi^- p \to K^0 \Lambda$ at 6.0 GeV/c
POLARIZATION
1.0
0.5
0
-0.5
-1.0
0
0.2
0.4
0.6
0.8
1.0
1.2
1.4
$-t$ [(GeV/c)^2]

Fig. 8.

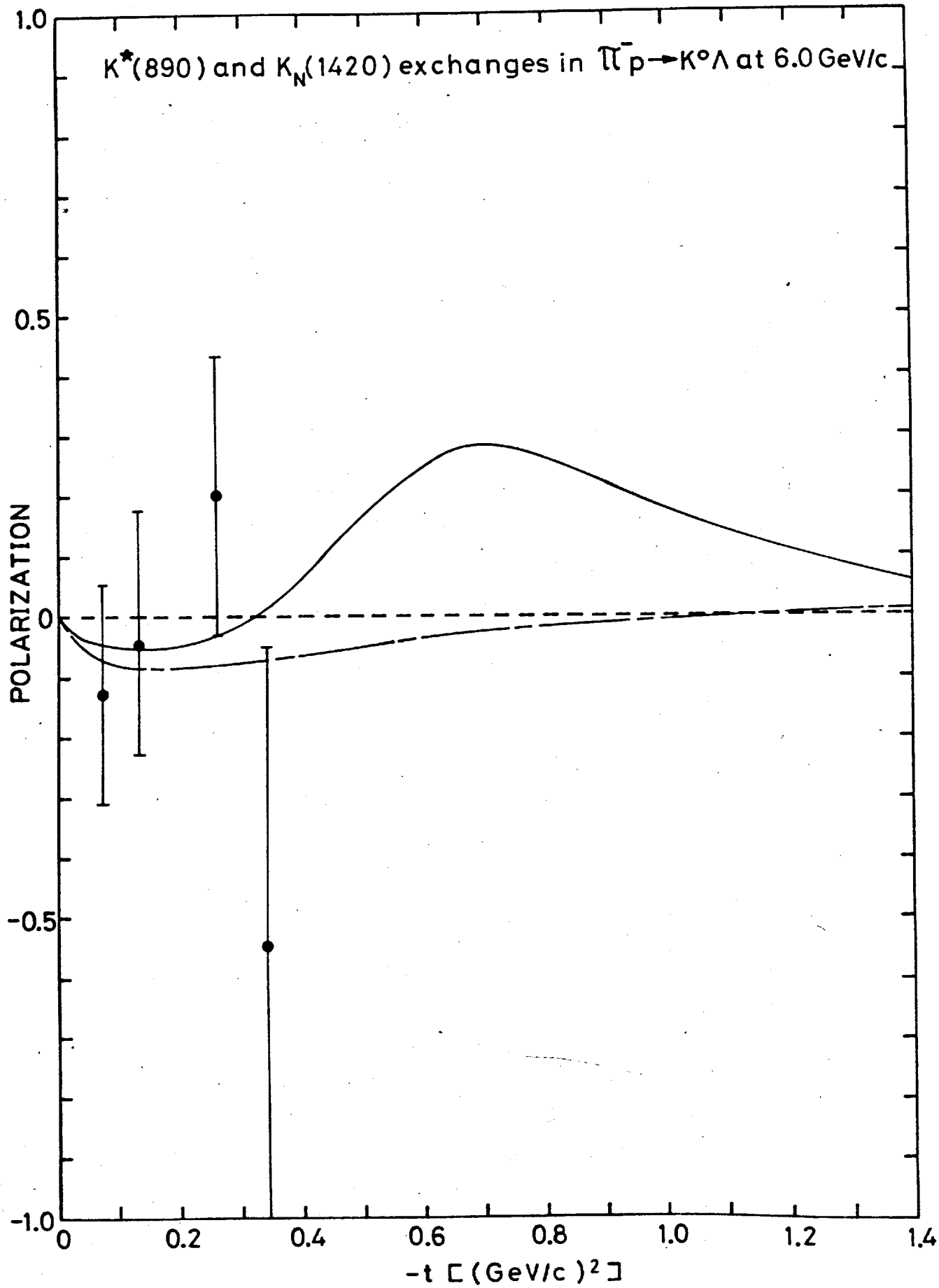
K*(890) and K_N(1420) exchanges in π⁻p→K°Λ at 6.0 GeV/c
POLARIZATION
1.0
0.5
0
-0.5
-1.0
0
0.2
0.4
0.6
0.8
1.0
1.2
1.4
-t [(GeV/c)²]

Fig. 9

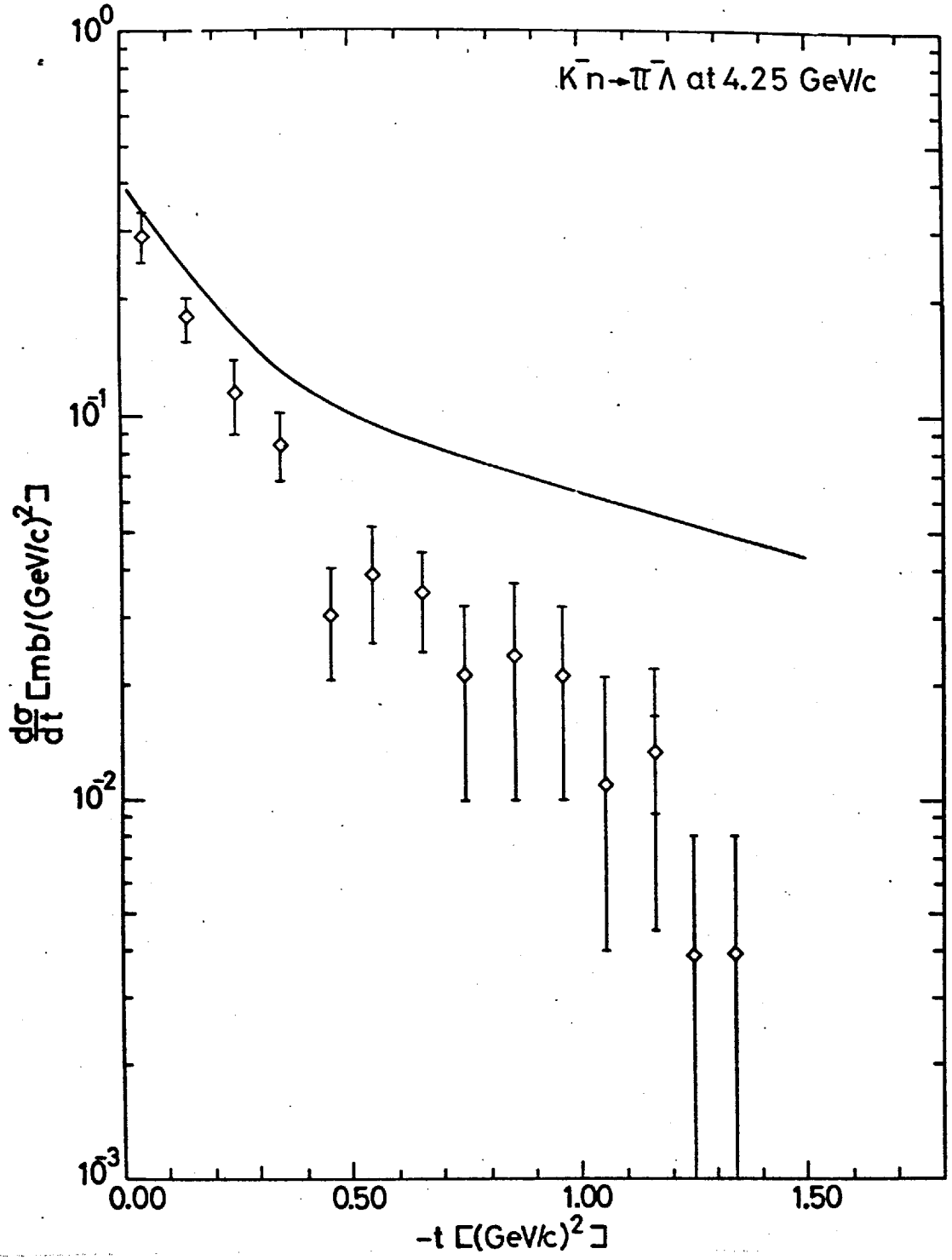
$K^-n \to \pi^-\Lambda$ at 4.25 GeV/c
10^0
10^{-1}
10^{-2}
10^{-3}
$\frac{d\sigma}{dt}$ [mb/(GeV/c)^2]
0.00
0.50
1.00
1.50
$-t$ [(GeV/c)^2]

Fig. 10.

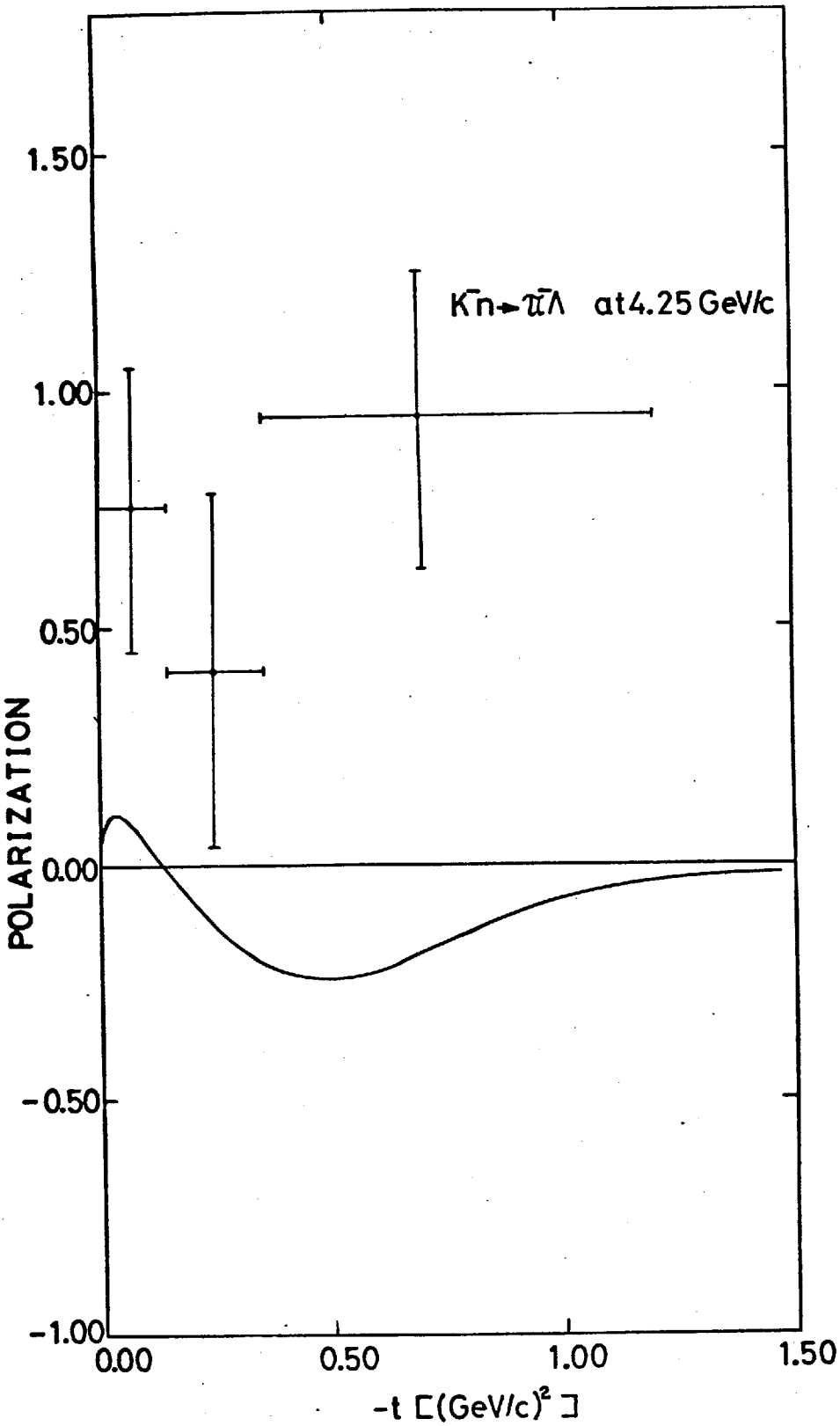
1.50
1.00
0.50
0.00
-0.50
-1.00
POLARIZATION
$K^-n \to \pi^-\Lambda$ at 4.25 GeV/c
0.00
0.50
1.00
1.50
$-t\ [(GeV/c)^2]$

Fig. 11.

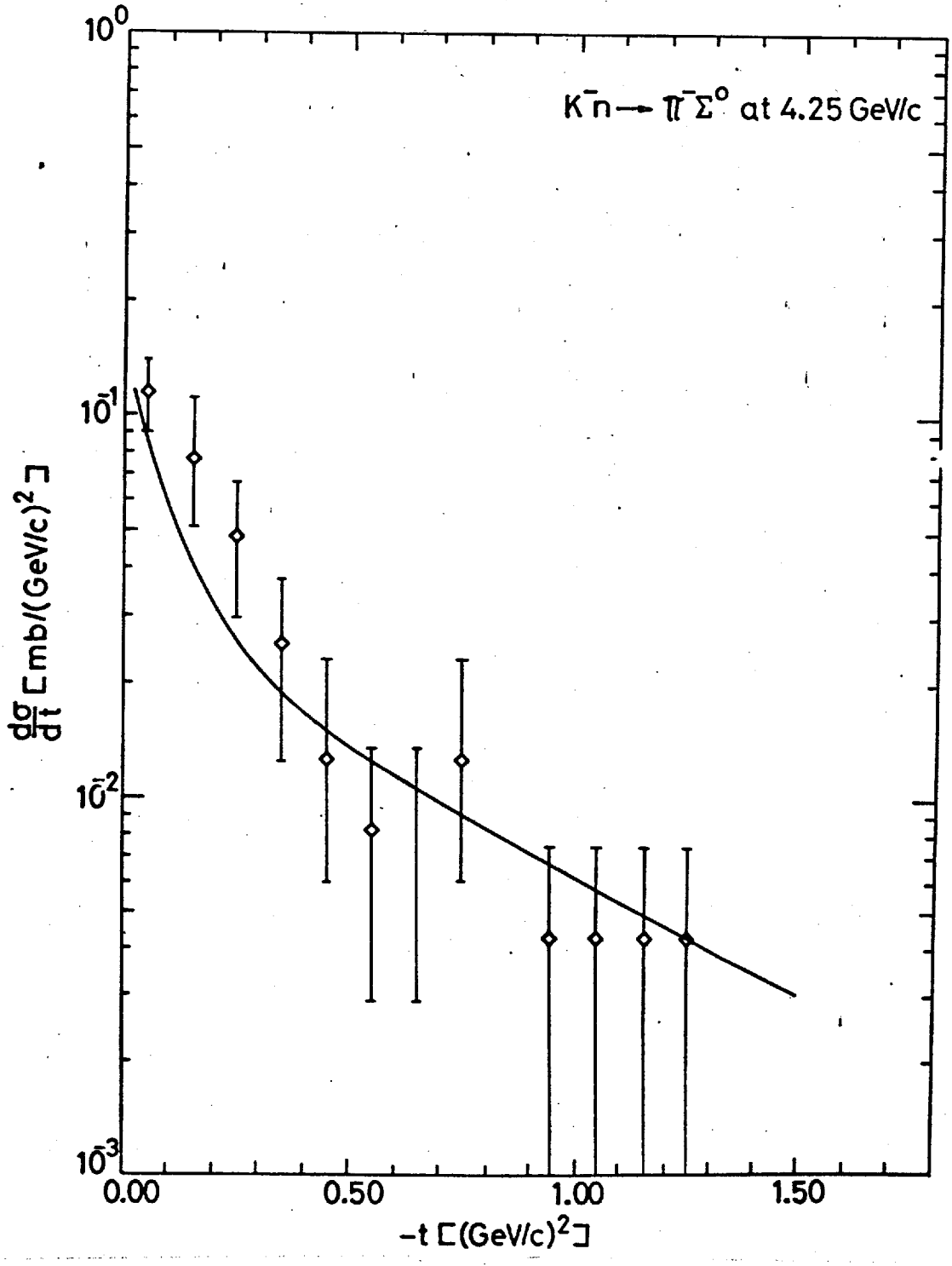
$K^-n \rightarrow \pi^-\Sigma^0$ at 4.25 GeV/c
10^0
10^{-1}
10^{-2}
10^{-3}
$\frac{d\sigma}{dt}$ [mb/(GeV/c)^2]
0.00
0.50
1.00
1.50
$-t$ [(GeV/c)^2]

Fig. 12.

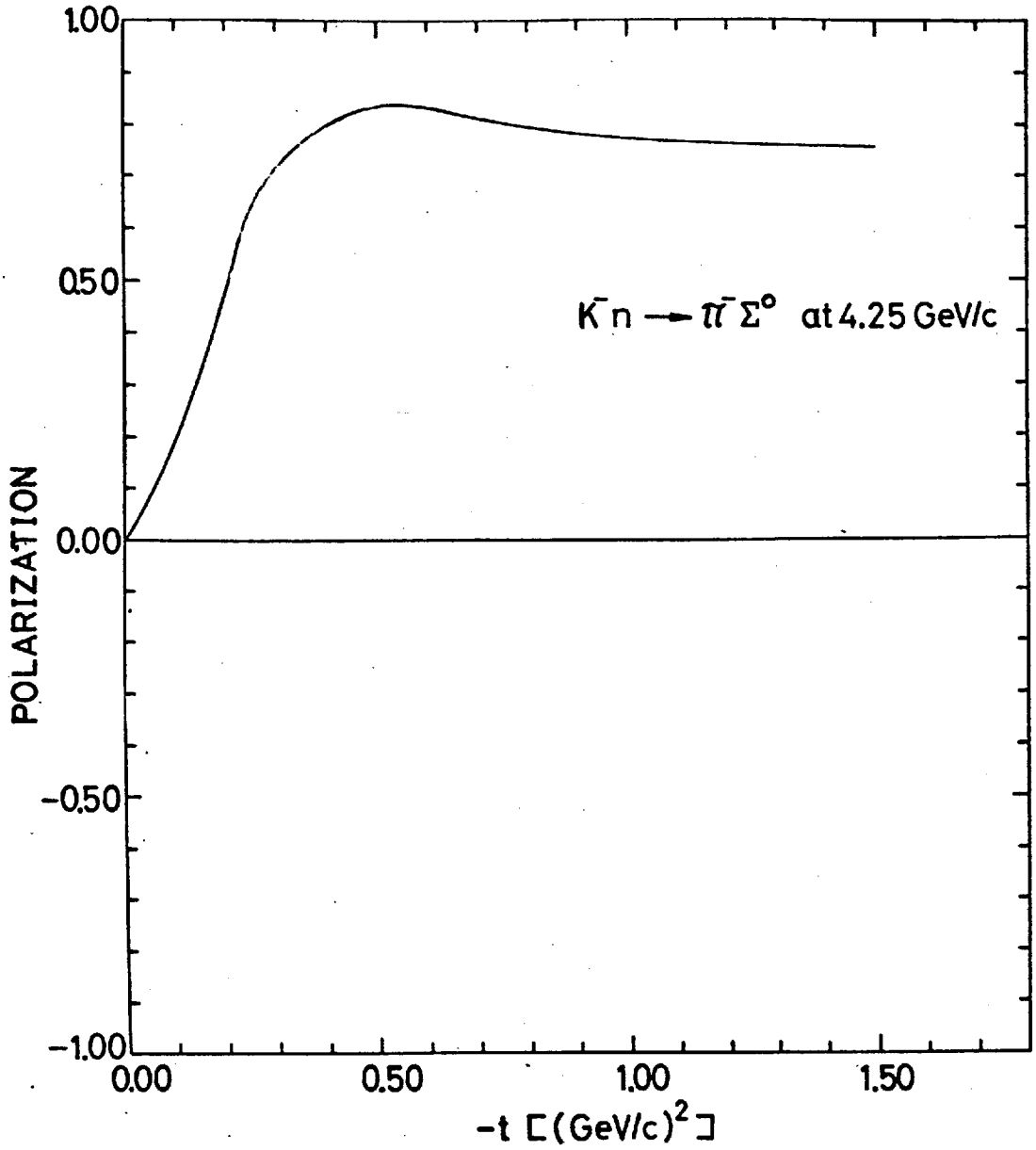
1.00
0.50
0.00
-0.50
-1.00
POLARIZATION
$K^- n \rightarrow \pi^- \Sigma^0$ at 4.25 GeV/c
0.00
0.50
1.00
1.50
$-t\ [(GeV/c)^2]$

Fig. 13

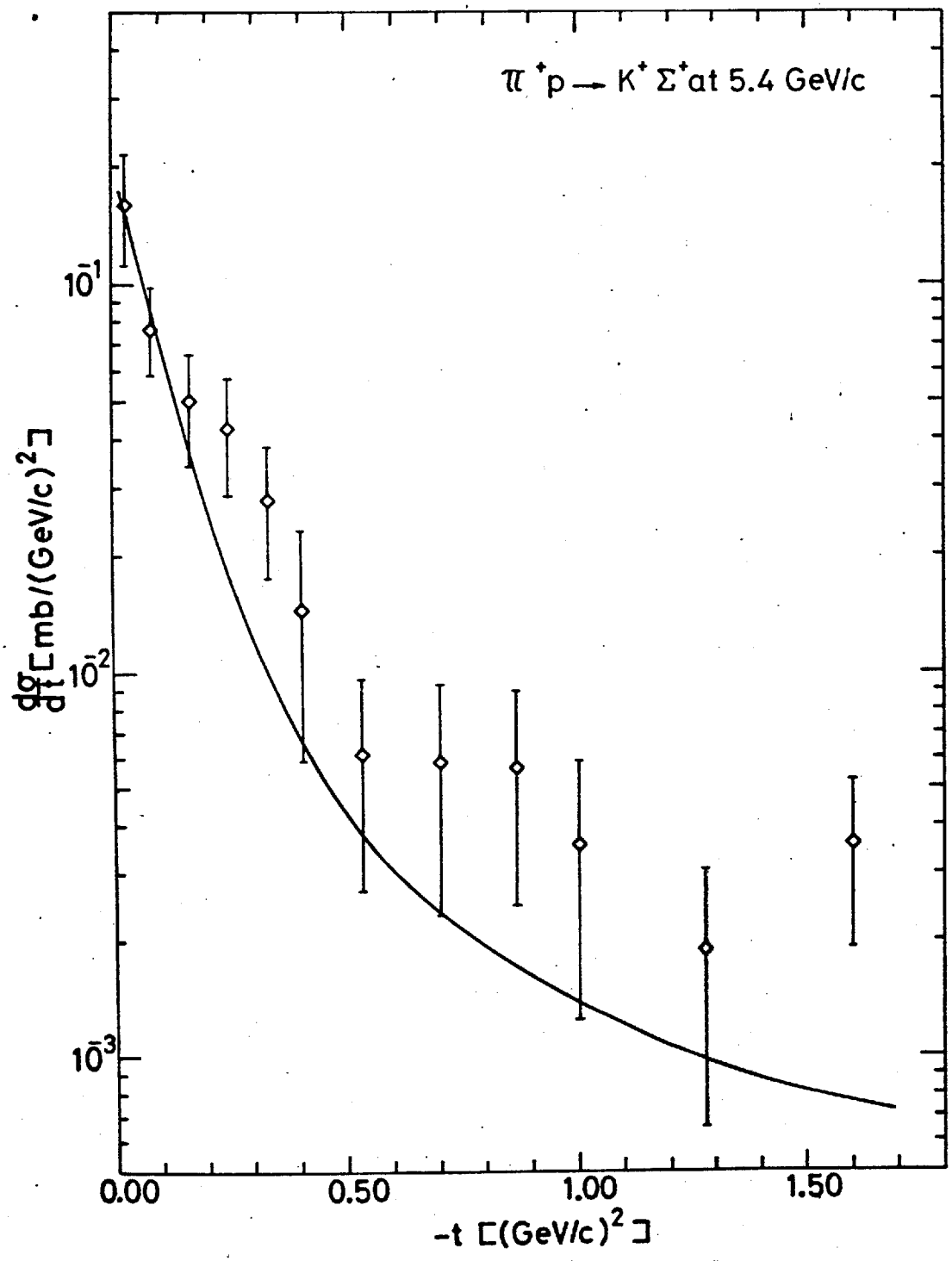
$\pi^+ p \rightarrow K^+ \Sigma^+$ at 5.4 GeV/c
$\frac{d\sigma}{dt}$ [mb/(GeV/c)^2]
10^{-1}
10^{-2}
10^{-3}
0.00
0.50
1.00
1.50
$-t$ [(GeV/c)^2]

Fig. 14.

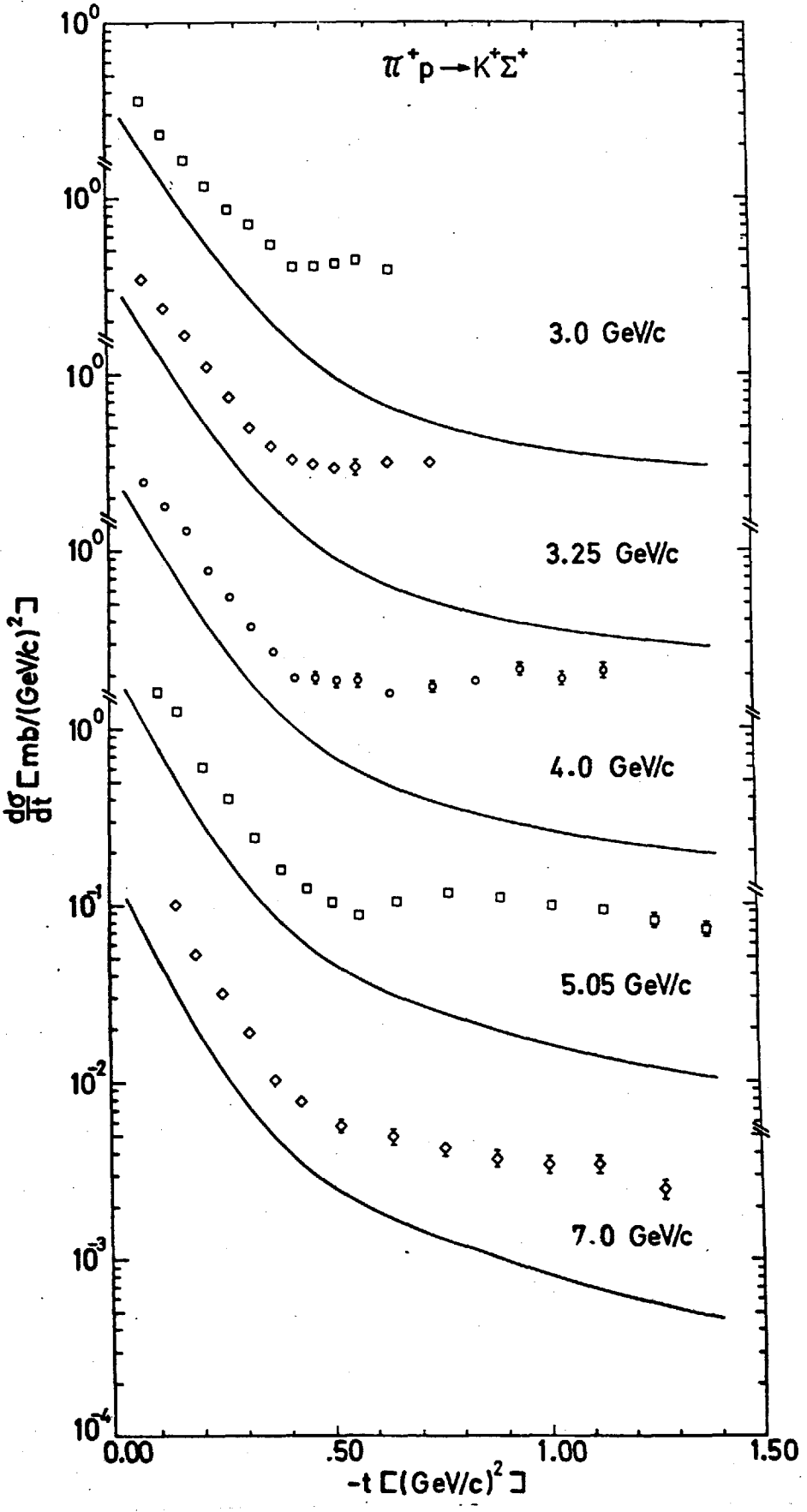
$\pi^+ p \rightarrow K^+ \Sigma^+$
3.0 GeV/c
3.25 GeV/c
4.0 GeV/c
5.05 GeV/c
7.0 GeV/c
$\frac{d\sigma}{dt}$ [mb/(GeV/c)^2]
-t [(GeV/c)^2]
10^0
10^{-1}
10^{-2}
10^{-3}
10^{-4}
0.00
.50
1.00
1.50

Fig. 15.

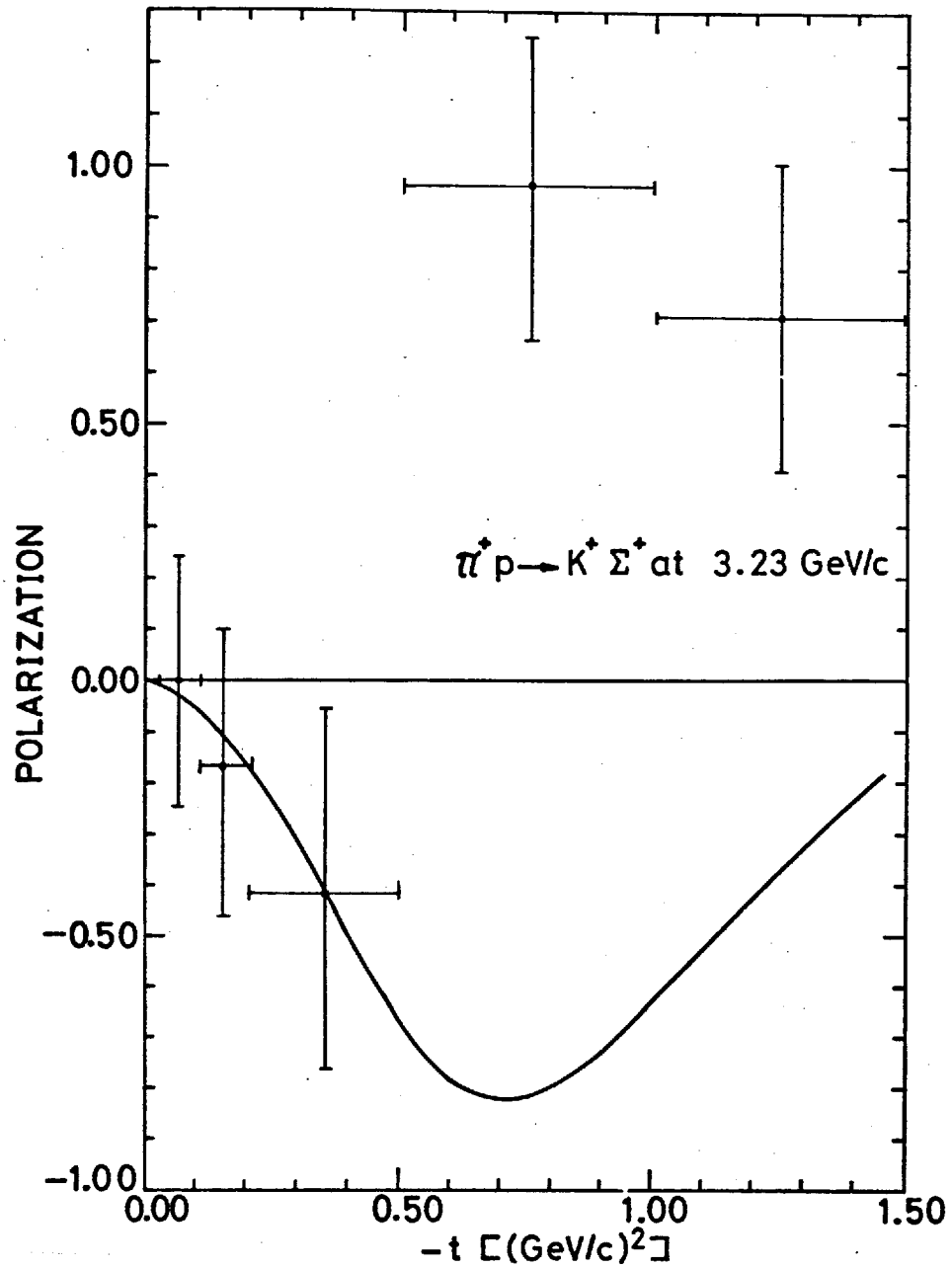
1.00
0.50
0.00
−0.50
−1.00
POLARIZATION
$\pi^+ p \rightarrow K^+ \Sigma^+$ at 3.23 GeV/c
0.00
0.50
1.00
1.50
$-t$ [(GeV/c)^2]

Fig. 16.

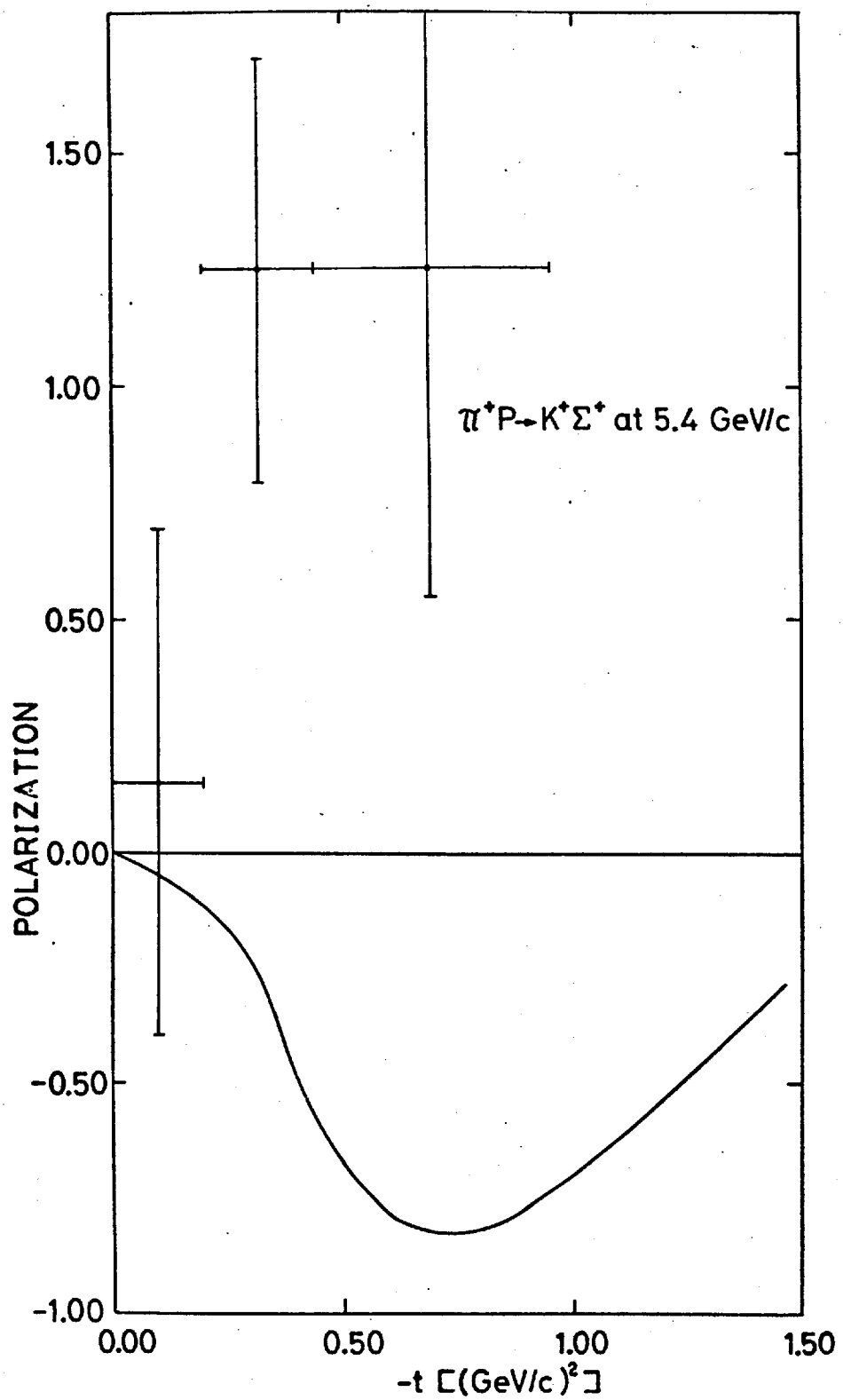
1.50
1.00
0.50
0.00
-0.50
-1.00
POLARIZATION
$\pi^+P \to K^+\Sigma^+$ at 5.4 GeV/c
0.00
0.50
1.00
1.50
$-t\ [(GeV/c)^2]$

Fig. 17.

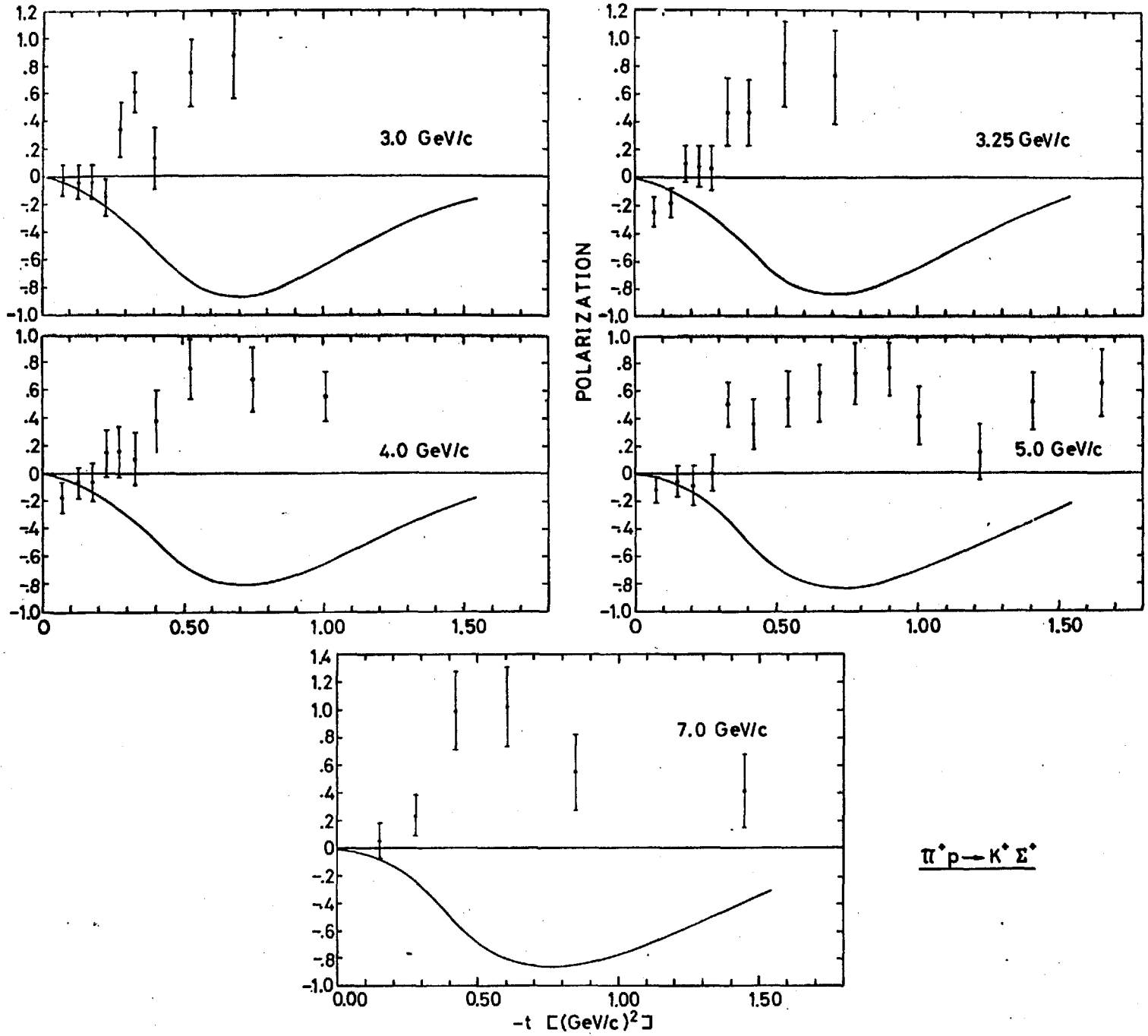
3.0 GeV/c
3.25 GeV/c
4.0 GeV/c
5.0 GeV/c
7.0 GeV/c
POLARIZATION
-t [(GeV/c)²]
π⁺p → K⁺Σ⁺

Fig. 18.

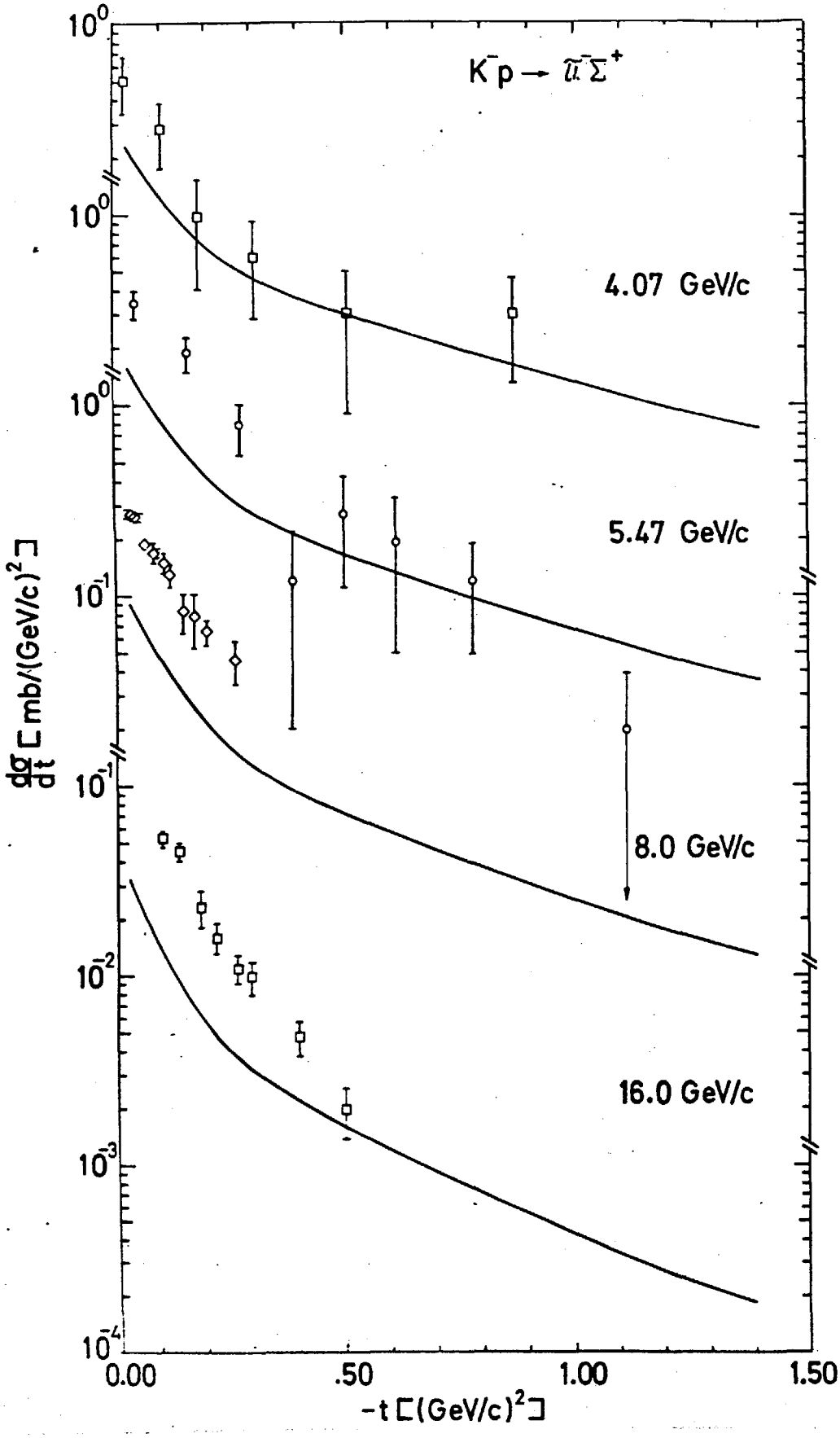
$K^- p \to \pi^- \Sigma^+$
4.07 GeV/c
5.47 GeV/c
8.0 GeV/c
16.0 GeV/c
$\frac{d\sigma}{dt}$ [mb/(GeV/c)^2]
$-t$ [(GeV/c)^2]
10^0
10^{-1}
10^{-2}
10^{-3}
10^{-4}
0.00
.50
1.00
1.50

Fig. 19.

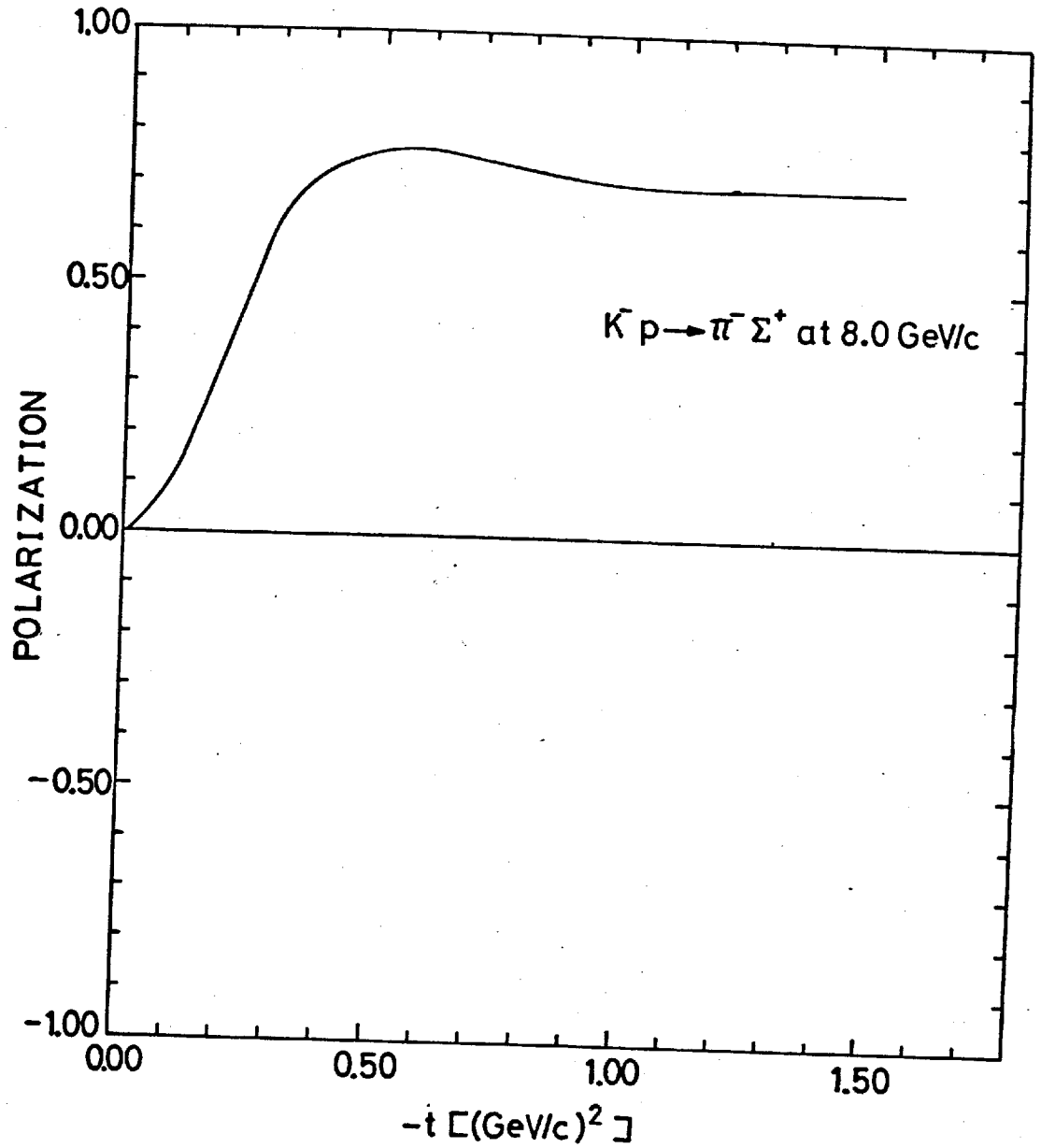
1.00
0.50
0.00
-0.50
-1.00
POLARIZATION
$K^- p \rightarrow \pi^- \Sigma^+$ at 8.0 GeV/c
0.00
0.50
1.00
1.50
$-t$ [(GeV/c)^2]

Fig. 20.

CHAPTER 5 DUALITY, EXCHANGE-DEGENERACY AND VENEZIANO MODELS

5.1 Duality and the Veneziano Model

It is generally believed that at low energies, the forward scattering cross-sections are dominated by s-channel resonances. This arises as at these low energies, cross-sections indicate peaks and dips which are readily explained by using a resonance saturation within either a fixed t-dispersion relation or a partial-wave expansion. The non-resonating background is of course neglected. However, as explained in Chapter 1, at higher energies and small momentum transfers, the forward scattering amplitudes are believed to be dominated by poles (to obtain the correct s-dependence, the poles must be Regge poles) in the crossed channel, neglecting the background integral and, at first, cuts in the t-channel. This latter fact is shown, for instance, in $K^-p \to \bar{K}^0 n$ where there are no non-exotic u-channel exchanges and so no backward peak. Vice versa, $K^-p \to \pi^+\Sigma^-$ has no t-channel exchanges and so no forward peak.(1)

An obvious advantage would be to find some sort of continuity between the two and this is provided by duality, which leads into the Veneziano model with its equivalence of infinite sets of s-channel resonances and t-channel Regge poles.

The concept of duality can be shown easily within the concept of finite energy sum rules (FESR)(48). Suppose, for example, that the amplitudes $T^{\pm}(\nu,t)$ [+ (-) means that the amplitude is even (odd) under s $\leftrightarrow$ u crossing and $\nu = \frac{s-u}{4m}$] satisfy fixed t dispersion relations :

$$T^{\pm}(\nu,t) = \frac{1}{\pi}\int_0^{\infty} d\nu' \, \mathrm{Im}\, T^{\pm}(\nu',t)\left[\frac{1}{\nu'-\nu} \pm \frac{1}{\nu'+\nu}\right] \quad (5.1)$$

where the integral has poles for $0 < \nu' < \nu_{th}$ and continuum contributions for $\nu' > \nu_{th}$ where ν_{th} is the threshold. Again, assume that for some $|\nu| > \nu_1$, $T^{\pm}(\nu,t)$ can be written as an expansion of t-channel Regge poles

$$T^{\pm}(\nu,t) = R^{\pm}(\nu,t) \qquad |\nu| > \nu_1$$

$$= \sum_j \beta_j(t)\, \nu^{\alpha_j(t)} \begin{Bmatrix} i - \cot\frac{\pi}{2}\alpha_j \\ i + \tan\frac{\pi}{2}\alpha_j \end{Bmatrix} \quad (5.2)$$

Defining $\Delta(\nu,t) = T(\nu,t) - R(\nu,t)$ the dispersion relation for this difference vanishes for $|\nu| > \nu_1$ as does the integrand for $|\nu'| > \nu_1$.

For $|\nu| > \nu_1$, expanding the integral in powers of $\left(\frac{\nu'}{\nu}\right)$ for $\Delta(\nu,t)$ leads to the FESR:

$$\int_0^{\nu_1} d\nu\, \nu^n \, \mathrm{Im}\, T^{\pm}(\nu,t) = \int_0^{\nu_1} d\nu\, \nu^n \, \mathrm{Im}\, R^{\pm}(\nu,t) \quad (5.3)$$

where n is even (odd) for $T^-(T^+)$. Carrying out the integral on the right-hand side of (5.3) leads to :

$$\int_0^{\nu_1} d\nu\, \nu^n \, \mathrm{Im}\, T^{\pm}(\nu,t) = \sum_j \frac{\beta_j(t)\, \nu_1^{\alpha_j(t)+n+1}}{\alpha_j(t)+n+1} \quad (5.4)$$

Hence, as the left-hand side is saturated with low-energy s-channel resonances while the right-hand side just has t-channel Regge poles, we have the concept of 'global duality'. The unknown here is ν_1 , the point at which the amplitude becomes 'Regge-like'.

Of course, this concept can be shown the other way round. We can take t-channel Regge poles, partial-wave analyse them and then plot the partial-waves in the complex plane[49]. These are typically in the form of circles so that at one point, we obtain a peak in $Im\,T_\ell$ where T_ℓ is the s-channel partial-wave amplitude. This is just what is expected from an s-channel resonance.

An even closer correspondence between direct channel resonances and cross-channel Regge poles comes from 'local duality'[50] where the infinite set of poles coming from the partial-wave analysis of s-channel resonances may give a Regge behaviour $S^{\alpha(t)}$. The converse also applies.

The Veneziano model has the features of both global and local duality, crossing symmetry, analyticity in s, t, and u, and the inclusion of poles from all contributing channels. Invoking the idea of duality enables us to look at the model as either an infinite set of t-channel Regge poles or an infinite set of s-channel resonances.

This can be seen as a typical meson-meson scattering Veneziano amplitude consists of Euler functions of the form, for the s and t channels with linear trajectories.

$$B(s,t) = \frac{\Gamma(-\alpha(s))\,\Gamma(-\alpha(t))}{\Gamma(-\alpha(s)-\alpha(t))} \qquad (5.5)$$

A similar expression exists for any two channels. (5.5) can be expanded, in terms of either s-channel poles or t-channel poles, but not both simultaneously i.e.

$$B(s,t) = \sum_{J=0}^{\infty} \binom{\alpha(t)+J}{J} \left(J-\alpha(s)\right)^{-1} \qquad (5.6)$$

$$= \sum_{J=0}^{\infty} \binom{\alpha(s)+J}{J} \left(J-\alpha(t)\right)^{-1} \qquad (5.7)$$

so showing the equivalence of an infinite set of s-channel poles and an infinite set of t-channel poles. (5.6) and (5.7) show that each infinite set consists of the parent and its daughters, all spaced by one unit of angular momentum.

In the Veneziano model which we will construct in Chapter 6 for $\bar{K}N$ and KN charge-exchange scattering, we take the asymptotic Reggeized U(6,6) model for $0^-\frac{1}{2}^+$ charge-exchange scattering in the forward peripheral region and obtain a Veneziano formula which agrees with this to leading order in s (center of mass energy squared). To this form for the pole graph, we add absorptive corrections as described in Chapter 3. These are still necessary with the Veneziano formalism as:

a) In the asymptotic limit of $s \to \infty$, we still obtain a Regge formalism with all its inherent difficulties.

b) Nonsense zeros are still present in the pole graph, and these must be filled in.

c) The first daughter of the f^0, for example, the ρ', lies one unit of angular momentum down in the Veneziano model[51]. However, when the ρ' is used as a phenomenological cut, for example in πN charge-exchange scattering, it turns out to be about half of a unit of angular momentum down.

The absorptive corrections of Chapter 3 may be regarded as 'duality-preserving'[52] in the sense that as the real Gaussian parameterization of the elastic scattering is equivalent to a fixed pole exchange of spin 1 (equation 3.35b). The amplitudes predicted to be real by the absence of non-exotic s-channels (e.g. $K^+n \to K^0p$) remain real after the addition of absorptive corrections. Similarly, those

predicted to be complex by duality, remain complex. However, the introduction of absorptive corrections in the t-channel destroys the crossing symmetry in the cut terms, but of course it still remains in the pole term.

The retention of the Veneziano form for the pole term produces one obvious problem. This is that the amplitude diverges at the s-channel resonances as we are above threshold in the s-channel. A remedy for this, which also agrees with unitarity, is to introduce an imaginary part into the s-channel fermion trajectories above threshold. As shown in Chapter 6, this is done in such a way as to give each resonance approximately the correct total width. However, the introduction of an imaginary part has the following difficulties :

a) The signature in the t-channel becomes $\{\exp[(\arg\alpha(s)/s - i\pi)\alpha(t)] \pm 1\}$ instead of $\{e^{-i\pi\alpha(t)} \pm 1\}$ (53) and so moves dips away from the nonsense points with resulting changes in the differential cross-sections.

b) The imaginary part gives all resonances at the same mass, the same total width[48], but partial wave analysis gives the daughters very different elastic widths from the parent.

c) Crossing symmetry is upset.

However, we will see that for the fermion trajectories used in the problem, the imaginary parts are small and we also do not have the explicit signature. Hence, we still use the Veneziano form with an imaginary part in $\alpha(s)$ in an effort to get a model valid for a wide range of s and t.

5.2 Regge Trajectories in the Veneziano Model

It has long been known that within the context of the Veneziano model that the real part of the Regge trajectories must be taken to be linear with the slope independent of the trajectory and the channel although the intercepts may be different. This violates the predictions of both potential and perturbation theory as discussed in section 2.7. Also in the limit of real linear trajectories, $\frac{\Gamma(a+\alpha(s))}{\Gamma(b+\alpha(s))} \not\to (\alpha' s)^{-b+a}$ $s\to\infty$ if s is real as we obtain infinitely many poles in taking this limit and so the limit is unattainable. However, as mentioned in 5.1, this is overcome with complex trajectories.

After making these criticisms, we will now discuss why, for real trajectories, it is necessary to make them linear with a common slope. As we have only introduced an imaginary part above threshold in one channel, we shall just note where this modifies the conclusions. There are three reasons, other than the many Regge pole fits, which have been successful in using linear trajectories, which indicate that the adoption of a linear parameterization may be sensible :

a) The Chew-Frautschi plots, which indicate, particularly in the case of fermions, that trajectories are linear[4].

b) If we take a dispersion relation with two subtractions for the trajectory :

$$\alpha(s) = as + b + \frac{s^2}{\pi}\int_{s_0}^{\infty} \frac{\mathrm{Im}\,\alpha(s')}{(s'-s)(s')^2}\,ds' \qquad (5.8)$$

$\longrightarrow as + b$ for real trajectories[54].

c) As seen from (5.4), global duality indicates a sum over Regge poles in the crossed channel. If one uses (5.4) within a

bootstrap scheme, this can be saturated with a ρ for $\pi\pi \to \pi\omega$ and get $\alpha = 0$ at a point consistent with that required for π N charge-exchange scattering. However, if more and more resonances (e.g. g) are included in the left-hand side of (5.4), the bootstrap stability is upset and one trajectory cannot sustain itself. This is rescued by Schmid's Partial-Wave projections of Regge exchanges which circle as the energy increases indicating more resonances. These can be identified as daughters of spacing $\Delta J = 2$ and in order to get good results they must be linear and parallel to the parent[55].

The introduction of the imaginary part to the s-channel trajectory only affects b) and c). The introduction of a linear imaginary part to (5.8) just bootstraps itself i.e. we get a linear imaginary part out to leading order, while the imaginary part implies the resonances in the low energy part for (c) have a finite width.

Having established the linearity of trajectories, it has to be shown that they have a common slope. There are five indications of this :

a) For a typical spinless Veneziano amplitude $\frac{\Gamma(-as-b)\Gamma(-a't-b')}{\Gamma(-as-b-a't-b')}$, $a' \neq a$ or else as s or t $\to \infty$ in the physical region with the scattering angle fixed and within a certain region, this diverges[56].

b) In certain reactions, such as πN charge-exchange scattering, signature is impossible in such models as Igi's[57] unless trajectories have a linear common slope.

c) Wagner[58] showed that if we expand the amplitude in a series of poles as in equation (5.6), and assume the positivity of the partial-wave projections of $\begin{pmatrix} \alpha(t)+J \\ J \end{pmatrix}$ and a universal slope, no ghosts (particles of negative decay width) exist.

d) Applying the Adler self-consistency condition to $\pi + A \to B + C$ i.e. $\rho_r^{\pi} \simeq 0$ where T_4-matrix $= 0 \Rightarrow$ Veneziano amplitude $= 0$ which happens at a pole in the denominator of the Euler functions. If the assumption of linear trajectories is now made, consistency implies a universal slope[59].

e) To avoid infinitely degenerate levels, the slope must be universal[60].

Of course, with the introduction of a linear imaginary part to one trajectory above threshold, all except b) are rigourously upset. However, in the region of scattering that we consider, t is small so problem a) never arises as we do not have an (s,u) term present.

5.3 Exchange Degeneracy in $\bar{K}N$ and KN Scattering

In connection with the general discussion on the Veneziano model, we must discuss the idea of strong exchange (or signature) degeneracy of Regge poles. As we will apply our model to $\bar{K}N$ and KN processes, we will discuss exchange degeneracy specifically in the context of these. In these processes, one channel has exotic exchanges. However, as the existence of these are not definitely established, we assume no exchange exists in such a channel.

From potential theory, it is known that both ordinary and exchange forces exist between scattering particles leading to even and odd signature trajectories in the crossed channels[22]. The breaking up into even and odd amplitudes is made necessary to avoid violating the Somerfeld-Watson transform i.e. alternately exponential increasing and decreasing in different parts of the complex ℓ-plane and also the destruction of unitarity except for real ℓ. Considering just spinless

particles, before reggeization, potential theory gives:

$$T^{(\substack{even\\odd})}_{(s,t)} = \frac{1}{2}\sum_{\ell}(2\ell+1)\,T^{\ell}(t)\left[P_{\ell}(z)\pm P_{\ell}(-z)\right] \qquad (5.9)$$

where T^{odd} is generated by the potential $V^{odd} = V_{ordinary} - V_{exchange}$ and only has odd ℓ values physical which in turn implies odd signature trajectories. A similar argument exists for T^{even}. Now one assumes that in the relativistic case that these forces for a given channel are built up of intermediate states in other channels. We use the convention that the s- and t-channel intermediate states generate direct forces while those associated with the u-channel generate exchange forces for forward scattering.

If we discuss $\bar{K}N$ charge-exchange scattering, the comments of the first paragraph implies no u-channel exchange which in turn implies that the forces governing this scattering in the near forward scattering are direct. Hence, both even and odd angular momentum values are physical so we no longer exists signature. Thus the t-channel meson trajectories are exchange degenerate, and similar arguments show that the s-channel fermion trajectories are also exchange degenerate. Similar arguments apply to $K^+n \to K^0p$.

Lastly, we can use the assumption of duality together with the absence of resonances in a given channel to obtain the sign between the exchange degenerate t-channel exchanges[48]. Thus, for forward scattering, this will either give a real amplitude or a complex one with t-dependent phases. Duality implies that an imaginary part as shown by resonances at low and medium energies, goes along with an imaginary part at high energies. Therefore, $\bar{K}N$ charge-exchange scattering has an imaginary part for t-channel exchanges which implies that we have the addition of the ρ and A_2. Similarly, KN charge-exchange scattering is almost

completely real so we have the cancellation of imaginary parts.

5.4 Veneziano Models for Meson-Meson Scattering

As mentioned in 5.1, these models have to exhibit duality, analyticity, crossing symmetry etc. and can be applied in its most simple form to pseudoscalar meson-meson scattering where only one spin-state exists. The Regge trajectories are here chosen in three exchange-degenerate sets according to the number of strange quarks which their constituent particles contain[61]. This is carried on into the case of meson-baryon scattering. The sets are :

a) ρ, A_2 f^0 and ω where the f^0 is often identified with the P'.

b) $K^*(890)$ and $K_N(1420)$

c) ϕ and f!

These are well verified by Chew-Frautschi plots.

The grouping is done in this way to comply with the requirements of various processes. To obtain (a), the first step is that the absence of a non-exotic u-channel in $\pi^+\pi^+$ implies ρ-f^0 exchange degeneracy[50]. Then it is noticed that for elastic KK scattering, the s-channel is exotic and as the $I_t = 0,1$ are separately constructed from the $I_s = 0,1$, we get ω-f^0 and ρ-A_2 exchange degeneracy. b) is implied by the absence of an $I = \frac{3}{2}$ exotic exchange in πK elastic scattering[50,62], while c) comes straight from Arnold's exchange degeneracy scheme[63].

The generalized Veneziano formulae for meson-meson scattering are :

$$\sum_{N=0}^{\infty} \sum_{R=N}^{2N} (-1)^R \beta_R^N \frac{\Gamma(N-\alpha(s))\,\Gamma(N-\alpha(t))}{\Gamma(R-\alpha(s)-\alpha(t))} \qquad (5.10)$$

for symmetry in s and t, and

$$\sum_{N=0}^{\infty} \sum_{R=N}^{2N} (-1)^R \beta_R^N \left\{ \frac{\Gamma(N-\alpha(s))\,\Gamma(N+1-\alpha(t))}{\Gamma(R-\alpha(s)-\alpha(t))} - (s \leftrightarrow t) \right\} \tag{5.11}$$

for antisymmetry in s and t. etc.

When these are applied to processes, the results have the following features :

a) Agreement with the Adler condition, $A(s,t) = 0$ at $s = m_\pi^2$ [64] given by $\alpha_\rho(m_\pi^2) = \frac{1}{2}$.

b) Good fits to the widths of the mesons [50].

c) Inability to use higher energy behaviour as the Pomeron has to be neglected to avoid the opening of many inelastic channels as the energy increases

d) The $I = 0$ s-wave has a large effective range and the ρ has a large width in agreement with other models [50].

e) In $p n \to \pi^+ \pi^+ \pi^-$ at rest, the initial state is a $^1S_0$ state and so is considered as an 'off-mass shell pion', and so this can be treated as a four pion process. The comparison with experiment is striking [64].

5.5 Extension to Meson-Baryon Scattering

The first problem encountered here is that linear trajectories for fermions imply, by Macdowell symmetry, that parity doubling is present. (The introduction of a linear imaginary part does not alter this). Explicitly, the Macdowell symmetry for fermion exchange [11] says

that the partial wave of total angular momentum J, signature τ, and parity P, taken at a given values of the total energy $W=\sqrt{s}$ is connected with the partial wave amplitude of total angular momentum J, signature τ, and parity -P, taken at a given value -W, by the relation

$$T^{J}_{\tau,P}(W) = -T^{J}_{\tau,-P}(-W) \tag{5.12}$$

Typically, suppose the fermion exchanges are Reggeized, and consider the pole at $\alpha(W) = J$, in the partial wave $T^{J}_{\tau,P}(W)$, then

$$T^{J}_{\tau,P}(W) = \frac{\beta_P(W)}{J-\alpha_P(W)} \tag{5.13}$$

Hence, (5.12) implies :

$$\beta_P(W) = -\beta_P(-W) \tag{5.14}$$

and

$$\alpha_P(W) = \alpha_{-P}(-W) \tag{5.15}$$

As the trajectories used in the Veneziano model are linear in W^2 (5.15) is always satisfied so the fermion trajectories are automatically parity doubled.

The second thing to be done is to modify Veneziano terms of the form $\frac{\Gamma(N-\alpha(s))\,\Gamma(N-\alpha(t))}{\Gamma(R-\alpha(s)-\alpha(t))}$, N and R integer, so that the fermion trajectories now have poles at odd half-integers. It is also necessary to adjust these constants so that the correct Regge asymptotic behaviour is obtained in all amplitudes and in both the forward and backward directions, e.g. in $0^{-}\frac{1}{2}^{+} \to 0^{-}\frac{1}{2}^{+}$ scattering, the invariant amplitudes A and B have a different asymptotic behaviour in S. (see for example, equation 2.62)). This is obtained very often at the expense of all terms

in a given amplitude having poles at all the particles on a given trajectory.

Having established the above facts, we will now give a short discussion of previous meson-baryon scattering Veneziano models. These have been applied to πN scattering, $\pi^- p \to \eta n$ and KN and $\bar{K}N$ scattering, the latter two processes being particularly simple due to the presence of an exotic channel.

In the πN scattering models[65], subsidiary terms were found to be necessary to fit the data. However, the greatest problem arising was with the Δ trajectory which is the sole contributor to $\pi^- p$ backward scattering. Previous Regge-pole fits have shown that there are difficulties in obtaining the correct differential cross-section at $u=0$, non-existent dip at $\alpha_\Delta(u) = -\frac{3}{2}$ and the extrapolation to the pole. With the Veneziano form as described by Berger and Fox, these difficulties still remain with the added problem of the inability to obtain the $\pi N \Delta$ coupling constant.

These difficulties led Miyamura[66] and Blackmon and Wali[67] to consider $\pi^- p \to \eta n$ where the Δ trajectory does not contribute. Signature conditions provide relations between the parameters, but the usual condition of taking the asymptotic limit to compare with experiment is still used.

The last class of models are those for KN scattering[53, 65, 68, 69]. Here, as stated before, one channel is always exotic implying exchange-degenerate trajectories in a given channel. These models have, in most cases, few satellites and are so constructed that the experimental absence of parity doublets is used to provide relations between the residues of various terms. The remaining parameters are fixed by a variety of methods,

ranging from the normalization at t = 0 of A' in Inami's model, the elastic widths of resonances in Lovelace's and Igi's, to the use of the differential cross-section data in Berger and Fox's. The last named were the only ones to use a full Veneziano formulation in any of the differential cross-sections. However, as they used a zero width approximation at all times, the Veneziano, as opposed to the Regge, formulation could only be used in cases where the fermion poles were in the u-channel, e.g. in KN charge-exchange and K^+p backward scattering. Otherwise, the Regge form with an added Pomeron, if necessary, was used. The usual difficulty of correlating $K^-p \to K^0 n$ and $K^+n \to K^0 p$ occurred.

All authors, with the exception of Lovelace, used just pole terms. Lovelace used the asymptotic form of the Veneziano amplitude in an absorptive K-matrix formulation to employ cuts of the form used by Imperial College and Argonne groups, i.e. choosing nonsense with small cuts, and to unitarize the model. However, crossing symmetry is completely lost, but considerable success at fitting the data was obtained.

CHAPTER 6. A VENEZIANO MODEL WITH ABSORPTIVE CORRECTIONS FOR $\bar{K}N$ AND KN CHARGE-EXCHANGE SCATTERING.

6.1 The Reggeized U(6,6) Model.

Previously, the application of models such as the Reggeized U(6) ⊗ U(6) ⊗ O(3) and the Reggeized U(6,6) models, both with absorptive corrections, to $K^- p \to \bar{K}^0 n$ and $K^+ n \to K^0 p$ have been successful at 5 GeV/c and above, but not below this energy, particularly in the case of $K^+ n \to K^0 p$ [26]. In an effort to improve this situation, we take note of the statement in 5.1, that cross-sections at low energies are dominated by direct channel resonances and so construct a Veneziano amplitude which agrees with that of the Reggeized U(6,6) to leading order in s when the asymptotic form of the Veneziano amplitude is used. However, to do this, we must first construct the Reggeized U(6,6) model.

This model is used in preference to the Reggeized U(6) ⊗ U(6) ⊗ O(3) model, as derived in Chapter 2, as the latter has certain problems associated with it. This first is that as we have a supermultiplet exchange with all possible meson multiplets included and evaluated 'off-shell', to avoid branch-point at $t = 0$, we have to add, rather artificially in the mode of fermions, a pseudoquark conspiring trajectory. The supermultiplet exchange principle gives the correct couplings i.e. $(\bar{N} \gamma_\mu N)$ and $(\bar{N}N)$, which we expect from vector and tensor particle exchanges, for $0^- \tfrac{1}{2}^+ \to 0^- \tfrac{1}{2}^+$ scattering. However, for higher spin scattering e.g. $\tfrac{1}{2}^+ \tfrac{1}{2}^+ \longrightarrow \tfrac{1}{2}^+ \tfrac{1}{2}^+$ or photoproduction, we obtain pseudoscalar couplings

$(\bar{N}\gamma_5 N)$ to nucleons as well as the above[76,70] for even - and odd - signature Regge poles, which we identify with trajectories of which the A_2 and ρ respectively are the lowest members.

In general, the pseudoscalar coupling (to whatever trajectory) leads to serious difficulties. When the invariant M-function for high spins is evaluated, we get a factor $\frac{1}{t}$ associated with this coupling. Reverting to our arguments of chapter 1, when we considered $\frac{1}{2}^+\frac{1}{2}^+ \to \frac{1}{2}^+\frac{1}{2}^+$ scattering, we see that now for the unabsorbed amplitude,

$$\phi_2^{\pi} \sim \frac{1}{t-m_\pi^2} \qquad (6.1)$$

for small t.

However, $\phi_4^{\pi} = \phi_2^{\pi}$ so that as $t \to 0$, $\phi_4^{\pi} \not\to 0$, which violates the conservation of angular momentum. An obvious solution, is to multiply the M-function by $t/4m_\mu$, but this leads to an unusual angular dependence for the non-pseudoscalar terms, which makes the reproduction of the differential cross-sections difficult. Hence, we are led to consider the Reggeized U(6,6) model for near forward scattering.

Here, we take the U(6,6) currents[19] on shell for the external particles and saturate with a fixed spin t-channel propagator. We then Reggeize the M-function. In the specific case that we consider i.e. $\bar{K}N$ and KN charge-exchange scattering, we have both spin 1^- and spin 2^+ fixed pole propagators to consider. Hence, we will first construct the T-matrix for spin 1^- exchange. The invariant 3-point effective Lagrangians are in the notation of chapter 2:

(a) Meson-Meson-Meson Vertex.

$$\mathcal{L}_{(a)} = \frac{h}{4\mu}\left[(p-q')\gamma_\mu T^i \phi_\mu^i(-q')\right]^D \left\{\Phi(p_2), \Phi(-p_4)\right\}_D^C \tag{6.2}$$

where h is the coupling constant and $q' = p_2 - p_4$.

(6.2) is unique as under charge conjugation,

$$Tr\left[\Phi'\Phi\Phi\right] = \tfrac{1}{2} Tr\left[\Phi'\{\Phi,\Phi\}\right] \tag{6.3}$$

where the trace is over U(6,6) indices.

This comes about as under charge conjugation:

$$\phi_5 \to \phi_5 \quad , \quad \phi_\mu \to -\phi_\mu$$

$$(C^{-1})^{\alpha\beta}(\gamma_5)_\beta^\gamma (C)_{\gamma\delta} = (\gamma_5)_\delta^\alpha \, , \quad (C^{-1})^{\alpha\beta}(\gamma_\mu)_\beta^\gamma (C)_{\gamma\delta} = -(\gamma_\mu)_\delta^\alpha \tag{6.4}$$

Carrying out the U(2,2) ⊗ SU(3) decomposition as in equation (2.4) and retaining only pseudoscalar external mesons, we obtain for (6.2),

$$\mathcal{L}_{(a)} = h\left(1 + \frac{q'^2}{2\mu^2}\right) P_\mu'(\phi_5,\phi_5)_F^i \phi_\mu^i(-q') \tag{6.5}$$

where q'^2 is interpreted 'on-shell' and the SU(3) couplings are defined equivalently to (2.50) and (2.51) as

$$(\phi_5,\phi_5)^i_F = Tr\left[\phi_5\left[T^i,\phi_5\right]\right] \tag{6.6}$$

and $$(\phi_5,\phi_5)^i_D = Tr\left[\phi_5\left\{T^i,\phi_5\right\}\right] \tag{6.7}$$

$$i = 1 \ldots 8.$$

(b) Baryon-Baryon-Meson Vertex.

$$\mathcal{L}_{(b)} = \frac{g}{2\mu}\,\bar{u}^{(ABC)}(p_3)\left[(q_\mu - q')\gamma_\mu, T^j\phi^j_{\mu'}(q)\right]_C u^{D}_{(ABD)}(p_1) \tag{6.8}$$

where $q = -q'$ and g is the coupling constant. Again, carrying out the $U(2,2) \otimes SU(3)$ decomposition as in equation (2.15) and retaining only the spin $\frac{1}{2}^+$ parts for the baryons, we get, after introducing the mass splitting of section (6.5),

$$\mathcal{L}_{(b)} = g\left[\frac{p_{\mu'}}{2m_1}\left(1+\frac{q^2}{2\mu}\right)(\bar{N},N)^j_F + \left(1+\frac{2\mu}{\mu}\right)\left(\frac{\bar{N}\,\gamma_{\mu'}\,N}{4m_1^2}\right)^j_{D+\frac{2}{3}F}\right]\phi^j_{\mu'}(q) \tag{6.9}$$

where $\gamma_{\mu'} = \varepsilon_{\mu'\nu\kappa\lambda}\, p_\nu\, q_\kappa\, \gamma_\lambda\, \gamma_5$

Upon evaluation, the kinematics given for 'on-shell',

$$\frac{\gamma_{\mu'}}{4m_1^2} = \frac{p^2}{4m_1^2}\gamma_{\mu'} - \frac{p_{\mu'}}{2m_1} \tag{6.10}$$

$$= \left(1-\frac{M^2}{4m_1^2}\right)\gamma_{\mu'} - \frac{p_{\mu'}}{2m_1} \tag{6.11}$$

where M is a mass associated with the exchange.

Hence, $$\mathcal{L}_{(6)} = g\left[\frac{p_{\mu'}}{2m_i}\left[\left(1+\frac{q^2}{2m_\rho}\right)(\bar N, N)_F^j - \left(1+\frac{2m}{\rho}\right)(\bar N, N)^j_{D+\frac{2}{3}F}\right] + \left(1+\frac{2m}{\rho}\right)\left(1-\frac{M^2}{4m_i^2}\right)(\bar N \gamma_\rho N)^j_{D+\frac{2}{3}F}\right]\phi_\rho^j(-q) \quad (6.12)$$

Defining the spin 1^- propagator as in equation (2.34), we construct the T-matrix as in equations (2.44) and (2.45) to give

$$T = \frac{-gh}{t-M^2}\left(1+\frac{q'^2}{2\mu^2}\right)\left[\frac{p\cdot p'}{2m_i}\left[\left(1+\frac{q^2}{2m_\rho}\right)(\bar N, N)_F^i - \left(1+\frac{2m}{\rho}\right)(\bar N, N)^i_{D+\frac{2}{3}F}\right] + \left(1+\frac{2m}{\rho}\right)\left(1-\frac{M^2}{4m_i^2}\right)(\bar N \not{p}' N)^i_{D+\frac{2}{3}F}\right](\phi_S, \phi_{\bar S})_F^i \quad (6.13)$$

where pair-wise equal mass kinematics give $p\cdot q = p'\cdot q' = 0$.

Hence, following chapter 2, we have for the invariant amplitudes:

$$A = \frac{-gh}{t-M^2}\, h_F\left(\frac{s+\frac{t}{2}-m^2-\mu^2}{m_i}\right)\left(1+\frac{q'^2}{2\mu^2}\right)\left[\left(1+\frac{q^2}{2m_\rho}\right)g_F - \left(1+\frac{2m}{\rho}\right)g_{D+\frac{2}{3}F}\right] \quad (6.14)$$

$$B = \frac{-2gh}{t-M^2}\, h_F\, g_{D+\frac{2}{3}F}\left(1+\frac{q'^2}{2\mu^2}\right)\left(1+\frac{2m}{\rho}\right)\left(1-\frac{M^2}{4m_i^2}\right) \quad (6.15)$$

To construct the amplitude for spin 2^+ exchange, we note that the A_2 lies in the (6,6,1) multiplet whereas the ρ was in the (6,6;0). Hence, the field for the exchanged particle is $\phi^i_{(\rho\nu)}(-q')$, and to saturate the extra $O(3)_j$ label, we take the currents for the vector exchange and multiply them by p_μ as in chapter 2. Thus, we

are led to the Lagrangians, with the appropriate mass splitting:

a) Meson-Meson-Meson Vertex.

$$\mathcal{L}_{(a)} = h\left(1+\frac{q^{12}}{2\mu^2}\right)\frac{p_\mu' p_\nu'}{\chi\mu_1}\,(\phi_5,\phi_5)^i_D\,\phi^i_{(\mu\nu)}(-q') \qquad (6.16)$$

b) Baryon-Baryon-Meson Vertex.

$$\mathcal{L}_{(b)} = \frac{g p_{\mu'}}{\chi m_1}\left[\frac{p_{\nu'}}{2m_1}\left[\left(1+\frac{q^2}{2m\mu}\right)(\bar N, N)^j_F - \left(1+\frac{2m}{\mu}\right)(\bar N, N)^j_{D+\frac{2}{3}F}\right]\right.$$

$$\left. + \left(1+\frac{2m}{\mu}\right)\left(1-\frac{M^2}{4m_1^2}\right)(\bar N\gamma_\nu, N)^j_{D+\frac{2}{3}F}\right]\phi^j_{(\mu\nu)}(-q) \qquad (6.17)$$

where the D-type coupling in (6.16) comes about as under charge conjugation $\phi_{(\mu\nu)} \to \phi_{(\mu\nu)}$ so we need a coupling of the form $\frac{1}{2}\mathrm{Tr}\left[\bar\Phi'[\bar\Phi,\bar\Phi]\right]$. X is a quantity, which can be, in principle, determined by the observed decay rates of $\rho \to \pi\pi$ and $A_2 \to \eta\pi$. The 'saturation factors' $\frac{p_\mu'}{\chi\mu_1}$ in (6.16) and $\frac{p_\mu}{\chi m_1}$ in (6.17) are chosen as Sharp and Wagner[71] have demonstrated in the concept of A_2 universality that if the A_2 system is strongly coupled to both the $\eta\pi$ and NN systems, in the limit of zero mass, then for coupling constants

$$g^{-1}_{A_2\eta\pi} \approx \frac{m_{\eta\pi}}{m_{NN}}\, g^{-1}_{A_2 NN} \qquad (6.18)$$

Generalizing to the U(6,6) case, we may write

$$g^{-1}(\phi_{(\mu\nu)}\phi_5\phi_5) \approx \frac{m_1}{m_1} g^{-1}(\phi_{(\mu\nu)}\bar{N}N) \tag{6.19}$$

so giving our saturation factors.

The spin 2^+ propagator is[72]:

$$\Delta_{\mu\nu\mu'\nu'}(q,q') = \frac{1}{t-m^2}\left\{ g_{\mu\mu'}g_{\nu\nu'} + g_{\mu\nu'}g_{\mu'\nu} - \frac{2}{3}g_{\mu\nu}g_{\mu'\nu'} \right.$$
$$+\frac{1}{m^2}\left[\frac{2}{3}g_{\mu\nu}q_{\mu'}q_{\nu'} + \frac{2}{3}g_{\mu'\nu'}q_\mu q_\nu - g_{\mu\mu'}q_\nu q_{\nu'}\right.$$
$$\left.\left. - g_{\mu\nu'}q_\nu q_{\mu'} - g_{\mu'\nu}q_\mu q_{\nu'} - g_{\mu'\nu'}q_\mu q_\nu\right] + \frac{1}{m^4}\frac{4}{3}q_\mu q_\nu q_{\mu'}q_{\nu'}\right\} \tag{6.20}$$

In the construction of the invariant amplitudes, pair-wise equal mass kinematics are used giving $P\cdot q = P'\cdot q' = 0$. Applications of the Bargmann-Wigner equations as in (2.13) gives such terms as

$$\bar{N}(p_3)\not{P}N(p_1) = 2m \tag{6.21}$$

leaving

$$A = \frac{gh}{t-m^2}\frac{h_0}{\lambda^2 m_1^2 \mu_1}\left(1+\frac{q'^2}{2\mu^2}\right)\left[4\left(s+\frac{t}{2}-m^2-\mu^2\right)^2 - \frac{16}{3}m_1^2\mu_1^2\left(1-\frac{M^2}{4m_1^2}\right)\right.$$
$$\left.\left(1-\frac{M^2}{4\mu_1^2}\right)\right]\left[\left(1+\frac{q^2}{2m\mu}\right)g_F - \left(1+\frac{2m}{\mu}\right)g_{D+\frac{2}{3}F}\right] \tag{6.22}$$

$$B = \frac{g\,h}{t-M^2}\,\frac{h_e}{X^2_{m_1\mu_1}}\left(1+\frac{q'^2}{2\mu^2}\right)\delta\left(s+\frac{t}{2}-m^2-\mu^2\right)\left(1+\frac{2m}{\mu}\right)$$
$$\left(1-\frac{M^2}{4m_1^2}\right) g_{D+\frac{2}{3}F} \qquad (6.23)$$

Using the mass-splitting of section 6.5,

$$\left(1-\frac{M^2}{4m_1^2}\right)\left(1-\frac{M^2}{4\mu_1^2}\right) \gtrsim 0.2 \qquad (6.24)$$

and this, together with the knowledge that the lowest energy we consider is $S \sim 6.0\,(\text{GeV})^2$ and the largest momentum transfer $t \sim -1.5\ (\text{GeV/c})^2$ gives,

$$\left(s+\frac{t}{2}-m^2-\mu^2\right)\sim 10\,,\quad \frac{4}{3}\,m_1^2\mu_1^2\left(1-\frac{M^2}{4m_1^2}\right)\left(1-\frac{M^2}{4\mu_1^2}\right)\sim 0.1 \qquad (6.25)$$

Hence, the second term in A can be neglected.

To Reggeize the invariant amplitudes (6.14), (6.15), (6.22) and (6.23), we shall use a method similar to that of chapter 2, and in particularly equations (2.54) and (2.55) and the associated text. The Gell'Mann 'ghost-killing' mechanism is again used. We first see that both the A amplitudes $\sim s^J$ and the B ones $\sim s^{J-1}$, so we use the prescription that

$$J \to \alpha(t) \qquad (6.26)$$

and using a Taylor expansion, we have:

for spin 1^- exchange,

$$\frac{1}{t-m^2} = -\pi \left.\frac{d\alpha}{dt}\right|_{t=m^2} \sin\pi\alpha_t \longrightarrow -\alpha' \Gamma(1-\alpha_t) \tag{6.27}$$

for the Gell'Mann mechanism and linear trajectories.

Similarly, for spin 2^+ exchange

$$\frac{1}{t-m^2} \longrightarrow \alpha' \Gamma(1-\alpha_t) \tag{6.28}$$

Finally, the signature factors for spin 1^- and 2^+ exchanges are taken to be $\frac{1}{2}(1-e^{-i\pi\alpha_t})$ and $\frac{1}{2}(1+e^{-i\pi\alpha_t})$ respectively. As explained in chapter 2, these are necessary to remove wrong signature poles as required by the presence of exchange forces.

Hence, combining (6.14) with (6.22) and (6.15) with (6.23) and taking common group theoretic masses and exchange degenerate trajectories, we have :

$$A = \frac{gh}{2m_1} \Gamma(1-\alpha_t) (\alpha' s)^{\alpha_t} \left(1+\frac{q'^2}{2\mu^2}\right)\left[\left(1+\frac{q^2}{2m\mu}\right) g_F - \left(1+\frac{2m}{\mu}\right) g_{D+\frac{2}{3}\bar{t}}\right]$$
$$\left[h_F\left(1-e^{-i\pi\alpha_t}\right) + \frac{4}{x^2 m_1 \mu_1 \alpha'} h_D \left(1+e^{-i\pi\alpha_t}\right)\right] \tag{6.29}$$

$$B = gh\,\Gamma(1-\alpha_t)(\alpha' s)^{\alpha_t - 1}\left(1+\frac{q'^2}{2\mu^2}\right)\left(1+\frac{2m}{\mu}\right)\left(1-\frac{M^2}{4m_1^2}\right)\alpha' g_{D+\frac{2}{3}\bar{t}}$$
$$\left[h_F\left(1-e^{-i\pi\alpha_t}\right) + \frac{4}{x^2 m_1 \mu_1 \alpha'} h_D \left(1+e^{-i\pi\alpha_t}\right)\right] \tag{6.30}$$

In the application of (6.29) and (6.30) to $\bar{K}N$ and KN charge-exchange scattering, $q^2 = q'^2$, and as explained in section 5.3, strong exchange degeneracy is required. This implies that

$$\frac{4}{X^2 m_1 \rho_1 \alpha'} = 1 \tag{6.31}$$

which is acceptable as X^2 cannot be determined from the ratio $\Gamma_{\rho\to\pi\pi} / \Gamma_{A_1\to\eta\pi}$ as these branching ratios are largely unknown. Hence,

$K^- p \to \bar{K}^0 n$

$$A = \frac{2gh}{m_1} e^{-i\pi\alpha_t} \Gamma(1-\alpha_t)(\alpha' s)^{\alpha_t}\left(1+\frac{q^2}{2\rho^2}\right)\left[\left(1+\frac{q^2}{2m\rho}\right) - \frac{5}{3}\left(1+\frac{2m}{\rho}\right)\right] \tag{6.32}$$

$$B = \frac{20}{3} gh\alpha' e^{-i\pi\alpha_t} \Gamma(1-\alpha_t)(\alpha' s)^{\alpha_t - 1}\left(1+\frac{q^2}{2\rho^2}\right)\left(1+\frac{2m}{\rho}\right)\left(1-\frac{M^2}{4m_1^2}\right) \tag{6.33}$$

$K^+ n \to K^0 p$

$$A = \frac{2gh}{m_1} \Gamma(1-\alpha_t)(\alpha' s)^{\alpha_t}\left(1+\frac{q^2}{2\rho^2}\right)\left[\left(1+\frac{q^2}{2m\rho}\right) - \frac{5}{3}\left(1+\frac{2m}{\rho}\right)\right] \tag{6.34}$$

$$B = \frac{20}{3} gh \Gamma(1-\alpha_t)(\alpha' s)^{\alpha_t - 1}\left(1+\frac{q^2}{2\rho^2}\right)\left(1+\frac{2m}{\rho}\right)\left(1-\frac{M^2}{4m_1^2}\right)\alpha' \tag{6.35}$$

These amplitudes are complex for $K^- p \to \bar{K}^0 n$ and real for $K^+ n \to K^0 p$ as required by duality.

Lastly, we have to determine the coupling constants g and h. These are calculated for fixed spin exchange, and as the lowest poles on the Regge trajectory are expected to dominate, we leave g and h untouched during Reggeization.

Firstly, to calculate g, we use the Chew-Low Extrapolation which gives:

$$\frac{G^2_{\pi NN}}{4\pi} = 14.9 \tag{6.36}$$

In the U(6,6) model, we write a 3-point coupling , similar to (6.8), but for a (56,1;0) - (56,1;0) - pseudoscalar meson interaction:

$$\mathcal{L} = -\frac{g}{2\mu}\,\bar{u}^{(ABC)}(p_3)\left((-q+p)\gamma_5 T^i\right)^D_c\, u_{(ABD)}(p_1)\,\phi_5^i(-q) \tag{6.37}$$

which reduces to, under U(2,2) ⊗ SU(3) decomposition and mass splitting:

$$\mathcal{L} = g\left(1+\frac{2m}{\mu^2}\right)\left(1-\frac{M_1^2}{4m_1^2}\right)(\bar{N}\gamma_5 N)^c_{D+\frac{2}{3}F}\,\phi_5^i(-q) \tag{6.38}$$

Taking the $\pi\bar{p}p$ vertex, (6.38) becomes

$$\mathcal{L} = g\,\frac{5}{3}\left(1+\frac{2m}{\mu^2}\right)\left(1-\frac{M_1^2}{4m_1^2}\right)(\bar{p}\gamma_5 p)\,\pi \tag{6.39}$$

In an ordinary space-time theory, the Lagrangian would be :

$$\mathcal{L} = G_{\pi NN}\,(\bar{p}\gamma_5 p)\,\pi \tag{6.40}$$

where $\bar{p}$, p and π are Dirac fields as in (6.39). On comparison

$$14.9 = \frac{g^2}{4\pi}\left(\frac{5}{3}\right)^2\left(1+\frac{2m}{\mu_2}\right)^2\left(1-\frac{M_1^2}{4m_1^2}\right)^2 \qquad (6.41)$$

h is determined from the $\rho \to 2\pi$ decay width as obtained from the Novisibirsk colliding beam experiment[73] $e^+e^- \to \rho^0 \to \pi^+\pi^-$ giving $\Gamma_{\rho\to 2\pi}$ = 122 MeV for m_ρ = 0.764 GeV/c^2. The decay width is determined by:

$$\Gamma = \frac{|\underline{p}|}{2m_\rho^2}\frac{1}{4\pi}\overline{\sum_{\substack{\text{average}\\ \text{over}\\ \text{spins}}}}|T|^2 \qquad (6.42)$$

where $|\underline{p}|$ is the C.M. 3-momentum for the decay products. The factor for spin averaging $= \frac{1}{2s_\rho+1} = \frac{1}{3}$. For ℓ , we use equation (6.5). Hence,

$$|T|^2 = 16\,h^2\left(1+\frac{q_2^2}{2\mu_2^2}\right)|\underline{p}|^2 \qquad (6.43)$$

giving

$$\frac{h^2}{4\pi}\left(1+\frac{q_2^2}{2\mu_2^2}\right) = 2.15 \qquad (6.44)$$

6.2 A Veneziano Extension.

We have now constructed Regge amplitudes for the high energy behaviour of $\bar{K}N$ and KN charge exchange scattering. In converting these into dual amplitudes, we use the form of Inami, and are thus led to :

$$A_{\bar{K}N}(s,t,u) = \Lambda_{A_1}\frac{\Gamma(1-\alpha_t)\Gamma(\frac{3}{2}-\alpha_s^{Y_0^*})}{\Gamma(\frac{3}{2}-\alpha_t-\alpha_s^{Y_0^*})} + \Lambda_{A_2}\frac{\Gamma(1-\alpha_t)\Gamma(\frac{1}{2}-\alpha_s^{Y_0^*})}{\Gamma(\frac{3}{2}-\alpha_t-\alpha_s^{Y_0^*})} + \sum_{A_1}\frac{\Gamma(1-\alpha_t)\Gamma(\frac{3}{2}-\alpha_s^{Y_1^*})}{\Gamma(\frac{3}{2}-\alpha_t-\alpha_s^{Y_1^*})} \qquad (6.45)$$

$$B_{\bar{K}N}(s,t,u) = \Lambda_{B_1}\frac{\Gamma(1-\alpha_t)\Gamma(\frac{1}{2}-\alpha_s^{Y_0^*})}{\Gamma(\frac{3}{2}-\alpha_t-\alpha_s^{Y_0^*})} + \sum_{B_1}\left(1-\frac{t}{M}\right)\frac{\Gamma(1-\alpha_t)\Gamma(\frac{3}{2}-\alpha_s^{Y_1^*})}{\Gamma(\frac{5}{2}-\alpha_t-\alpha_s^{Y_1^*})} \qquad (6.46)$$

where numerically,

$$\Lambda_{A_1} = \frac{2gh}{m_1}\left(1+\frac{q^2}{2p^2}\right)\left[\left(1+\frac{q^2}{2mp}\right)-\frac{5}{3}\left(1+\frac{2m}{p}\right)\right]\frac{\Lambda'}{\Sigma'+\Lambda'}$$

$$\Lambda_{A_2} = X\frac{(\Sigma'+\Lambda')}{\Lambda'}\Lambda_{A_1} \quad , \quad \Sigma_{A_1} = \frac{\Sigma'}{\Lambda'}\Lambda_{A_1}$$

$$\Lambda_{B_1} = -\frac{20}{3}gh\left(1+\frac{q^2}{2p^2}\right)\left(1+\frac{2m}{p}\right)\left(1-\frac{M^2}{4m_1^2}\right)\alpha'\frac{\Lambda}{\Sigma+\Lambda}$$

$$\Sigma_{B_1} = \frac{\Sigma}{\Lambda}\Lambda_{B_1} \qquad (6.47)$$

and α_t is the exchange degenerate $\rho - A_2$ t-channel trajectory, $\alpha_s^{Y_1^*}$ is the exchange degenerate $\Sigma_\beta - \Sigma_\delta$ s-channel trajectory and $\alpha_s^{Y_0^*}$ is the exchange degenerate $\Lambda_\alpha - \Lambda_\gamma$ s-channel trajectory. In common with other authors, we have neglected $\Lambda_\beta - \Lambda_\delta$ and $\Sigma_\alpha - \Sigma_\gamma$ trajectories as experimental analyses show no evidence for their presence. In (6.47), Σ', Λ', Σ, Λ, X and N are parameters, which are reduced to 2 independent ones, $(\frac{\Sigma}{\Lambda})$ and N by the following methods:

(i) The removal of the $\frac{1}{2}^-$ parity partner on the Y_0^* trajectory relates X to $(\frac{\Sigma}{\Lambda})$. In fact the amplitude in $A_1 \Lambda_{A_2} \frac{\Gamma(1-\alpha_t)\,\Gamma(\frac{1}{2}-\alpha_s^{Y_0^*})}{\Gamma(\frac{3}{2}-\alpha_t-\alpha_s^{Y_0^*})}$, must be included to remove the above parity doublet, to get the correct relation for the removal of the $\frac{3}{2}^+$ parity doublet on the Y_0^* trajectory, and to make the amplitude diverge at the $\Lambda(1115)$ pole. This term gives the asymptotic behaviour $-\Lambda_{A_2}\,\Gamma(1-\alpha_t)\,e^{-i\pi\alpha_t}\,(\alpha' s)^{\alpha_t - 1}$ and so is a subsidiary term. However, its presence will not upset our required asymptotic limit of the Reggeized U(6,6) model, as at the lowest energy considered, $s \sim 6$ (GeV)^2, $\Lambda_{A_2} \sim -\frac{1}{15}\Lambda_{A_1}$.

(ii) The removal of the $\frac{3}{2}^+$ parity partner on the Y_0^* trajectory relates $(\frac{\Sigma'}{\Lambda'})$ to $(\frac{\Sigma}{\Lambda})$.

The term proportional to $(\frac{\Sigma}{N})$ is also not present in our desired asymptotic limit. To make this negligible, the condition that $N \gg 1$, is imposed. The presence of this term is necessary in order to obtain the 'correct' behaviour of the Y_1^* trajectory in the backward direction for $K^+ n \to K^0 p$.

We stated that the parameters were equivalent to the U(6,6) factors numerically as, according to Kugler[74], factorization may not be true for the Veneziano model. He considered 3 scattering processes:

(i) $\pi^0\pi^0 \rightarrow \pi^0\pi^0$ - f^0 exchange in the t-channel.

(ii) $\pi^0\pi^0 \rightarrow \sigma\sigma$ - π or A_1 exchange in the t-channel.

(iii) $\sigma\sigma \rightarrow \sigma\sigma$ - f^0 exchange in the t-channel.

A partial wave projection of the Veneziano formula gives for $\ell < \sqrt{s_n}$,

$$g_\ell(s_n) = \frac{s_n^{\alpha(t=0)-1}}{\log_e s_n} + (t \leftrightarrow u) \qquad (6.48)$$

Hence, for the above scattering interaction, factorization gives:

$$g_\ell^{(i)}(s_n)\, g_\ell^{(iii)}(s_n) = \left[g_\ell^{(ii)}(s_n) \right]^2 \qquad (6.49)$$

implying $$\alpha_{f^0}(0) + \alpha_{f^0}(0) = 2\alpha_\pi(0) \qquad (6.50)$$

As $\alpha_{f^0}(0) \simeq \frac{1}{2}$, $\alpha_\pi(0) \simeq 0$, (6.50) implies

$$\alpha_{f^0}(0) = -\frac{1}{2} \qquad (6.51)$$

which is untrue. Thus the conclusions are that either f^0 decouples from (iii) or factorization fails.

For (6.45) and (6.46), we can obtain the KN charge-exchange amplitudes by $s \Leftrightarrow u$ crossing and time reversal. This is because the s-channel $K^- p \to \bar{K}^0 n$ is the time reversed u-channel of $K^+ n \to K^0 p$. Under time reversal, the helicity amplitudes behave as (using the notation of section 2.6):

$$\langle \lambda_3 \lambda_4 | \phi(\theta,\phi) | \lambda_1 \lambda_2 \rangle \to \eta_T \, e^{-2i(\lambda - \mu)\phi} \langle \lambda_1 \lambda_2 | \phi(\theta, \phi+\pi) | \lambda_3 \lambda_4 \rangle \quad (6.52)$$

where η_T is a phase factor and so can be neglected as it does not affect experimental quantities. As we evaluate our amplitudes at $\phi = 0$, (6.52) gives

$$\phi_1 \to \phi_1, \quad \phi_2 \to -\phi_3 = \phi_2 \quad \text{(by parity invariance)} \quad (6.53)$$

Now as (6.52) does not affect any of the energies in the s-channel helicity amplitude decomposition as given by equations (2.77) and (2.78), the amplitudes A and B are invariant. Hence, the amplitudes for $K^+ n \to K^0 p$ in terms of those for $K^- p \to \bar{K}^0 n$ by

$$A_{KN}(s,t,u) = A_{\bar{K}N}(u,t,s) \quad (6.54)$$

$$B_{KN}(s,t,u) = -B_{\bar{K}N}(u,t,s) \quad (6.55)$$

satisfying our required asymptotic limit.

We conclude this section by writing the asymptotic limit for $K^+n \to p K^0$ backward scattering, which will show the importance of the $\left(\frac{t}{N}\right)$ term for the Y_1^* contribution to B. We must first remark that for terms such as $\frac{\Gamma(1-\alpha_t)}{\Gamma(\frac{3}{2}-\alpha_t-\alpha_u^{Y_0^*})}$, when we take the asymptotic limit for u fixed, $s \to \infty$, we would pass through an infinity of poles. Hence, the limit must be taken off the real s-axis. Thus, the backward $K^+n \to pK^0$ asymptotic limit is:

$$A_{KN}(s,t,u) = \left[\Lambda_{A_1}\Gamma(\tfrac{3}{2}-\alpha_u^{Y_0^*}) + \Lambda_{A_2}\Gamma(\tfrac{1}{2}-\alpha_u^{Y_0^*})\right](\alpha' s)^{\alpha_u^{Y_0^*}-\frac{1}{2}}$$
$$+ \Sigma_{A_1}\Gamma(\tfrac{3}{2}-\alpha_u^{Y_1^*})(\alpha' s)^{\alpha_u^{Y_1^*}-\frac{1}{2}} \qquad (6.56)$$

$$B_{KN}(s,t,u) = \Lambda_{B_1}\Gamma(\tfrac{1}{2}-\alpha_u^{Y_0^*})(\alpha' s)^{\alpha_u^{Y_0^*}-\frac{1}{2}}$$
$$+\Sigma_{B_1}\Gamma(\tfrac{3}{2}-\alpha_u^{Y_0^*})\left[(\alpha' s)^{\alpha_u^{Y_1^*}-\frac{3}{2}} + \frac{1}{N\alpha'}(\alpha' s)^{\alpha_u^{Y_1^*}-\frac{1}{2}}\right] \qquad (6.57)$$

6.3. Regge Trajectories.

As we consider only forward scattering in this chapter, both t and u are ≤ 0 for the energy range considered. Thus, no problems exist with poles in the t and u channel exchanges. Thus we can write down the real linear trajectories with a common slope for the t and u channel exchanges in $K^-p \to \bar{K}^0n$ and $K^+n \to K^0p$ in such a way that the first few poles on each trajectory as given by a Chew-Frautschi plot, lie on the trajectory. Thus the t and u channel trajectories are :

$\rho - A_2$ trajectory: $\alpha_t = 0.44 + 0.95\, t$ (6.58)

$\Lambda_\alpha - \Lambda_\gamma$ trajectory: $\alpha_u^{Y_0^*} = -0.67 + 0.95\, u$ (6.59)

$\Sigma_\beta - \Sigma_\delta$ trajectory: $\alpha_u^{Y_1^*} = -0.33 + 0.95\, u$ (6.60)

However, as explained in section 5.2, the s-channel exchanges in $K^- p \to \bar{K}^0 n$ have $s \geq s_{\text{threshold}}$, so we need an imaginary part to the fermion trajectories to give approximately the correct width to the resonances and to avoid the divergences. We choose our trajectories so that $Re\,(\alpha_s^{Y_0^*})$ and $Re\,(\alpha_s^{Y_1^*})$ are given by $s \leftrightarrow u$ crossing from (6.59) and (6.60) respectively, but the addition of the imaginary part must upset the crossing symmetry. Hence, for both the Y_0^* and Y_1^* s-channel trajectories, we choose a form above threshold as follows :

$$\alpha_s = \alpha_0 + \alpha' s + i\,\alpha_I (s - s_0) \tag{6.61}$$

where $\alpha_I \geq 0$ and $s_0 = (m_\rho + m_K)^2$, the s-channel threshold.

To construct a simple model for α_I, we see that near a pole at $Re(\alpha_s) = J$, the partial wave amplitude is of the form: (for example, see the Veneziano decomposition in equation (5.6)).

$$T^J \approx \frac{r(s,J)}{J - \alpha_s}$$

$$= \frac{r(s,J)}{J - \alpha_0 - \alpha' s - i\alpha_I (s - s_0)} \tag{6.62}$$

The resonance would have a pole at

$$J = \alpha_0 + \alpha' s_{res}. \tag{6.63}$$

on the real axis. Assuming that the resonance is of a Breit-Wigner form, at half-width[75]:

$$\alpha_I (s_{res} - s_0) = J - \alpha_0 - \alpha' s_{\frac{1}{2}}$$

$$= \alpha' (s_{res} - s_{\frac{1}{2}})$$

$$\therefore \alpha_I = \frac{\alpha' \Gamma_{m_{res}}}{(m^2_{res} - s_0)} \tag{6.64}$$

For the purpose of the model, α_I is determined for each of the first few resonances on a given trajectory and then averaged as shown in Table 4. Thus, the first few resonances have approximately the correct total width. Combining Table 4 with equations (6.59) and (6.60) the s-channel fermion trajectories for $K^- p \to \bar{K}^0 n$ above threshold are:

$$\Lambda_\alpha - \Lambda_\gamma \text{ trajectory}: \quad \alpha_s^{Y_0^*} = -0.67 + 0.95 s + i\, 0.09 (s - s_0) \tag{6.65}$$

$$\Sigma_\beta - \Sigma_\delta \text{ trajectory}: \quad \alpha_s^{Y_1^*} = -0.33 + 0.95 s + i\, 0.15 (s - s_0) \tag{6.66}$$

As explained in section (5.1) the introduction of an imaginary part to the s-channel trajectories modifies the asymptotic limit. For $K^- p \to \bar{K}^0 n$, the limit for fixed t, $s \to \infty$, is now:

$$A_{\bar{\pi}N}(s,t,u) = \Gamma(1-\alpha_t)\left[\left\{\Lambda_{A_1}\left(1+\frac{i\alpha_I^{Y_0^*}}{\alpha'}\right)^{\alpha_t} + \sum_{A_1}\left(1+i\frac{\alpha_I^{Y_1^*}}{\alpha'}\right)^{\alpha_t}\right\}\right.$$
$$\left.(\alpha' s)^{\alpha_t} - \Lambda_{A_2}\left(1+\frac{i\alpha_I^{Y_0^*}}{\alpha'}\right)^{\alpha_t-1}(\alpha' s)^{\alpha_t-1}\right] e^{-i\pi\alpha_t} \qquad (6.67)$$

$$B_{\bar{\pi}N}(s,t,u) = -\Gamma(1-\alpha_t)\, e^{-i\pi\alpha_t}(\alpha' s)^{\alpha_t-1}\left[\Lambda_{B_1}\left(1+\frac{i\alpha_I^{Y_0^*}}{\alpha'}\right)^{\alpha_t-1}\right.$$
$$\left.+\sum_{B_1}\left(1-\frac{t}{N}\right)\left(1+\frac{i\alpha_I^{Y_1^*}}{\alpha'}\right)^{\alpha_t-1}\right] \qquad (6.68)$$

Expanding factors such as $\left(1+\frac{i\alpha_I^{Y_0^*}}{\alpha'}\right)^{\alpha_t}$ by a binomial expansion allows us to recover the desired asymptotic limit to first order. However, the real part of this factor remains close to unity, but we get a small t-dependent imaginary part.

6.4 Removal of parity doublets on the Y_0^* trajectory.

Taking the case of the azimuthal angle $\phi = 0$ and using the notation of section 2.6, we can define the s-channel helicity amplitudes as

$$\phi_1 = (f_1+f_2)\cos\frac{\theta}{2} \qquad (6.69)$$

$$\phi_2 = (f_1-f_2)\sin\frac{\theta}{2} \qquad (6.70)$$

Then, the s-channel partial wave amplitudes with $J=\ell\pm\frac{1}{2}$ [ℓ is the

orbital angular momentum] and definite parity can be written as :

$$f_{\ell+} = \frac{1}{2}\int_{-1}^{+1} d(\cos\theta)\left[d^{J}_{\frac{1}{2}\frac{1}{2}}(\theta)\,\phi_1 + d^{J}_{-\frac{1}{2}\frac{1}{2}}(\theta)\,\phi_2\right] \qquad (6.71)$$

$$f_{(\ell+1)-} = \frac{1}{2}\int_{-1}^{+1} d(\cos\theta)\left[d^{J}_{\frac{1}{2}\frac{1}{2}}(\theta)\,\phi_1 - d^{J}_{-\frac{1}{2}\frac{1}{2}}(\theta)\,\phi_2\right] \qquad (6.72)$$

with parity $\pm(-1)^{J-\frac{1}{2}}$ respectively. Combining (6.69), (6.70), (6.71) and (6.72) and using equations (3.5) and (3.6) gives:

$$f_{\ell\pm} = \frac{1}{2}\int_{-1}^{+1} d(\cos\theta)\left[f_1 P_{\ell}(\cos\theta) + f_2 P_{\ell\pm1}(\cos\theta)\right] \qquad (6.73)$$

where $$f_1 = \frac{E_1+m_1}{8\pi W}\left[A + B(W-m_1)\right] \qquad (6.74)$$

and $$f_2 = -\frac{E_1-m_1}{8\pi W}\left[A - B(W+m_1)\right] \qquad (6.75)$$

where $E_1 = \dfrac{W^2-m_1^2-\mu_1^2}{2W}$, $W^2 = s$ and m_1 and μ_1 are the masses of the initial nucleon and meson respectively.

The Y_0^* trajectory lies in the $J = \ell-\frac{1}{2}$ partial wave, and the poles on this are defined with the mass $W = -m_{res.}^{(11)}$. The discussion of Macdowell symmetry in section 5.5 then puts the parity doublets in the $J = \ell-\frac{1}{2}$ partial wave with mass $W = m_{res.}$ Hence, to remove

unwanted parity doublets(i.e. ones not appearing in nature), it is necessary to make the residue of (6.73) vanish for the f_{e-} wave[69]. This implies that

$$f_1(w) = 0 \qquad \text{for} \qquad w = m_{res} \tag{6.76}$$

Taking (6.76) and (6.74), the condition for the removal of a Y_0^* parity doublet of mass $w = m_{res}$ is:

$$\frac{A}{B} = -(m_{res} - m_1) \tag{6.77}$$

There are 2 particles that we want to remove. These are the $\Lambda\ (115)\frac{1}{2}^-$ particle (S_{01}) and the $\Lambda\ (1520)\ \frac{3}{2}^+$ particle (P_{03}). The relations between the parameters in the amplitudes given in equations (6.45) and (6.46) obtained from the removal of these are:

a) Elimination of the $\Lambda\ (1115)\frac{1}{2}^-$ particle (S_{01}).

The term in A and B considered are those containing Λ_{A_2} and Λ_{B_1}, as these only have the $\alpha_s^{Y_0^*} = \frac{1}{2}$ pole. (6.77) gives:

$$\frac{\Lambda_{A_2}}{\Lambda_{B_1}} = -0.177 \tag{6.78}$$

b) Elimination of the Λ (1520) $\frac{3}{2}^+$ particle (P_{03}).

The $\alpha_s^{Y_0^*} = \frac{3}{2}$ pole is contained in the terms proportional to Λ_{A_1}, Λ_{A_2} and Λ_{B_1}. Hence (6.77) gives

$$\frac{-(1+2i\times10^{-3})\Lambda_{A_1} + \Lambda_{A_2}}{\Lambda_{B_1}} = -0.582 \qquad (6.79)$$

Hence neglecting the small imaginary part,

$$\frac{\Lambda_{A_1}}{\Lambda_{B_1}} = 0.405 \qquad (6.80)$$

The relations between $\left(\frac{\Sigma'}{\pi'}\right)_\chi$ and $\left(\frac{\Sigma}{\pi}\right)$ obtained from these are given in Table 5. Hence we have specifically removed the doublets for $K^-p \to \bar{K}^0 n$, but crossing also removes them from $K^+n \to K^0 p$.

6.5 Discussion of Results.

The previous part of the chapter was concerned with setting up a Veneziano form for the pole graph in the hope that the lower energy behaviour of our model would be improved. Absorptive corrections are still required as explained in section 5.1, but as they are introduced just in the t-channel, as explained in Chapter 3, we destroy crossing symmetry in the cut terms. Thus, for the purposes of this model, we are forced to interpret the

Veneziano contributions to the cut terms just as an infinite set of Regge poles. The importance of this inclusion of the daughters can be seen from the fact that the first daughter in the Λ_{A_1} term has a larger effect than the subsidiary term Λ_{A_2}.

The absorption coefficients for elastic $K^- p$ scattering are given in Table 2, but as no elastic $K^+ n$ scattering data exists, $K^+ p$ elastic scattering absorption coefficients were used for $K^+ n \longrightarrow K^0 p$ and these are given in Table 6.

From previous sections, we see that our model is left with two free parameters, $\left(\frac{\Sigma}{\Lambda}\right)$ and N. These were determined, as in chapter 4, by fitting the 'pole+cut' amplitudes in the differential cross-sections to the data using a χ^2 minimization and MINUITS. The results are displayed in Figs. 21 to 24. These fits were remarkably insensitive to N, when it was chosen such that $N >> 1$, so N was chosen as 20. $\left(\frac{\Sigma}{\Lambda}\right)$ came out to be 0.0423 so giving a χ^2 of 617 on 101 data points.

The mass splitting used in determining the U(6,6) factors involved in the parameters Λ_{A_1} etc. was

$q_i^2 = \mu_i^2$ i.e. 'on-shell'

m = average of $\frac{1}{2}^+$ SU(3)octet and $\frac{3}{2}^+$ SU(3)decuplet = 1.27 GeV/c^2.

μ = average of 0^- nonet, 1^- and 2^+ nonets = 0.88 GeV/c^2.

M = average of 1^- and 2^+ nonets = 1.115 GeV/c^2.

M_1 = average of 0^- nonet = 0.42 GeV/c^2.

m_1 = average of $\frac{1}{2}^+$ octet = 1.15 GeV/c^2.

μ_2 = average of the 35 SU(6) multiplets = 0.63 GeV/c^2. (6.81)

This was motivated as follows. In the coupling constants, with the exception of the kinematic factor $p^2/4m_1^2$, SU(6) masses were used. These were preferred as at the meson vertex, both 0^- and 1^- particles are involved and these compose the SU(6) $\underline{35}$ multiplets. Thus, for consistency, we use the SU(6) $\underline{56}$ multiplet at the baryon vertex. The kinematic factor $\frac{p^2}{4m_1^2} = \left(1 - \frac{M_1^2}{4m_1^2}\right)$ was conveniently interpreted in terms of SU(3) masses.

For masses external to g and h, the same form of mass splitting must exist by consistency, but the meson masses must be modified to include an effect from the 2^+ exchange with equal weight as the 0^- and 1^- exchange as we have used exchange degeneracy.

The figs. 21 to 24 show that reasonable success was obtained, but we still failed to reproduce the low energy normalization for $K^+n \to K^0p$ although this was an improvement over our previous fits for this process. As shown by Berger and Fox, the introduction of many satellites might solve this problem. The diagrams also show that at wide angles, the differential cross sections for $K^-p \to \bar{K}^0n$ were too large whereas those for $K^+n \to K^0p$ were too small. This is a factor in common with our previous Reggeized absorption models, although we are rather better here probably due to the inclusion of other channels, so indicating that this is a 'cut' effect. This seems to be borne out by figures 21 and 23 which shows that the cut is probably too steep in $K^-p \to \bar{K}^0n$ and too shallow in $K^+n \to K^0p$, so giving too little destructive interference in the first case and too much in the latter case. We also see that the cut shape is non-flip as expected.

The defects in the 'cut' are not really unexpected as this is an essentially high energy parameterization and pure non-flip. We expect the flip contribution to give an effect at wider angles so its introduction to the absorption may be important.

The comparison of our model with Inami , who used a similar pole form, but without absorptive corrections, is interesting. Our parameters turn out to be :

$$\Lambda_{A_1} = -64.4, \quad \Lambda_{A_2} = 28.1, \quad \Sigma_{A_1} = -14.1 \quad \text{in units of } (GeV)^{-1}$$

$$\Lambda_{B_1} = -159.5, \quad \Sigma_{B_1} = -6.72, \quad \text{in units of } (GeV)^{-2}$$

$$\text{and } N = 20.0 \ (GeV)^2 \qquad (6.82)$$

Those of Inami are

$$\Lambda_{A_1} = -55.5, \quad \Lambda_{A_2} = 24.4, \quad \Sigma_{A_1} = -22.4 \quad \text{in units of } (GeV)^{-1}$$

$$\Lambda_{B_1} = -138.7, \quad \Sigma_{B_1} = -22.5, \quad \text{in units of } (GeV)^{-2}$$

$$\text{and } N = 2.3 \ (GeV)^2 \qquad (6.83)$$

The trajectories were :

$$\alpha_s^{Y_0^*} = -0.74 + s$$

$$\alpha_s^{Y_1^*} = -0.4 + s \qquad (6.84)$$

$$\alpha_t = 0.5 + t$$

His relations $\Sigma_{A_1}/\Sigma_{B_1}$ and N were obtained by the requirement

of removal of the $\Sigma(1385)\frac{3}{2}^-$ and $\frac{1}{2}^+$ daughter, which we did not attempt to do because of restrictions on the Σ_{β_1} term. The overall normalization was obtained from $\bar{K}N$ and KN total cross sections.

Our model gives a larger Y_0^* term, but a much smaller Y_1^* term than Inami's. We require an increased normalization as we have a destructive effect between pole and cut, which of course is not present in Inami's model so this must be given by the Y_0^* term. The smallness of the Y_1^* contribution is not unreasonable as if we treat our model as a pure phenomenological one, the α_t can be treated as an exchange-degenerate $\rho - A_2 - f^0 - \omega$ trajectory and thus, by using isospin and crossing arguments, generate K^+p backward scattering amplitudes at high energies (where the Pomeron contribution would be negligible). Barger[76] fitted this data with a Y_0^* contribution only and neglected the Y_1^* term by SU(3) and dispersion relation arguments. However, resolution of this problem must wait for K^+n elastic backward scattering data.

Using the same phenomenological argument for a $\rho - A_2 - \omega - f^0$ trajectory being equivalent to α_t, we can generate the K^-p elastic scattering amplitude from that of $K^-p \to \bar{K}^0 n$ by isospin i.e. for pole terms only

$$A(K^-p \to \bar{K}^0 n) = \tfrac{1}{2}(-A^{(0)} + A^{(1)}) \qquad (6.85)$$

$$A(K^-p \to K^-p) = \tfrac{1}{2}(A^{(0)} + A^{(1)}) \qquad (6.86)$$

where the superscripts define the s-channel isospin terms. (B similar)

Thus we can obtain the low energy resonance properties. The first is the coupling constants, for which we have to make the questionable assumption of factorization. Assuming that, we have[53]

$$g_{\Lambda}^2 = \frac{[\Lambda_{A_2} - (m_\Lambda + m_\rho)\Lambda_{B_1}]}{16\pi\alpha' m_\Lambda} \tag{6.87}$$

and $$\frac{g^2_{\Sigma(1385)}}{4\pi} = -\frac{m_\rho^2 \Sigma_{A_1}}{8\pi m_{\Sigma(1385)}} \tag{6.88}$$

giving $g^2_\Lambda = 6.46$ and $\frac{g^2_{\Sigma(1385)}}{4\pi} = 0.36$

compared with 5.5 and 0.77 respectively for Inami's model.

The next thing we wish to calculate are the elastic widths of the s-channel resonances. Again we use the pole graph contribution only. From equations (6.69), (6.70), (6.71) and (6.72) we can write :

$$f_1 = \sum_J \left[f_{\ell+} P'_{J+\frac{1}{2}}(\cos\theta) - f_{(\ell+1)-} P'_{J-\frac{1}{2}}(\cos\theta) \right] \tag{6.89}$$

$$f_2 = \sum_J \left[f_{(\ell+1)-} P'_{J+\frac{1}{2}}(\cos\theta) - f_{\ell+} P'_{J-\frac{1}{2}}(\cos\theta) \right] \tag{6.90}$$

Now the Y_0^* particles lie in $J = \ell - \frac{1}{2}$ wave, and the Y_1^* ones in $J = \ell + \frac{1}{2}$ wave. Hence, for large t, the Y_0^* lies almost entirely in f_2 while the Y_1^* is in f_1.

Considering a pole at $J = j$ on the Y_0^* trajectory

$$f_2(w) \approx f_{(\ell+1)-} P'_{j+\frac{1}{2}}(\cos\theta) \tag{6.91}$$

For large t,

$$P'_{j+\frac{1}{2}}(\cos\theta) \sim \frac{2\Gamma(j+1)}{\Gamma(\frac{1}{2})\Gamma(j+\frac{1}{2})}\left(\frac{t}{Q^2}\right)^{j-\frac{1}{2}} \tag{6.92}$$

where Q is the C.M momentum at the resonance pole. Again, $f_{(\ell+1)-}$ is approximatedby a Breit-Wigner at the pole, giving[77]

$$f_{(\ell+1)-} = \frac{\Gamma_{el}^{(0)j-} m_{res}}{Q(m_{res}^2 - s - i\Gamma^{(0)}_{m_{res}})} \tag{6.93}$$

where $\Gamma_{el}^{(0)}$ is the elastic width and $\Gamma^{(0)}$ is the total width of the resonance.

$$\therefore f_{(\ell+1)-} P'_{j+\frac{1}{2}}(\cos\theta) = \frac{2\Gamma(j+1)\Gamma_{el}^{(0)j-} m_{res}}{\sqrt{\pi}\,\Gamma(j+\frac{1}{2})} \frac{1}{(Q^2)^j} \frac{(t)^{j-\frac{1}{2}}}{(m_{res}^2 - s - i\Gamma^{(0)}_{m_{res}})} \tag{6.94}$$

Near the pole, from equation (6.64);

$$m_{res}^2 - s - i\Gamma_{m_{res}} \simeq \frac{1}{\alpha'}\left(j - \alpha_s^{Y_0^{\pm}}\right) \tag{6.95}$$

and

$$\frac{1}{j - \alpha_s^{Y_0^{\pm}}} \simeq \Gamma\left(j - \alpha_s^{Y_0^{\pm}}\right)\Gamma\left(1 - j + \alpha_s^{Y_0^{\pm}}\right) \tag{6.96}$$

Using equations (6.75) gives:

$$\Gamma_{el}^{(0)j-} = -\frac{\sqrt{\pi}\,\Gamma(j+\frac{1}{2})\,(Q^2)^j}{16\pi W \alpha'(t)^{j-\frac{1}{2}} m_{res}} \frac{(E_1 - m_p)}{\Gamma\left(j - \alpha_s^{Y_0^{\pm}}\right)\Gamma\left(1 - j - \alpha_s^{Y_0^{\pm}}\right)} \tag{6.97}$$
$$\left[A^{(0)} - (W + m_p)B^{(0)}\right] \frac{1}{\Gamma(j+1)}$$

Taking the asymptotic limit for fixed s, $t \to \infty$, at the pole $\alpha_s^{\gamma\sigma} = j$ with $\omega = m_{\rho_3}$ (this way round or else we obtain the condition for vanishing f_2):

$$\Gamma_{21}^{(0)j-} = \frac{\sqrt{\pi}\left[(m_\rho^2+Q^2)^{\frac{1}{2}} - m_\rho\right](\alpha' Q^2)^j}{16\pi\, m_{\rho_3}^2\,(\alpha')^{\frac{3}{2}}\,\Gamma(j+1)}\left[\Lambda_{A_2} - (j-\tfrac{1}{2})\,\Lambda_{A_1} - (m_{\rho_3}+m_\rho)\,\Lambda_{B_1}\right] \tag{6.98}$$

Similarly for the $\gamma_1^{\sigma\sigma}$ widths,

$$\Gamma_{21}^{(1)j+} = \frac{-(j-\frac{1}{2})\sqrt{\pi}\left[(m_\rho^2+Q^2)^{\frac{1}{2}} + m_\rho\right](\alpha' Q^2)^j}{16\pi\, m_{\rho_3}^2\,(\alpha')^{\frac{3}{2}}\,\Gamma(j+1)}\left[\Sigma_{A_1} + \frac{(m_{\rho_3}-m_\rho)}{\alpha' N}\,\Sigma_{B_1}\right] \tag{6.99}$$

The widths are displayed in Table 7. They are too small in common with Inami's analysis and provide a powerful argument for the introduction of satellite terms.

In conclusion, we can make the following comments:

a) The arguments for the introduction of satellite are powerful, but not feasible within the restrictions of our model.

b) A 'low energy' form for the absorptive corrections appears to be necessary.

c) Instead of using imaginary parts to trajectories to avoid

singularities, a 'smoothing' Veneziano form as suggested by Martin[78], where one takes the Veneziano amplitude $V(\sigma, \tau)$ and creates a new one,

$$V(s,t) = \int_{1-a}^{1} \psi(x)\, V(x\sigma, x\tau)\, dx \qquad (6.100)$$

where $\psi(x)$ is an averaging function, may provide an effective solution with cuts.

Trajectory	Resonance	J^P	Contribution to α_I
Y_0^*	$\Lambda_\alpha(1115)$	$\frac{1}{2}^+$	below threshold
	$\Lambda_\gamma(1520)$	$\frac{3}{2}^-$	0.075
	$\Lambda_\alpha(1815)$	$\frac{5}{2}^+$	0.099
	$\Lambda_\gamma(2100)$	$\frac{7}{2}^-$	0.084
Average			0.09
Y_1^*	$\Sigma_\beta(1385)$	$\frac{3}{2}^+$	below threshold
	$\Sigma_\delta(1770)$	$\frac{5}{2}^-$	0.186
	$\Sigma_\beta(2030)$	$\frac{7}{2}^+$	0.110
Average			0.15

Table 4

Contributions to the imaginary parts of the trajectories.

Parity Partner	Relation obtained.
$\Lambda\ (1115)\frac{1}{2}^-$	$X = -\dfrac{0.362}{\frac{\Sigma}{\Lambda} + 1}$
$\Lambda\ (1520)\ \frac{3}{2}^+$	$\dfrac{\frac{\Sigma}{\Lambda} + 1}{\frac{\Sigma'}{\Lambda'} + 1} = 0.829$

Table 5.

Relations given by absence of parity partners.

p_{lab}	V_1^{-1}(GeV)	C_1
2.3	0.38	1.00
2.97	0.36	0.91
5.5	0.31	0.68

Table 6

Absorption coefficients for K^+p elastic scattering.

Resonance		$\Lambda_\gamma(1520)D_{03}$	$\Lambda_\alpha(1815)F_{05}$	$\Lambda_\gamma(2100)G_{07}$
Γ_{el} (MeV)	experi-mental	7.2	52	42
	theore-tical	2.16	11.6	15

Y_o^* Elastic Widths.

Resonance		$\Sigma_\beta(1770)D_{15}$	$\Sigma_\delta(2030)F_{17}$
Γ_{el} (MeV)	experi-mental	45	12
	theor-etical	5.5	4.9

Y_1^* Elastic Widths.

Table 7.

FIGURE CAPTIONS.

Figure 21. Contributions from the pole (---), cut (— - — - —) and pole + cut (—) to the differential cross-section for $K^- p \to K^o n$. Data from ref. (79).

Figure 22. Differential cross-section for $K^- p \to \bar{K}^o n$. Data from ref. 79 and 80.

Figure 23. Contributions from the pole (---), cut (— - — - —), and pole + cut (–) to the differential cross-section for $K^+ n \to K^o p$. Data from ref. 71.

Figure 24. Differential cross-section for $K^+ n \to K^o p$. Data from refs. 71 and 82.

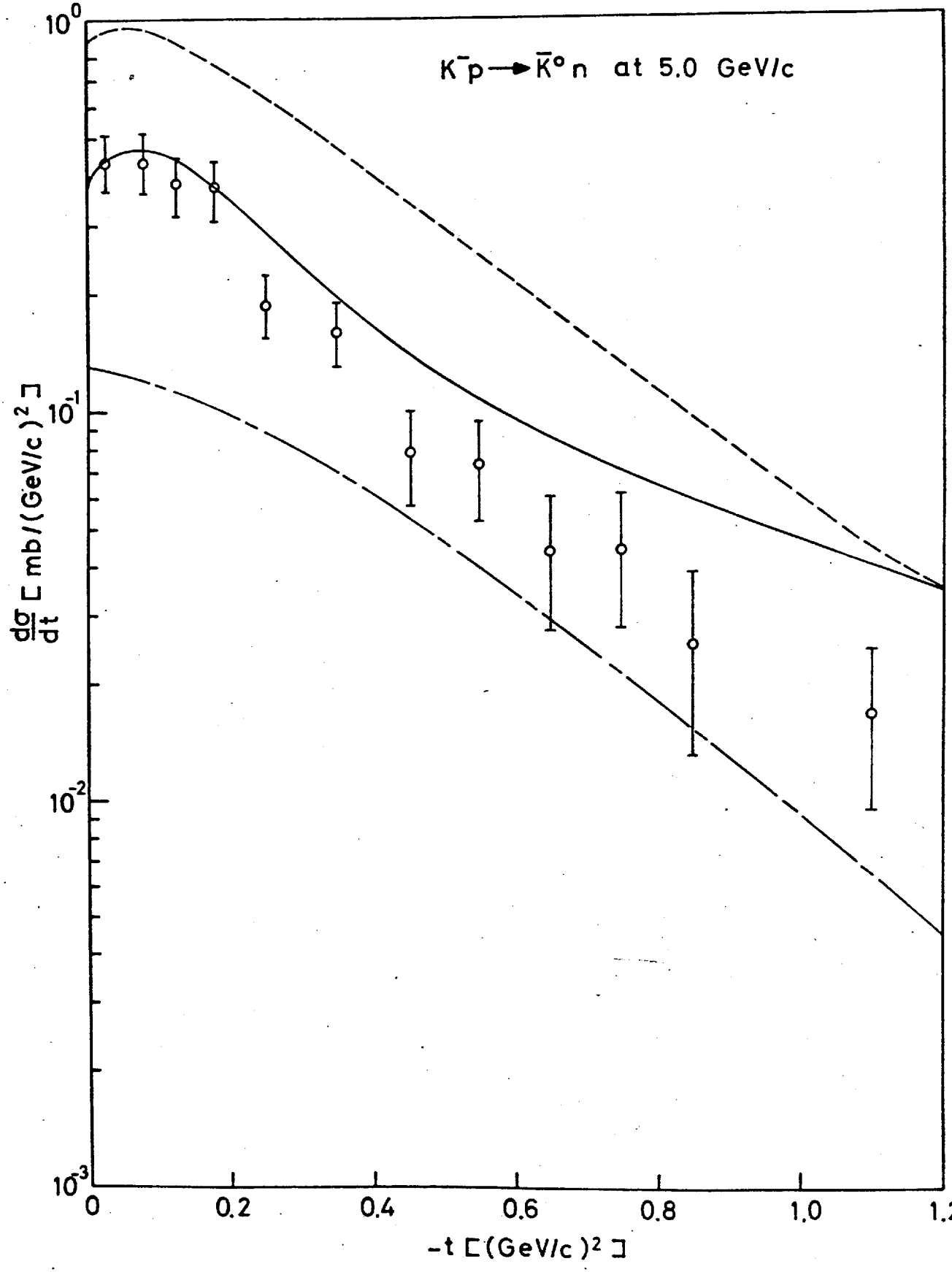
$K^- p \rightarrow \bar{K}^0 n$ at 5.0 GeV/c
10^0
10^{-1}
10^{-2}
10^{-3}
$\frac{d\sigma}{dt}$ [mb/(GeV/c)^2]
0
0.2
0.4
0.6
0.8
1.0
1.2
$-t$ [(GeV/c)^2]

Fig. 21

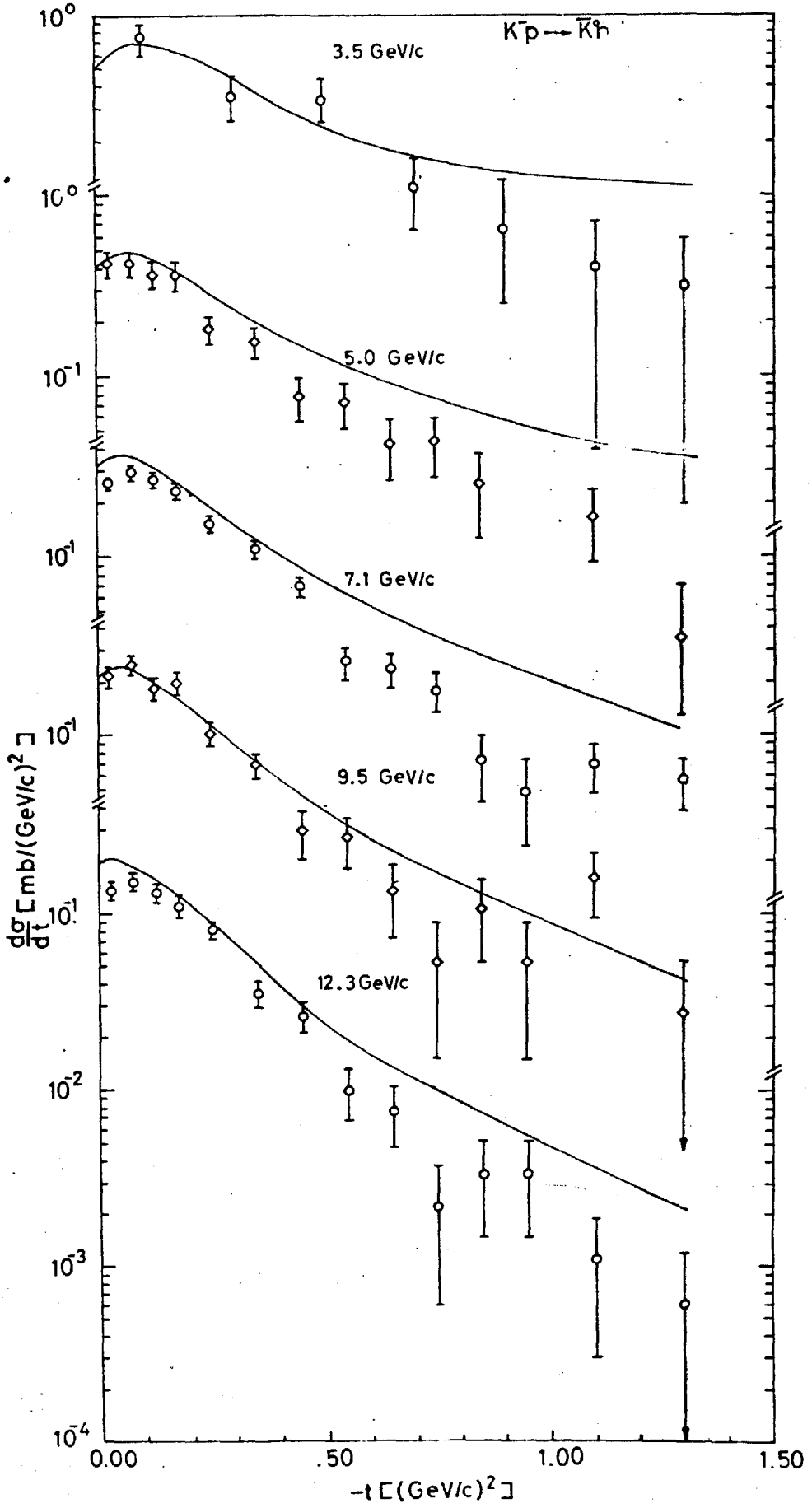
$K^-p \to \bar{K}^0 n$
3.5 GeV/c
5.0 GeV/c
7.1 GeV/c
9.5 GeV/c
12.3 GeV/c
$\frac{d\sigma}{dt}$ [mb/(GeV/c)^2]
$-t$ [(GeV/c)^2]
10^0
10^0
10^{-1}
10^{-1}
10^{-1}
10^{-1}
10^{-2}
10^{-3}
10^{-4}
0.00
.50
1.00
1.50

Fig. 22.

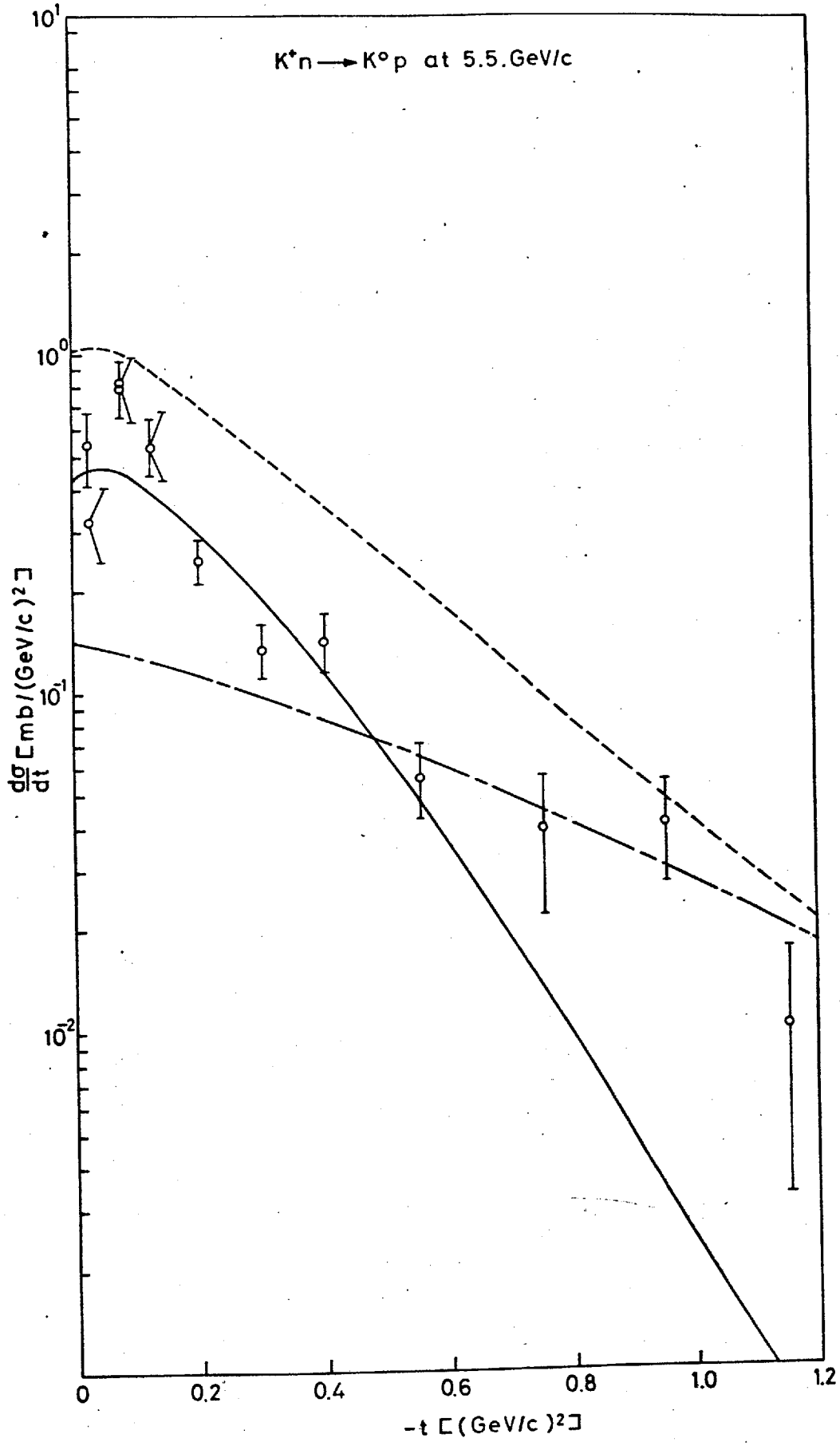
$K^+n \longrightarrow K^0p$ at 5.5.GeV/c
10^1
10^0
10^{-1}
10^{-2}
$\frac{d\sigma}{dt}$ [mb/(GeV/c)^2]
0
0.2
0.4
0.6
0.8
1.0
1.2
-t [(GeV/c)^2]

Fig. 23.

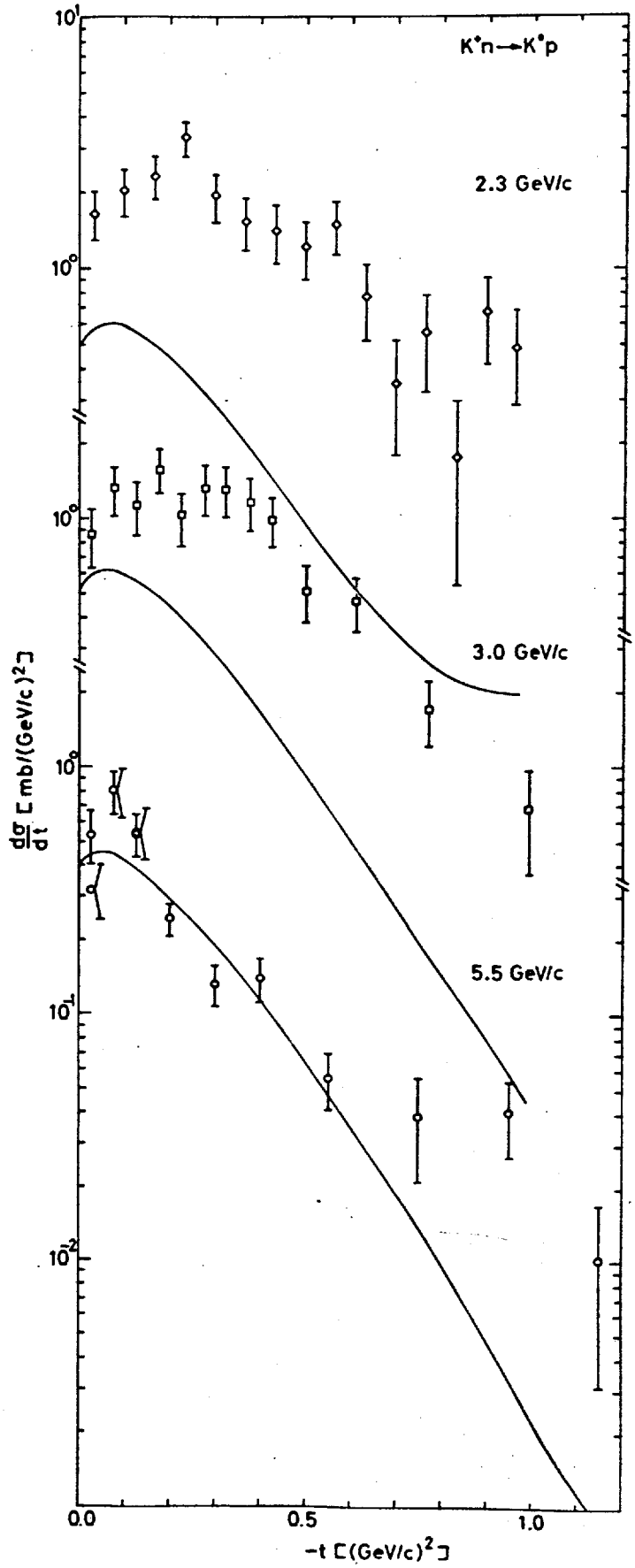
K⁺n→K⁰p
2.3 GeV/c
3.0 GeV/c
5.5 GeV/c
dσ/dt [mb/(GeV/c)²]
-t [(GeV/c)²]
10¹
10⁰
10⁰
10⁰
10⁻¹
10⁻²
0.0
0.5
1.0

Fig. 24.

APPENDIX

Numerical Analysis of the Problem[83]

As in the above analyses, we have free parameters, it was necessary to use a standard minimization program to determine these. This program was MINUITS (CERN Program library No. D506).

To this were added sub-routines which presented the parameters to be minimized on to MINUITS and carried out the Regge calculations, which involved partial-wave analysing the helicity amplitudes for the pole graph, modifying them with absorption corrections to obtain the cut graphs and then resuming the modified series and comparing the theoretical results with the experimental data by means of a χ^2 where

$$\chi^2 = \sum_{\substack{\text{no. of} \\ \text{data points}}} \left(\frac{\text{experimental } \frac{d\sigma}{dt} - \text{theoretical } \frac{d\sigma}{dt}}{\text{error on experimental } \frac{d\sigma}{dt}} \right)^2$$

Many passes were made through MINUITS which altered the parameters for each pass until this χ^2 found a minimum.

The partial-wave analysis of the helicity amplitudes were carried out by means of the equation :

$$\langle \lambda_3 \lambda_4 | T^J(s) | \lambda_1 \lambda_2 \rangle = \tfrac{1}{2} \int_{-1}^{+1} \langle \lambda_3 \lambda_4 | \phi(s,t) | \lambda_1 \lambda_2 \rangle d^J_{\mu\lambda}(\theta)\, d(\cos\theta)$$

As this cannot be done analytically, the integration was carried out using an N-point Gaussian quadrature which says that for a range of integration symmetrically placed about the origin

$$\int_{-1}^{+1} f(x)\,dx = \sum_{m=1}^{N} W_m f(x_m)$$

This would integrate exactly a polynomial of degree 2N. In our case, this becomes:

$$\int_{-1}^{+1} \langle \lambda_3\lambda_4 | \phi(s,t) | \lambda_1\lambda_2 \rangle\, d^J_{\mu\lambda}(\cos\theta)\, d(\cos\theta)$$

$$= \sum_{m=1}^{N} \langle \lambda_3\lambda_4 | \phi(s,\cos\theta_m) | \lambda_1\lambda_2 \rangle\, d^J_{\mu\lambda}(\cos\theta_m)\, W_m$$

where W_m is the quadrature weight associated with the point $\cos\theta_m$. Clearly, the rotational matrices are independent of energy and depend only on the value of the angle θ_m, which in turn, depend only on the order of the Gaussian quadrature.

This enables us to write the integration in terms of new weights

$$W'_m = d^J_{\mu\lambda}(\cos\theta_m)\, W_m$$

which need to be evaluated only once, so saving much computing time.

The checks involved were, for the given no. of partial waves and given order of Gaussian quadrature :

a) Re S^J_{++} became 1.0 within the allowed number of partial waves i.e. no absorption is taking place outside this region.

b) The contributions from the helicity amplitudes must be zero by the time the last partial wave is reached.

c) Resummation of the unmodified partial-waves must give the original pole graph helicity amplitudes.

The structure of the program is shown in the flow diagram.

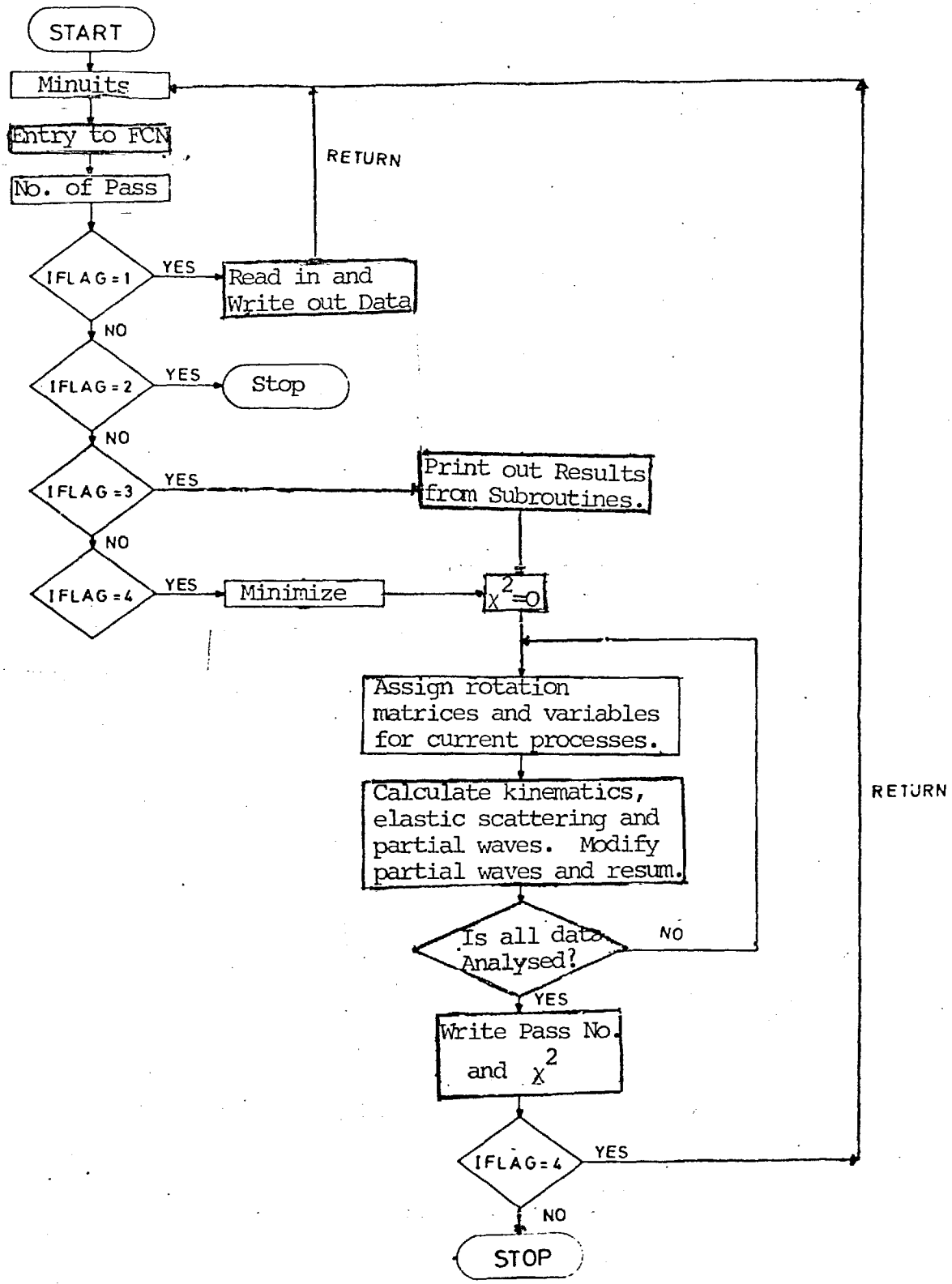

FLOW DIAGRAM.

REFERENCES

1. J.D. Jackson. Proceedings of the XIIIth International Conference on High Energy Physics, Berkeley (1967).

2. P.T. Matthews. Brandeis Summer School (1963).

3. H.D.D. Watson and J.H.R. Migneron, Phys. Letters 19, 424 (1965);
J.H.R. Migneron and K.M.J. Moriarty, Phys. Rev. Letters 18, 978 (1967);
J.H.R. Migneron and H.D.D. Watson, Phys. Rev. 166, 1654 (1968);
H.D.D. Watson et al., Nuovo Cimento 62A, 127 (1969);
D.G. Fincham et al., Nucl. Phys. B13, 161 (1969);
F.D. Gault et al, Nuovo Cimento 62, 269 (1969).

4. G.E. Hite, Rev. Mod. Phys. 41, 669 (1969).

5. H.D.D. Watson, Ph.D. Thesis (1965).

6. P. Bonamy et al, Phys. Letters 23, 501 (1966).

7. W.A. Cooper et al, Phys. Rev. Letters 20, 472 (1968).

8. S.M. Pruss et al, Phys. Rev. Letters 23, 189 (1969).

9. R.R. Kofler et al, Phys. Rev. 163, 1479 (1967).

10. G. McCellan et al, Phys. Rev. Letters 23, 718 (1969).

11. L. Bertocchi, Proceedings of the Heidelberg International Conference on Elementary Particles (1967).

12. M. Le Bellac, Phys. Letters 25B, 524 (1967).

13. V. Barger and R.J.N. Phillips, Phys. Rev. Letters 24, 291 (1970).

14. V. Barger. Topical Conference on High Energy Collisions of Hadrons. CERN (1968).

15. A.V. Stirling et al, Phys. Rev. Letters 14, 763 (1963);
ibid 20, 75 (1966);
M.A. Wahlig et al, Phys. Rev. 168, 155 (1968).

16. R.C. Arnold. Proceedings of the 1969 Regge Cut Conference Wisconsin (1969).

17. Q. Shafi, Nuovo Cimento 62A, 290 (1969).

18. R. Delbourgo, A. Salam and J. Strathdee, Phys. Rev. 179 1487 (1968); 172, 1727 (1968); 186, 1516 (1969).

19. R. Delbourgo et al. High Energy Physics and Elementary Particles. I.A.E.A., Vienna (1965).

20. V.N. Gribov et al, JETP 18, 769 (1964).

21. M. Jacob and G.C. Wick, Annals of Physics 7, 404 (1959).

22. R.G. Newton. The Complex j-Plane. (W.A. Benjamin, Inc. New York, 1964).

23. These are plotted in Chapter 12 of reference 22.

24. R.J. Eden et al. The Analytic S-Matrix. (Cambridge University Press, New York 1966).

25. D.P. Owen et al, Phys. Rev. 181, 1794 (1969).

26. B.J. Hartley et al, Phys. Rev. 187, 1921 (1969);
ibid D1(3) 954 (1970);
P.A. Collins et al, Phys. Rev. D1(9), 2619 (1970);
P.A. Collins et al, Phys. Rev. D1(11), 3195 (1970);
S.A. Adjei, et al, ICTP/69/23. Presented at Kiev Conference (1970).

27. R.C. Arnold and M. Blackmon, Phys. Rev. 176, 2082 (1968) and subsequent material.

28. P.A. Collins, et al, Nucl. Phys. B20, 381 (1970).

29. F. Henyey et al, Phys. Rev. 182, 1579 (1969) and subsequent material;
M. Ross, Regge Pole Conference, Irvine, California (1969).

30. R.J.N. Phillips, Ninth Winter School, Schladming (1970).

31. H.D.D. Watson, Phys. Letters 17, 72 (1965).

32. D. Amati, et al, Phys. Letters 1, 29 (1962);
Nuovo Cimento 26, 897 (1962).

33. S. Mandelstam, Nuovo Cimento 30, 1113, 1127, 1148 (1963).

34. M. Ross, Proceedings of the 1969 Regge Cut Conference, Wisconsin (1969).

35. P.V. Landshoff. Ninth Winter School, Schladming (1970).

36. G.E. Hite. Ninth Winter School, Schladming (1970).

37. L. Caneschi, Phys. Rev. Letters 23, 254 (1969).

38. K.J.M. Moriarty, Ph.D. Thesis (1970).

39. D.D. Reeder and K.V.L. Sarma, Phys. Rev. 172, 1566 (1968).

40. A. Krzywicki and J. Tran Thanh Van, Phys. Letters 30B, 185 (1969).

41. C. Meyers et al. Bordeaux preprint PTB-36 (1970).

42. E. Bertolucci et al, Nuovo Cimento Letters 2, 149 (1969).

43. R. Erlich et al, Phys. Rev. 152, 1194 (1966).

44. D.J. Crennell et al, Phys. Rev. Letters 18, 86 (1967).

45. W.L. Yen et al, Phys. Rev. Letters 22, 963 (1969).

46. J.S. Loos et al, Phys. Rev. 173, 1330 (1968).

47. D. Burnbaum et al. Paper submitted to XIVth International Conference on High-Energy Physics, Vienna 91968).

48. J.D. Jackson. Proceedings of the Lund International Conference on Elementary Particles (1969).

49. See, for instance, H. Harari, Brookhaven Summer School (19698).

50. M. Jacob, Proceedings of the Lund International Conference on Elementary Particles (1969).

51. C. Lovelace, Irvine Conference on Regge Poles (1969).

52. A. Kryzwicki. Fifth Moriond Meeting (1970).

53. C. Lovelace, Nucl. Phys. B12, 253 (1969).

54. S. Mandelstam, Brandeis Summer School (1970).

55. W.R. Frazer, XIVth International Conference on Elementary Particles, Vienna (1968).

56. S. Mandelstam, Phys. Rev. Letters 21, 1724 (1968).

57. K. Igi, Phys. Letters 28B, 230 (1968).

58. F. Wagner, Nuovo Cimento 63A, 393 (1969).

59. M. Ademollo et al,Phys. Rev. Letters 22, 83 (1969).

60. P. Olesen, CERN Preprint TH.1100 (1969).

61. O.W. Greenberg. Proceedings of the Lund International Conference on Elementary Particles (1969).

62. M. Jacob. Eighth Winter School, Schladming (1969).

63. R.C. Arnold. Phys. Rev. Letters 14, 657 (1965).

64. C. Lovelace, Phys. Letters 28B, 264 (1968).

65. E.L. Berger and G.C. Fox, Phys. Rev. 188, 2170 (1969) and references therein.

66. O. Miyamura, Tokyo Report No. TU/69/41 (1969).

67. M. Blackmon and K.C. Wali, Syracuse Preprint no. SU-1206-215.

68. T. Inami, Nuovo Cimento 63A, 987 (1969).

69. K. Igi and J.K. Storrow, Nuovo Cimento 62A, 972 (1969); K. Pretzl and K. Igi, ibid 63A, 609 (1969).

70. R. Delbourgo, ICTP/68/21.

71. D.H. Sharp and W.G. Wagner, Phys. Rev. 131, 2237 (1963).

72. F.D. Gault, private communication.

73. V.L. Auslander et al, Phys. Letters 25B, 433 (1967).

74. M. Kugler, Ninth Winter School Schladming (1970).

75. C.F. Chew, S.C. Frautschi and S. Mandelstam, Phys. Rev. 126, 1202 (1962).

76. V. Barger, Phys. Rev. 179, 1371 (1969).

77. M.A. Virasoro, Phys. Rev. 184, 1621 (1969).

78. A. Martin, Phys. Letters 29B, 431 (1969).

79. P. Astbury et al, Phys. Letters 23, 396 (1966).

80. A.D. Brodz and C. Lyons, Nuovo Cimento 45A, 1027 (1966).

81. D. Cline et al, Wisconsin Report (1969).

82. I. Butterworth et al, Phys. Rev. Letters 15, 734 (1965); Y. Goldschmidt-Clemont et al, Phys. Letters 27B, 602 (1968).

83. S.A. Adjei et al, ICTP/69/25